



University of Kentucky  
UKnowledge

---

Theses and Dissertations--Chemical and  
Materials Engineering

Chemical and Materials Engineering

---

2017

## PORE-CONFINED CARRIERS AND BIOMOLECULES IN MESOPOROUS SILICA FOR BIOMIMETIC SEPARATION AND TARGETING

Shanshan Zhou

*University of Kentucky*, [shs.zhou@hotmail.com](mailto:shs.zhou@hotmail.com)

Digital Object Identifier: <https://doi.org/10.13023/ETD.2017.383>

[Right click to open a feedback form in a new tab to let us know how this document benefits you.](#)

---

### Recommended Citation

Zhou, Shanshan, "PORE-CONFINED CARRIERS AND BIOMOLECULES IN MESOPOROUS SILICA FOR BIOMIMETIC SEPARATION AND TARGETING" (2017). *Theses and Dissertations--Chemical and Materials Engineering*. 78.

[https://uknowledge.uky.edu/cme\\_etds/78](https://uknowledge.uky.edu/cme_etds/78)

This Doctoral Dissertation is brought to you for free and open access by the Chemical and Materials Engineering at UKnowledge. It has been accepted for inclusion in Theses and Dissertations--Chemical and Materials Engineering by an authorized administrator of UKnowledge. For more information, please contact [UKnowledge@lsv.uky.edu](mailto:UKnowledge@lsv.uky.edu).

## **STUDENT AGREEMENT:**

I represent that my thesis or dissertation and abstract are my original work. Proper attribution has been given to all outside sources. I understand that I am solely responsible for obtaining any needed copyright permissions. I have obtained needed written permission statement(s) from the owner(s) of each third-party copyrighted matter to be included in my work, allowing electronic distribution (if such use is not permitted by the fair use doctrine) which will be submitted to UKnowledge as Additional File.

I hereby grant to The University of Kentucky and its agents the irrevocable, non-exclusive, and royalty-free license to archive and make accessible my work in whole or in part in all forms of media, now or hereafter known. I agree that the document mentioned above may be made available immediately for worldwide access unless an embargo applies.

I retain all other ownership rights to the copyright of my work. I also retain the right to use in future works (such as articles or books) all or part of my work. I understand that I am free to register the copyright to my work.

## **REVIEW, APPROVAL AND ACCEPTANCE**

The document mentioned above has been reviewed and accepted by the student's advisor, on behalf of the advisory committee, and by the Director of Graduate Studies (DGS), on behalf of the program; we verify that this is the final, approved version of the student's thesis including all changes required by the advisory committee. The undersigned agree to abide by the statements above.

Shanshan Zhou, Student

Dr. Barbara L. Knutson, Major Professor

Dr. Thomas D. Dziubla, Director of Graduate Studies

PORE-CONFINED CARRIERS AND BIOMOLECULES IN MESOPOROUS SILICA  
FOR BIOMIMETIC SEPARATION AND TARGETING

---

DISSERTATION

---

A dissertation submitted in partial fulfillment of the  
requirements for the degree of Doctor of Philosophy in the  
College of Engineering  
at the University of Kentucky

By

Shanshan Zhou

Lexington, Kentucky

Director: Dr. Barbara L. Knutson, Professor of Chemical Engineering

Lexington, Kentucky

2017

Copyright© Shanshan Zhou 2017

## ABSTRACT OF DISSERTATION

### PORE-CONFINED CARRIERS AND BIOMOLECULES IN MESOPOROUS SILICA FOR BIOMIMETIC SEPARATION AND TARGETING

Selectively permeable biological membranes composed of lipophilic barriers inspire the design of biomimetic carrier-mediated membranes for aqueous solute separation. This work imparts selective permeability to lipid-filled pores of silica thin film composite membranes using carrier molecules that reside in the lipophilic self-assemblies. The lipids confined inside the pores of silica are proven to be a more effective barrier than bilayers formed on the porous surface through vesicle fusion, which is critical for quantifying the function of an immobilized carrier. The ability of a lipophilic carrier embedded in the lipid bilayer to reversibly bind the target solute and transport it through the membrane is demonstrated. Through the functionalization of the silica surface with enzymes, enzymatic catalysis and biomimetic separations can be combined on this nanostructured composite platform. The successful development of biomimetic nanocomposite membrane can provide for efficient dilute aqueous solute upgrading or separations using engineered carrier/catalyst/support systems.

While the carrier-mediated biomimetic membranes hold great potential, fully understanding of the transport processes in composite synthetic membranes is essential for improve the membrane performance. Electrochemical impedance spectroscopy (EIS) technique is demonstrated to be a useful tool for characterizing the thin film pore accessibility. Furthermore, the effect of lipid bilayer preparation methods on the silica thin film (in the form of pore enveloping, pore filling) on ion transport is explored, as a lipid bilayer with high electrically insulation is essential for detecting activity of proteins or biomimetic carriers in the bilayer. This study provides insights for making better barriers on mesoporous support for carrier-mediated membrane separation process.

Porous silica nanoparticles (pSNPs) with pore sizes appropriate for biomolecule loading are potential for encapsulating dsRNA within the pores to achieve effective delivery of dsRNA to insects for RNA interference (RNAi). The mobility of dsRNA in the nanopores of the pSNPs is expected to have a functional effect on delivery of dsRNA to insects. The importance of pores to a mobile dsRNA network is demonstrated by the lack of measurable mobility for both lengths of RNA on nonporous materials. In addition, when the dsRNA could not penetrate the pores, dsRNA mobility is also not measurable at the

surface of the particle. Thus, the pores seem to serve as a “sink” in providing a mobile network of dsRNA on the surface of the particle. This work successfully demonstrates the loading of RNA on functionalized pSNPs and identified factors that affects RNA loading and releasing, which provides basis for the delivery of RNA-loaded silica particles *in vivo*.

**KEYWORDS:** Biomimetic membrane, mesoporous silica, carrier-mediated, pore-confined lipid, RNA delivery

Shanshan Zhou  
August 14<sup>th</sup>, 2017

PORE-CONFINED CARRIERS AND BIOMOLECULES IN MESOPOROUS SILICA  
FOR BIOMIMETIC SEPARATION AND TARGETING

By

Shanshan Zhou

Dr. Barbara L. Knutson

*Director of Dissertation*

Dr. Thomas D. Dziubla

*Director of Graduate Studies*

August 14<sup>th</sup>, 2017

## ACKNOWLEDGEMENTS

The completion of this work would not have been possible without the input, and guidance of many people. First of all, I would like to thank my advisor Dr. Barbara L. Knutson, who have been a tremendous mentor for me. I am grateful for her patience, support, and encouraging in my research and for allowing me to grow as a research scientist. I would also like to thank Dr. Stephen E. Rankin for always being there and giving thoughtful advice and kindly help. Also, thanks to my committee members, Dr. Dibakar Bhattacharyya, Dr. Folami T Ladipo and Dr. Bruce A Webb, who give insightful advice to make this work better.

I'm thankful for Nicolas Briot's help on FIB-SEM, Dali Qian's assistant on TEM and, James Begley on the support of confocal microscopy. With their technical support I would not have been able to complete as much as I could have. Specially, I would like thank my lab mates: Daniel Schlipf, Ravinder Garlapalli, Kaitlyn Wooten, Suraj Nagpure, Syed Islam, Airf Khan, Kwabena Darkwah, Yuxin He and Mahsa Moradipour for their endless support and being always more than willing to help me when I needed it.

Finally, to my family, thank you for supporting in me on anything that I decided to do. Without your love and caring, I can't image how life will be like.

## TABLE OF CONTENTS

<b>ACKNOWLEDGEMENTS .....</b>	<b>iii</b>
<b>LIST OF TABLES .....</b>	<b>vii</b>
<b>LIST OF FIGURES .....</b>	<b>viii</b>
<b>Chapter 1: Introduction .....</b>	<b>1</b>
<b>Chapter 2: Background.....</b>	<b>5</b>
<b>2.1 Ordered mesoporous silica materials .....</b>	<b>5</b>
2.1.1 Surfactant templating for synthesis of ordered mesoporous silica materials .....	5
2.1.2 Synthesis of silica thin films with orthogonally oriented 2-D hexagonally close packed (HCP) pore structure on porous support .....	7
<b>2.2 Biomimetic carrier-mediated membrane for dilute aqueous solute separation...9</b>	
2.2.1 Structure of biological membrane .....	9
2.2.2 Biomimetic carrier-mediated membranes .....	10
<b>2.3 Supported lipid bilayers.....</b>	<b>12</b>
2.3.1 Types of supported lipid bilayer .....	12
2.3.2 Pore-confined lipids.....	14
<b>2.4 Techniques for characterizing membrane properties.....</b>	<b>16</b>
2.4.1 Electrochemical impedance spectroscopy .....	16
2.4.2 Grazing-incidence small angle X-ray scattering .....	19
2.4.3 Confocal laser scanning microscopy .....	20
2.4.4 Transport in a diffusion cell.....	22
<b>Chapter 3: Lipid Pore-Filled Silica Thin Film Membranes for Biomimetic Recovery of Dilute Carbohydrates .....</b>	<b>25</b>
<b>3.1 Abstract .....</b>	<b>25</b>
<b>3.2 Introduction .....</b>	<b>26</b>
<b>3.3 Experimental sections .....</b>	<b>29</b>
<b>3.4 Results and discussion.....</b>	<b>36</b>



3.4.1 Synthesis of mesoporous silica thin film on porous support as separation platform .....	36
3.4.2 Lipid Pore-Filled Silica Thin Film Membranes as a Transport Barrier .....	38
3.4.3 Incorporation of boronic acid carrier into lipid bilayers.....	45
3.4.4 Glucose transport through supported lipid bilayers with boronic acid carrier .	47
<b>3.5 Conclusion.....</b>	<b>56</b>
<b>Chapter 4: Impedance Analysis of Ion Transport through Supported Lipid Bilayers on Accessible Mesoporous Silica Thin Films.....</b>	<b>57</b>
<b>4.1 Abstract .....</b>	<b>57</b>
<b>4.2 Introduction .....</b>	<b>58</b>
<b>4.3 Experimental sections .....</b>	<b>61</b>
<b>4.4 Results and discussion.....</b>	<b>65</b>
4.4.1 Electrochemical analysis of the mesoporous silica thin film structure .....	65
4.4.2 Electrochemical analysis of lipid supported by mesoporous silica thin film ...	70
<b>4.5 Conclusion.....</b>	<b>76</b>
<b>Chapter 5: Enzyme Immobilization on Synthetic Biomimetic Membranes for Dilute Aqueous Solute Upgrading and Recovery .....</b>	<b>77</b>
<b>5.1 Abstract .....</b>	<b>77</b>
<b>5.2 Introduction .....</b>	<b>78</b>
<b>5.3 Experimental methods .....</b>	<b>82</b>
<b>5.4 Result and discussion .....</b>	<b>85</b>
5.4.1 Characterization of glucose isomerase immobilized thin film silica membrane .....	85
5.4.2 Glucose conversion through glucose isomerase immobilized silica composite membranes.....	88
5.4.3 Transport model development for biocatalyst and carrier-mediated separation integrated membrane at continuous flowing system .....	91

5.5 Conclusion.....	100
<b>Chapter 6: Size-Dependent Loading and Mobility of RNA in Porous Silica Nanoparticles.....</b>	<b>102</b>
6.1 Abstract.....	102
6.2 Introduction.....	103
6.3 Experimental methods.....	107
6.4 Results and discussion.....	111
6.4.1 Amine functionalization of silica particles for RNA loading.....	111
6.4.2 Loading of dsRNA to silica particles and its mobility.....	113
6.5 Conclusion.....	120
<b>Chapter 7: Conclusion and Future Directions.....</b>	<b>122</b>
7.1 Conclusion.....	122
7.2 Future directions.....	124
<b>Appendix A: Characterization of Orthogonally Oriented Silica Thin Film with 2-D HCP Structure Supported by AAO support.....</b>	<b>129</b>
<b>Appendix B: MATLAB Code for the Model Describing the Transport Process in Biocatalysis and Selective Separation Integrated Membrane.....</b>	<b>130</b>
<b>References.....</b>	<b>132</b>
<b>VITA.....</b>	<b>150</b>

## LIST OF TABLES

<b>Table 4.1</b> Resistance and active electrode areas of silica thin films with varying structures and lipid supported by o-HCP silica estimated by an equivalent circuit model R (RCW) for EIS measurements with hydrophilic probe FDM. (Error based on three samples). ....	69
<b>Table 5.1</b> Glucose and fructose concentrations in the donor and receptor sides of the static diffusion cell separated by the GI immobilized separation membrane at 6 hrs. (The initial glucose concentration was on the donor side is 2g/L or 11.1mM.) .....	91
<b>Table 6.1</b> Brunauer–Emmett–Teller (BET) specific surface area, amount of amine grafted and % of monolayer silica surface coverage by amine group for amine functionalized micron-sized nonporous and porous particles.....	112

## LIST OF FIGURES

<b>Figure 2.1</b> Chemistry of Sol-gel process and template synthesis procedure. ....	7
<b>Figure 2.2</b> Schematic of dip coating process shown from the cross sectional view of the (a) AAO membrane; (b) AAO membrane modified with cross-linked polymer acting as a neutral surface; (c) silica thin film cast on neutral surface to achieve vertical pore alignment; (d) silica thin film membrane following calcination to achieve accessible pores. ....	9
<b>Figure 2.3</b> Structure of biological membrane. ....	10
<b>Figure 2.4</b> Reversible interaction between boronic acid and diols. ....	11
<b>Figure 2.5</b> Preparation of supported lipid bilayers: (a) Langmuir-Blodgett (LB) deposition; (b) Vesicle fusion. ....	13
<b>Figure 2.6</b> Types of model lipid bilayers: (a) Black lipid membrane; (b) polymer cushioned lipid bilayer; (c) tethered bilayer lipid membrane. ....	14
<b>Figure 2.7</b> (a) Preparation of pore-confined lipid; (b) Diffusivity of pore-confined lipid in mesoporous silica particles as a function of pore size and position.....	16
<b>Figure 2.8</b> Impedance spectrum (Nyquist plot) in the complex plane (each point on the spectrum represents the impedance vector at one frequency). ....	18
<b>Figure 2.9</b> Interface of electrode with redox probes and corresponding circuit model. .	19
<b>Figure 2.10</b> Diffusion cell for characterizing membrane transport properties. ....	24
<b>Figure 3.1</b> Glucose transport through lipid pore-filled silica thin film supported by macroporous support (anodic aluminum oxide) using boronic acid carrier. ....	27
<b>Figure 3.2</b> Plane-view SEM images of (a) AAO support and (b) silica thin film coated AAO.....	38
<b>Figure 3.3</b> Confocal microscopy image of (a) lipid enveloped silica particle; (b) lipid filled silica particles; (c) lipid-BA enveloped silica particle; (d) lipid-BA filled silica particles; (e) scheme of competitive complexation between Alizarin Red S (ARS) and glucose to boronic acid. Lipid is tagged with green fluorescent DiO and boronic acid (BA) is complexed with ARS to give red fluorescence. All confocal images showed the cross-section of the core of the particle (pore diameter: 11.8 nm). ....	40

<b>Figure 3.4</b> Glucose flux through different membrane (5.6 mM initial glucose solutions in donor side of diffusion cell). The error bars are based on the sampling times at 1 h, 1.5 h, 3 h of diffusion). .....	42
<b>Figure 3.5</b> ATR-FTIR spectra of bare AAO, silica, lipid filled AAO and lipid filled silica membrane.....	44
<b>Figure 3.6</b> Gel to fluid phase behavior of lipid filled silica particle (dash line) and boronic acid immobilized lipid filled silica particle (solid line) as measured by DSC (59 mol% boronic acid, pore diameter: 11.8 nm).....	47
<b>Figure 3.7</b> Glucose flux through lipid filled membrane with or without boronic acid carriers as a function of temperature (room temperature versus 45°C) and pH (pH 7.4 versus a pH 10 (donor)/pH 5 (receptor) gradient), (5.6 mM initial glucose solutions, 59 mol% BA and error based the sampling at 2 h, 3 h, 4 h of diffusion ). .....	50
<b>Figure 3.8</b> Relative glucose flux through boronic acid immobilized lipid filled membrane during multiple temperature-switch cycles (At each cycle, the same membrane started with 5.6 mM initial glucose solutions and sampling at 2 h of diffusion. Flux reported was normalized to flux measured on cycle 2).....	51
<b>Figure 3.9</b> Relative reduced fluorescent intensity after adding glucose to ARS-BA complex (fluorescent) to competitively form ARS-glucose (no fluorescent) as a function of pH. (Fluorescence intensity change was normalized to the original intensity at experimental pH. Error based on three replicates).....	53
<b>Figure 3.10</b> Selective separation of carbohydrate mixture (5.6mM glucose, 5.6mM xylose, 5.6mM cellobiose) through boronic acid immobilized lipid filled membrane at as a function of temperature (room temperature versus 45oC) and pH (pH 7.4 versus a pH 10 (donor)/pH 5 (receptor) gradient. (Sampling time: 2 h, S=Selectivity).....	55
<b>Figure 4.1</b> (a) Electrochemical cell setup for EIS measurement; (b) Impedance spectrum and corresponding equivalent circuit model for silica thin film. ....	65
<b>Figure 4.2</b> 2D GISAXS patterns of (a) parallel oriented; (d) orthogonal oriented mesoporous silica thin film after calcination. ....	66
<b>Figure 4.3</b> Nyquist plots of silica thin films with different pore structures and lipid enveloped o-HCP silica on FTO electrodes measured using the hydrophilic redox probe	

(FDM). The insert presents the Nyquist plots for the nonporous silica and lipid filled o-HCP silica on FTO.....	68
<b>Figure 4.4</b> Phase angle (black) and absolute impedance (Z, red) profile with experimental frequency for bare, lipid enveloped, lipid filled o-HCP silica on FTO electrode. The probe for this measurement was FDM.....	71
<b>Figure 4.5</b> Impedance spectra of FTO electrode, bare, lipid enveloped and lipid filled o-HCP silica using hydrophobic redox probes (DBD).....	75
<b>Figure 5.1</b> Scheme for recovery and upgrading of the fructose from glucose using an enzyme-immobilized biomimetic integrated membrane. ....	80
<b>Figure 5.2</b> SEM images of (a) AAO support; (b) silica thin film coated AAO; (c) glucose isomerase immobilized membrane. ....	86
<b>Figure 5.3</b> FTIR spectra of silica, epoxy modified silica, GI immobilized silica through covalent coupling with epoxy or physical adsorption.....	87
<b>Figure 5.4</b> Fructose permeability through the bare, epoxy modified, and GI epoxy-modified silica membrane at 50°C.....	88
<b>Figure 5.5</b> Fructose concentration in the static diffusion cell as a function of time through the GI immobilized membranes for the silica composite membrane (GI-silica), the lipid-filled silica composite membrane, (lipid-GI-silica) and the lipid-filled silica composite membrane with immobilized boronic acid as a sugar carrier (Lipid-BA-GI-silica). The initial glucose concentration was on the donor side is 2g/L or 11.1mM. ....	90
<b>Figure 5.6</b> Concentration profile through the reaction-diffusion membrane (v: flow rate; C: concentration; N: species flux; A: substrate; B: product; d: donor phase; r: receiving phase; i: interface between enzyme layer and the membrane). ....	93
<b>Figure 5.7</b> Model prediction and experimental measurement of glucose (a) and fructose (b) concentration in the static diffusion cell as a function of time through the lipid-filled silica composite membrane with immobilized boronic acid as a sugar carrier (Lipid-BA-GI-silica). The initial glucose concentration was on the donor side is 2000 mg/L. ....	97
<b>Figure 5.8</b> (a) Model prediction of selectivity (fructose over glucose) on the receptor phase as a function of the value of Thiele modulus. (b) Fructose profiles in the enzyme layer when the value of Thiele modulus is $2.5 \times 10^{-5}$ .....	99

<b>Figure 5.9</b> Model predication of selectivity (fructose over glucose) on the receptor phase as a function of relative permeability under given Thiele modulus.....	100
<b>Figure 6.1</b> Scheme of dsRNA loading into amine group functionalized micron-sized porous silica nanoparticles (pSNPs) .....	106
<b>Figure 6.2</b> Confocal images through the middle section of silica particles as a function of fragment length and pore size. ....	114
<b>Figure 6.3</b> 84 bp and 282 bp dsRNA diffusivity as a function of pore size and dsRNA location (cap and core) at a loading concentration of 0.25 mg dsRNA /mg particles. The role of RNA concentration on mobility is important designing dsRNA loading strategy. ....	117
<b>Figure 6.4</b> Loading (confocal images) and corresponding diffusivity of 84 bp dsRNA in pSNPs of 11.8 nm pores with varying loading concentration. ....	118
<b>Figure 6.5</b> Fluorescence recovery after incubating pSNPs (11.8 nm pore) saturated with unlabeled dsRNA (84 bp) in labelled dsRNA solution for <b>(a)</b> 10min; <b>(b)</b> 40mins. ....	120
<b>Figure 7.1</b> Glucose upgrading process on composite silica thin film membranes.....	128
<b>Figure A.1</b> TEM image of oriented silica film after dissolving the AAO support in 5 M HCl.....	129
<b>Figure A.2</b> Ethanol flux as a function of pressure drop. ....	129

## **Chapter 1: Introduction**

The recovery of dilute aqueous solutes from biological processing such as organic solvents, amino acid, proteins from fermentation processes is critical to the development of biotechnology applications. In the case of relative low value added products, the limited options for product recovery and upgrading may act as bottlenecks for commercialization. Dilute aqueous separation processes are usually costly and energy-intensive due to the low concentration feeds.[1-3] For example, improved separation of carbohydrates from biomass hydrolysate mixtures resulting from the enzymatic deconstruction of lignocellulose would address significant challenges to the biochemical and catalytic production of biofuels and chemicals. Sugars with six or five carbon can be directly converted into biofuel through bacterial fermentation,[4] which typically has an optimal sugar concentration of at least 100 g/L. [5, 6] But the sugar concentration produced from enzymatic hydrolysis (1~20 g/L) [7, 8] results inefficient fermentation. Alternatively, sugars can be catalytically dehydrated into platform chemicals for further processing into a variety of value-added chemicals.[9] In industry, chromatography is the most used method for sugar separation and concentration, which is an expensive process and has low production efficiency.[3, 10]

In order to address the low efficiency of dilute aqueous solute separation, a robust lipid pore-filled silica thin film membrane combined with a specific binding carrier is proposed to achieve low energy usage, high permeability and high selectivity separation. **Chapter 2** summarizes the design and configuration of a biomimetic carrier-mediated separation membrane. The synthesis mechanism of orthogonally oriented ordered mesoporous thin film membrane with 2-D hexagonal close packed (HCP) structure, which acts separation



platform for the proposed biomimetic membrane, is discussed. The preparation of different types of synthetic lipid membrane (black lipid bilayer, polymer cushioned lipid bilayer, tethered bilayer lipid membrane and pore-confined lipid membrane) to mimic the structure of biological membrane is also compared. Finally, the principle and application of the surface analysis techniques (electrochemical impedance spectroscopy (EIS), grazing incidence small angle X-ray scattering (GISAXS), confocal laser scanning microscopy (CLSM) and a diffusion cell for characterizing the biomimetic membrane is presented.

In **Chapter 3**, solute rejection of lipid assemblies (1, 2-dipalmitoyl-sn-glycero-3-phosphocholine (DPPC)) confined in mesopores silica thin film is demonstrated and compared to lipid bilayers suspended over pores. Sugar separation through the biomimetic membrane using a lipophilic boronic acid (4-(N-Boc-aminomethyl) phenylboronic acid) as carbohydrate transporter is examined for proof of concept and also provides insights for sugar purification from processed biomass mixture. In addition, the glucose permeability through this biomimetic boronic carrier-mediated membrane is investigated under environmental factors of pH gradient (related to carrier-solute association) and temperature (related to the lipid bilayer diffusivity) to optimize the performance of the separation membrane. The membrane selectivity for three major sugars (glucose, xylose, and cellobiose) is also compared.

An understanding of transport process through pore-confined lipid is essential for optimizing the proposed biomimetic membrane separation. Thus, **Chapter 4** examines ion transport through the lipid filled mesoporous silica thin films using electrochemical impedance spectroscopy (EIS). The capability of EIS to quantify mass transport and accessibility of mesoporous silica thin film is compared for different mesoporous thin films

with known structure. The EIS is then extended to quantify the ion transport through supported lipid bilayers using different preparation methods (in the form of lipid filling and lipid enveloping). The hydrophilic redox probe and hydrophobic redox probe are used to quantify the lipid bilayer resistance to hydrophilic molecules or ion and diffusion of hydrophobic carriers in the lipid membrane respectively. This study is expect to quantify the configuration and ion transport through the mesoporous silica thin film supported lipid membrane, which provide insights for making better barriers on mesoporous support as carrier-mediated membrane separation platform for biomimetic membrane. Besides, the silica thin film supports provide various covalent coupling strategies for immobilizing the biocatalyst to integrate the reaction and separation in one single membrane process. **Chapter 5** then focuses on the feasibility of combining an enzymatic membrane reactor with integrated biomimetic separation for one-step upgrading and separation of dilute aqueous solutes using mesoporous silica thin film. The model system is the enzymatic catalysis of glucose to fructose using glucose isomerase, which is covalently bound to epoxy group modified thin film silica. The upgrading and separation efficiency of the enzyme immobilized selective separation membrane is then quantified using a static diffusion cell. The chemical reaction and selective mass transfer through the composite membrane is further described by a mathematical model for identifying the dominant factors in membrane performance.

In **Chapter 6**, the concept of pore confinement of biomolecules in mesoporous silica materials is further extended to encapsulate the double-stranded (ds) RNA in porous silica nanoparticles for dsRNA delivery to cells to achieve RNA interference. This chapter examines the mobility of pore-confined dsRNA as function of pore size, length of dsRNA

and loading concentration ratio of dsRNA to the silica particles measured by FRAP (fluorescence recovery after photobleaching) using confocal laser scanning microscopy (CLSM). These factors affect the loading capacity of dsRNA into particles and release of dsRNA to act on the targeted sites after the delivery by the nanoparticle, which determines the effectiveness of RNA interference.

## Chapter 2: Background

### 2.1 Ordered mesoporous silica materials

Ordered mesoporous silica with tunable pore size, which offers a great potential for controlling the material structure and texture, has been studied widely due to its mechanical strength and stability at severe conditions such as high temperature, acid environment. [11, 12] Also its high specific surface area and the ability to functionalize the internal pore surface and external surface with other organic group (amines, aldehydes, hydrophilic, hydrophobic etc.) [13] make it a promising platform for catalysis, biomolecule carrier, drug delivery vehicle, and a selective absorbent.[14, 15] Mesoporous silica materials can also be synthesized in the form of particles or films. Since the discovery of template synthesis, ordered mesoporous silica thin films have found applications as separation membranes, optical sensors, semiconductors, nanostructure (wire, rod etc.) templates and photonic devices. [16, 17]

#### 2.1.1 Surfactant templating for synthesis of ordered mesoporous silica materials

Mesoporous (2 - 50 nm) silica materials are typically synthesized by a sol-gel process, which is low cost and easy to operate. This process involves the hydrolysis and polycondensation of alkoxide precursors under acidic or basic condition (**Figure 2.1**).[18] As the silica precursor, such as tetraethoxysilane (TEOS), is mixed with water (sol), the alkoxide group is hydrolyzed to yield  $\equiv Si - OH$ , which then condenses to form  $n \equiv Si - O - Si \equiv$ . As the condensation reaction proceeds and  $\equiv Si - O - Si \equiv$  bonds form, a three-dimensional  $SiO_2$  network (gel) develops. The  $H_2O$  and alcohol formed during hydrolysis and condensation remain in the network and are removed by drying, which

results in pore structure in the materials. The material can be prepared as monoliths, films or particles through the sol-gel process and the pore structures are disordered. The discovery of surfactant templating in 1992 [19, 20] revolutionized sol-gel synthesis.

During the surfactant templating synthesis, the precursors of final materials condense around surfactant micelles, which is called a templating or structure directing agent (SDA).[21] As the stable structure is formed after hydrothermal treatment, the surfactant template is then removed by calcination, solvent extraction or light irradiation. [22-24] The pore structure is then formed, which has the same shape and size as the assembly of surfactant templates (**Figure 2.1**). Thus, various pore morphologies (pore size and pore structure) can be obtained using different surfactant mesophases by varying the volume ratio between the surfactant and inorganic precursor solutions. For example, different arrangements of cylindrically shaped micelles can result in cubic bicontinuous and two-dimensional hexagonally close packed (2-D HCP) pore structures. [25, 26] Cubic discontinuous and 3-dimensional hexagonal structure are formed as spherical micelles are arranged in lattices at corresponding patterns.[27]

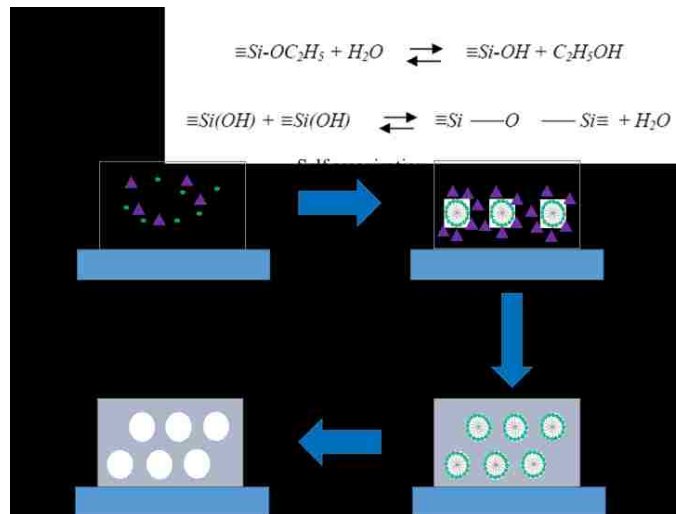


**Figure 2.1** Chemistry of Sol-gel process and template synthesis procedure.

### **2.1.2 Synthesis of silica thin films with orthogonally oriented 2-D hexagonally close packed (HCP) pore structure on porous support**

The application of mesoporous silica materials is matched to its structure. Cubic bicontinuous structures, while offers easy accessibility, limits diffusion as the interconnected pathways increase tortuosity, which makes it more appropriate as absorbents or for molecule storage.[28] For membrane applications, orthogonally oriented 2-D HCP pore array in thin film templated by cylindrical micelles is desirable due to its continuous channels which do not offer alternate pathway for the diffusion.[16] However, cylindrical surfactant micelles naturally tend to align with the substrate.[29] The parallel orientation makes the pores inaccessible, which against the requirement of separation and catalysis application.[30] There are some successful strategies to achieve orthogonally oriented HCP pore array on a substrate. Electro-assisted self-assembly (EASA), which utilizes the electric field to control the orientation of the cationic surfactant template, is reported to be capable of preparing silica thin films with vertical oriented pores around 3

nm in diameter and a uniform film thickness around 50-200 nm.[11, 31] However, this method can only be applied to conductive supports (carbon, platinum, gold, indium-tin oxide). Also, further characterization revealed that only thin films were well-structured and oriented.[11]

In our group, we reported a simple and versatile method to synthesize silica or titania thin films with ordered 2-D HCP structure orthogonal on supports, which is applicable to various substrates (porous, nonporous, conductive or insulated etc.).[16] By creating a chemically neutral (equally attractive to the head and tail of the surfactant template) supporting surface, which removes the affinity of the micelles to surface, parallel orientation of the micelles (and the resulting pores) is reduced.[32] In this approach, silica precursor (TEOS) and poly (ethylene oxide)-poly (propylene oxide)-poly (ethylene oxide) (PEO-PPO-PEO) triblock surfactant (P123) is dip-coated on a glass slide which is modified by cross linking P123 or other random copolymer (PEO-PPO-R) to make the vertical pore structure, as evident by XRD. To synthesize thin films greater than 100 nm, sandwiching the silica thin films between similarly modified glass slides is demonstrated to arrange pores vertical to the support.[32] The preparation of this vertically oriented mesoporous silica thin films is successfully extended to a macroporous support (anodic aluminum oxide, AAO), in which the composite silica thin film has an accessible pore structure.[33] In this case, the copolymer layer coated on AAO surface not only serves as a chemically neutral surface but also helps to prevent the penetration of the silica into the pores of AAO support during the dip coating process (**Figure 2.2**). This high surface area thin film silica membrane with accessible pores is proved to be a potential platform for nanofiltration and separation applications.

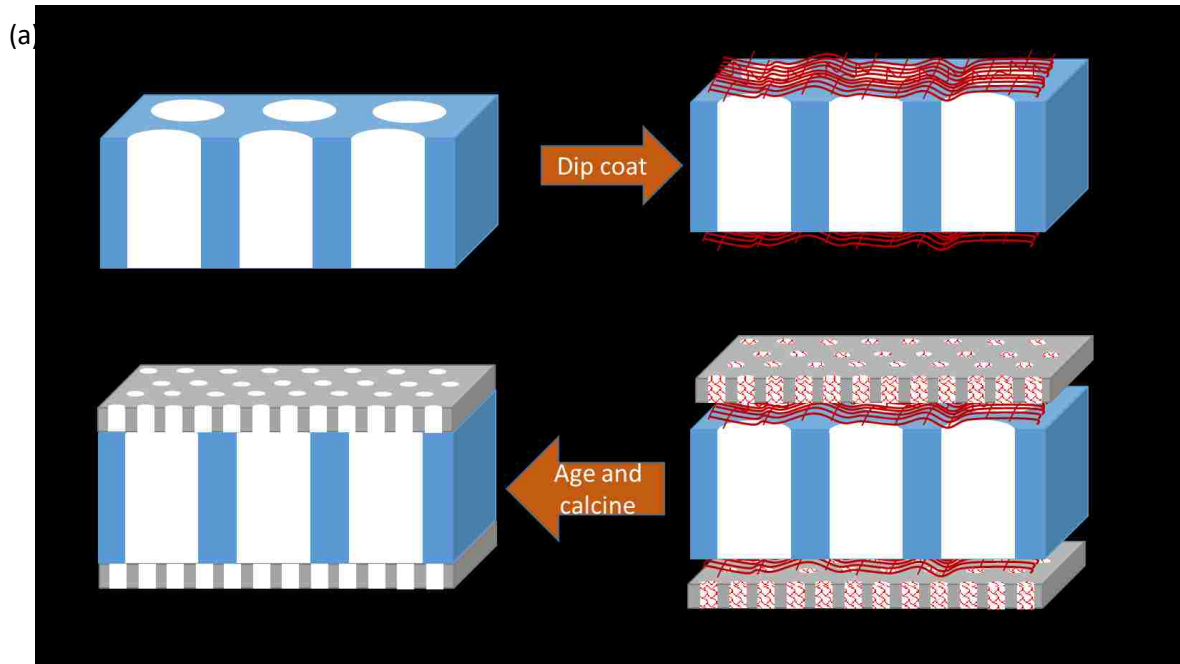


**Figure 2.2** Schematic of dip coating process shown from the cross sectional view of the (a) AAO membrane; (b) AAO membrane modified with cross-linked polymer acting as a neutral surface; (c) silica thin film cast on neutral surface to achieve vertical pore alignment; (d) silica thin film membrane following calcination to achieve accessible pores. Adapted from Wooten et al.[33]

## 2.2 Biomimetic carrier-mediated membrane for dilute aqueous solute separation

### 2.2.1 Structure of biological membrane

The semi-permeable biological cell membrane, which separates the external environment and components in the cells, selectively controls the transport of molecules and ions into and out of the cell, and the exchange of information between the environment and the cell, which is important for maintaining the life of living organisms.[34] The main component of biological membranes is lipid molecules, containing two hydrocarbon tails which link to a hydrophilic head group, which tend to form bilayer structure (**Figure 2.3**). Based on head group components, biological membrane lipids mainly can be divided into



three classification: phospholipids, glycolipids and sterols.[35] The lipid bilayer membrane is the key structure for maintaining the selective permeability of biological membrane. Its hydrophobic region prevents the direct passage of hydrophilic molecules and ions across the membrane. Meanwhile, the channel proteins or carrier proteins specific for given molecules are embedded in the cell membrane and facilitate the diffusion of desired molecules (carbohydrates, nucleotide, catecholamine and amino acid) and ions ( $\text{Cl}^-$ ,  $\text{K}^+$ ,  $\text{Na}^+$ ) across the membrane.[36]

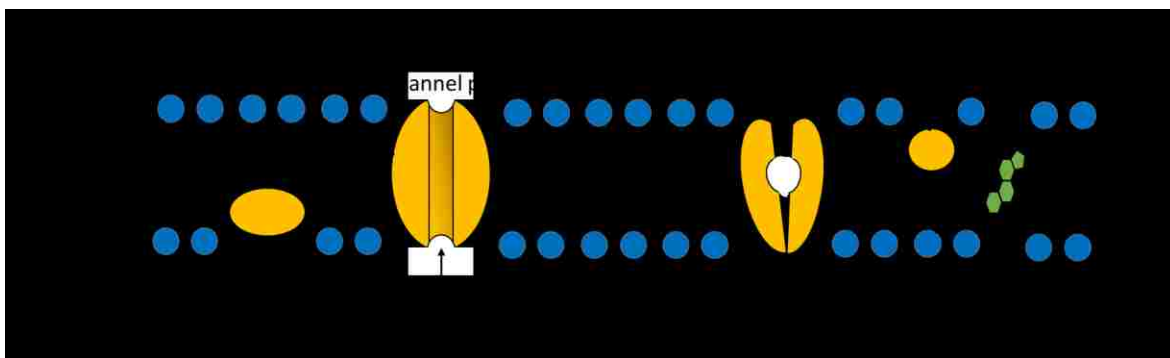


**Figure 2.3** Structure of biological membrane. Adapted from Freeman et al.[34]

### 2.2.2 Biomimetic carrier-mediated membranes

Thus, the biological membrane is a natural model of carrier mediated separation membrane, which can overcome the tradeoff between the high permeability and selectivity as the carrier/transporter only specifically interact with the target molecules.[36, 37] Based the configuration of biological membrane, biomimetic carrier-mediated membranes that allow for continuous, low-energy, high selectivity and high efficiency separation for dilute aqueous solutes can be designed. Firstly, a defect-free barrier is required to exclude the aqueous solutes to ensure selectivity. Synthetic lipid membranes, which mimic the structure of biological membranes, are promising to act as effective barriers and be compatible with carrier proteins or other hydrophobic transporters. Secondly, a carrier that

can reversibly and specifically react with the targeted molecules is required to mimic the function of embedded proteins. The native proteins or peptides in biological membrane can be ideal carriers. These include, for example, water-selective aquaporin protein,[38] amino acid-selective chloroplast outer envelope protein,[39] monovalent cation-selective gramicidin peptide,[40] and  $K^+$  ions-selective valinomycin.[41]

Specifically, for proof of concept, a biomimetic carrier-mediated membrane for carbohydrate separation is investigated in **Chapter 3** using boronic acid, which is commercially available and easier to obtain relative to proteins. The affinity of saccharides for boronic acids have been largely applied in detection and separation of sugar.[42, 43] The boronate ligands can reversibly interact with the 1, 2-diols or 1, 3-diols of saccharides to form cyclic esters with five or six member rings (**Figure 2.4**).[42, 43] The kinetics and thermodynamics of formation and dissociation of boronic acid-sugar complexes involve proton – hydroxide ion equilibria.[44] Because the boronic acid needs to be transformed to a tetrahedral anionic form before it can bind to diol, the pH becomes an important factor affecting the formation and dissociation of sugar-boronic acid complex .[43] The pH effect on the separation efficiency of biomimetic membrane using boronic acid as sugar carrier will also be examined in **Chapter 3**.

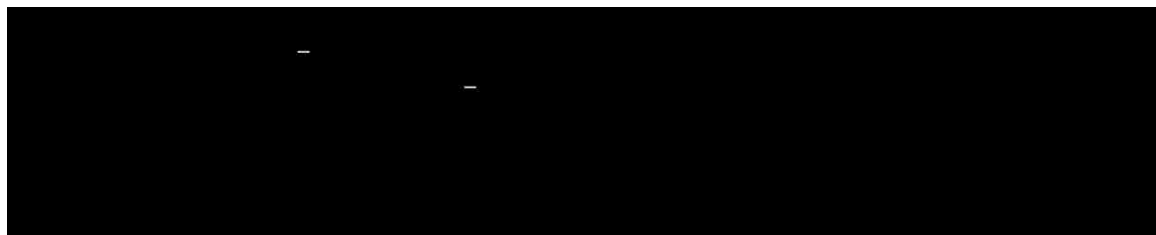


**Figure 2.4** Reversible interaction between boronic acid and diols. Adapted from Cheema et al. [45]

## 2.3 Supported lipid bilayers

To construct biomimetic membranes, lipid bilayers are usually assembled onto solid supports to mimic biological membranes (supported lipid bilayers, SLBs), which increases the bilayer stability. [46] On a solid support, the fluidity of lipids is preserved because the bilayers and solid supports are separated by a thin water layer (1-2 nm), which allows mobility of the lipids. [47] Confining the lipid bilayers to a flat surface allows the use of surface characterization techniques (electrochemical impedance spectroscopy, secondary ion mass spectrometry, fluorescence microscopy, atomic force microscopy, etc.) to study the property of lipid membranes, which is much more difficult to achieve with free-floating lipid vesicles. [47, 48] Due to its stability and mechanical robustness, SLBs are often used to investigate the function of transmembrane proteins or smaller lipophilic biomolecules.

### 2.3.1 Types of supported lipid bilayers

Generally, lipid layers are assembled onto supports using Langmuir-Blodgett (LB) deposition or vesicle fusion.[49] In the LB method, a single layer of lipids is formed by pulling the solid support out of a Langmuir trough which has a lipid monolayer spread at the air-water interface. The lipid monolayer interacts with the solid support through the polar head group and exposes the hydrophobic tails to the environment. A lipid bilayer is finally formed by immersing the support in the lipid monolayer interface again (**Figure 2.5a**). Compared to the LB technique, vesicle fusion is more popular and simpler. [50] To prepare SLBs, a suspension of small unilamellar vesicles (SUV, 50-200nm) is obtained from multilamellar vesicles (MLV, 0.1-10 $\mu$ m) by sonication or extrusion and added to the hydrophilic support. Then the vesicles adsorb to the surface, followed by deformation, flattening and rupture. Edges of lipid bilayer patches formed by individual vesicles fuse

through hydrophobic interactions and gives rise to a continuous lipid bilayer (**Figure 2.5b**). [35, 47, 48]. The surface chemistry, surface structure, temperature, vesicle size, and ion strength in solution have been shown to affect the vesicle fusion on surface. [51-53]

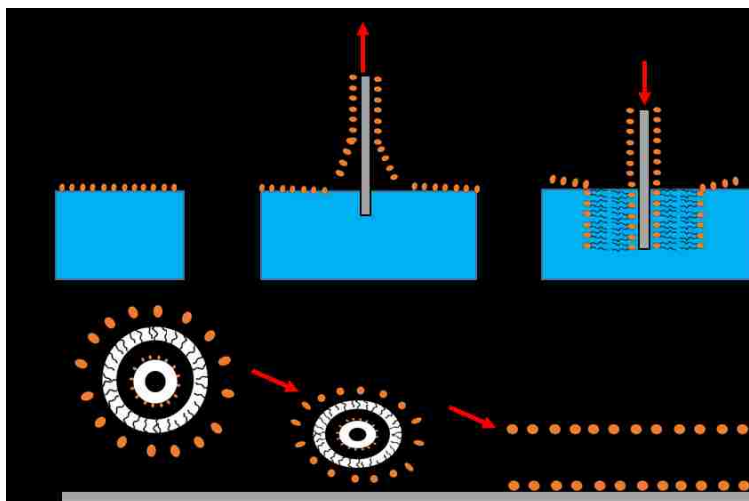


**Figure 2.5** Preparation of supported lipid bilayers: (a) Langmuir-Blodgett (LB) deposition; (b) Vesicle fusion. Adapted from Mingeot-Leclercq.[48]

However, solid supports for SLBs usually have direct contact with the incorporated proteins whose hydrophilic domains are protruding outside the bilayer, thus affecting their functionality and even causing denaturation.[54] Many effort have been taken to make defect-free supported lipid membranes with high stability while maintaining the activity of the incorporated proteins. Black lipid membrane (BLM, **Figure 2.6 a**) is a well-established model system, where the lipid is spanning the micrometer-sized apertures of Teflon film or polymer cup.[55] The configuration creates free spaces on both sides of the BLMs to accommodate the hydrophilic domains of the proteins.[56] However, the BLMs usually have short life time, which limit their application. To create aqueous environment under the SLBs while maintaining long term stability, polymer cushioned lipid bilayer (**Figure 2.6b**) has been utilized to avoid the protein-substrate interaction by raising bilayers above

the substrate using hydrophilic polymer spacers [57] However, the strong affinity between polymer cushion and lipid bilayer need to be careful maintained, which usually minimizes the lateral diffusivity of the lipid membrane.[58] Alternatively, tethered bilayer lipid membrane (tBLM, **Figure 2.6c**) is more extensively used to provide long-term stability and high electrical resistance to investigate ion transport through the ion channel or peptides.[59] tBLMs are chemically anchored to substrate using an anchoring group which has a hydrophilic spacer attached to the substrate and a lipid-like part, which mixes with the lower leaflet of the lipid bilayer. [60] One of the shortcoming of tBLMs is that its mobility is much smaller than the free standing SLBs, as the lower leaflet of the tBLMs is constrained by the immobile anchoring spacer, which limits the full function of the incorporated proteins.[61]

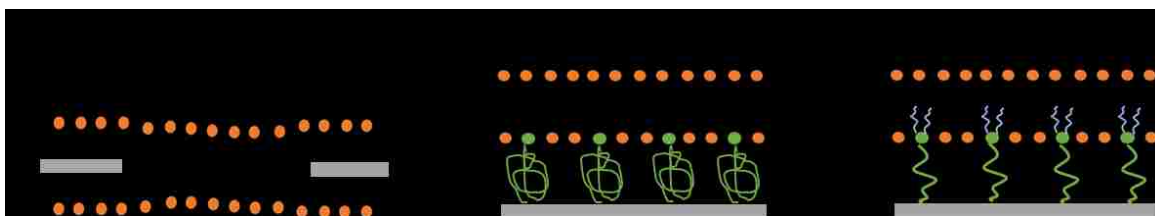


**Figure 2.6** Types of model lipid bilayers: (a) Black lipid membrane; (b) polymer cushioned lipid bilayer; (c) tethered bilayer lipid membrane. Adapted from Koper. [62]

### 2.3.2 Pore-confined lipids

Our group identified a model lipid system, pore-confined lipid assemblies supported by mesoporous silica, which is promising to offer long-term stability and high insulating resistance for functional incorporation of carriers for separation application. Unlike most model lipid membranes, which contains a single lipid bilayer, the amount of lipid confined in the pores is dependent on the dimension of the support. The confinement of the lipid

inside the pores is achieved using evaporation deposition (**Figure 2.7a**). [63] By dissolving lipid molecules in organic solvent to avoid the formation of vesicles, which are far larger than available pore size, the lipid molecules can be infiltrated into the pores. After removing organic solvent and rehydration, lipid assemblies are then formed inside the pores.

Schlipf et al.[64] characterized the location and mobility of pore-confined DPPC lipid in mesoporous silica particles using CLSM. It was found that pore size of mesoporous support affect the pore confinement of lipid. For pore diameter of 3.0 nm, the lipid bilayer only forms on the surface of silica particles (**Figure 2.7b**), while the lipid can be confined into the pores of 5.4 nm and 9.1 nm. This is greater than the dimension of DPPC bilayer, which has a thickness around 4 nm. Furthermore, the lipid diffusivity inside the silica particles is also pore size dependent (**Figure 2.7b**). The diffusivity of lipid at the core and middle core were found to be consistent with the surface suspending lipids, indicating the pore-confinement doesn't alter the lipid mobility, which is a big advantage compared to other supported lipid bilayers. Furthermore, the ease of surface functionalization of silica enables the tethered of lipids into the pores which is also demonstrated by Schlipf et al.[64] The mobile network of pore confined lipid has great potential for carrier immobilization to achieve separation. The extension of this pore-confined lipid in mesoporous silica to silica thin films to construct carrier-mediated biomimetic membrane will be described in **Chapter 3**.

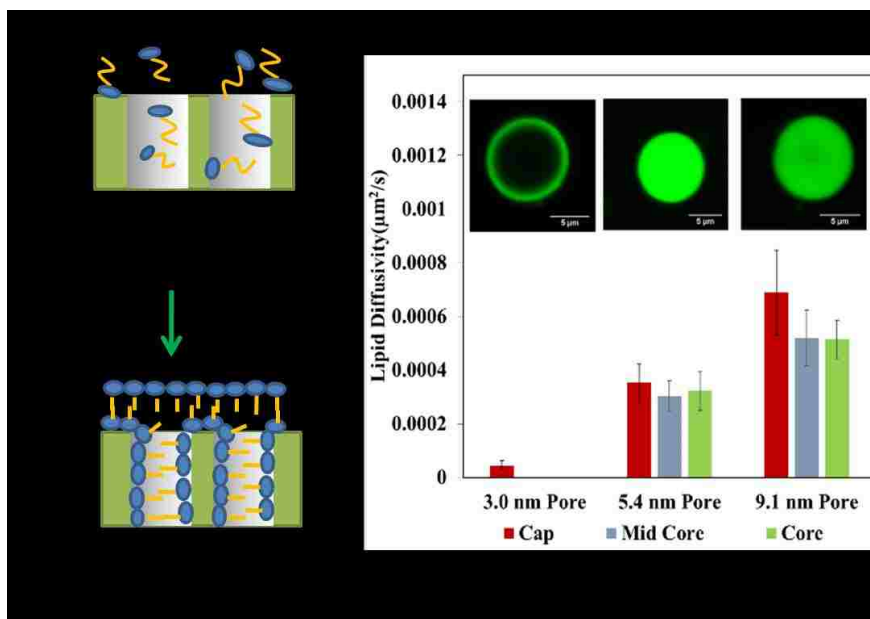


**Figure 2.7** (a) Preparation of pore-confined lipid; (b) Diffusivity of pore-confined lipid in mesoporous silica particles as a function of pore size and position. Diffusivity data Adapted from Schlipf et al.[64]

## 2.4 Techniques for characterizing membrane properties

### 2.4.1 Electrochemical impedance spectroscopy

Electrochemical impedance spectroscopy (EIS) is used to characterize the transport processes in composite synthetic lipid membranes in **Chapter 4**. EIS measures the systems impedance change when excited by a small alternating current (AC) potential along with a direct current (DC) potential, which reflects the multiple processes happening on the electrode surface. [65] The ability of EIS to distinguish electron transfer, chemical reaction and mass transport processes finds applications in studying transport through multilayer composite membranes with different structure,[66] including biomimetic membranes in this work. Wei and Hillhouse [67] first applied EIS to examine the mass transport in ordered mesoporous silica thin films with various pore structure and orientation, surfactant

template and order of the film, and the thin film stability as a function of pH. They provide a method for quantifying the species diffusivity in the porous thin films, which is critical for screening and optimizing silica thin films for separation application. In addition, EIS has been widely used to investigate the structure of synthetic lipid membrane, which provides the basis for identifying superior lipid barriers with high stability and electrical insulation for examining the functionality of incorporated transmembrane proteins and small lipophilic carriers.[41, 59, 68-70] These works suggest the potential application of EIS to characterize ion transport through the proposed biomimetic membrane, which is demonstrated in **Chapter 4**.

#### 2.4.1.1 Principle of EIS

Impedance ( $Z$ ) defines the ability of a circuit element to resist the flow of electrical current.[71] The application of AC potential  $E = E_o \sin(\omega t)$ , which has a amplitude of  $E_o$  and radial frequency of  $\omega = 2\pi f$ , to the system results in an AC current  $I = I_o \sin(\omega t + \varphi)$  with an amplitude of  $I_o$  and phase shift of  $\varphi$  at the same frequency ( $f$ ). [72] The impedance of the system is then calculated using Ohm's law (**Eq. 2.1**). Thus, the impedance is a vector defined by the length of  $|Z| = \sqrt{(Z')^2 + (Z'')^2}$  and phase angle of  $\varphi$  at different frequency as shown in the impedance spectrum (**Figure 2.8**).

$$Z(\omega) = \frac{E}{I} = \frac{E_o \sin(\omega t)}{I_o \sin(\omega t + \varphi)} = |Z|(\cos\varphi + j\sin\varphi) = Z' + j Z'' \quad (2.1)$$

The impedance spectrum is further analyzed by equivalent circuit models, which are built based on the physical configuration of the membrane, to quantify the transport processes occurring near the electrode surface.[73] **Figure 2.9** illustrates a general electrode surface during EIS measurement and its corresponding circuit model. When the



electrode is electrified by the DC potential applied, an electrical double layer formed on the electrode surface, which is considered a capacitor  $C_d$ . [65] When the AC potential is applied, the reduction or oxidation of the redox probes is induced. The electron transfer between the electrode and the redox species associated with the electrochemical reaction needs to overcome the activation barrier,[74] which is defined as charge transfer resistance  $R_{ct}$ . This resistance is considered to occur in parallel with the double layer capacitor in the circuit model. The diffusion rate of redox species from the bulk solution to the electrode surface also affects the electron interface rate, and the process is quantified by a mass transfer impedance ( $W$ ) in series with the charge transfer resistance. The capacitor, charge transfer resistance and mass transfer resistance then completes a (RCW) element. The solution resistance  $R_s$ , accounting for the potential drop in the solution, is also included in series with the (RCW) element. [73, 74] For complex systems, multiple elements may need to be included to fully describe the process.

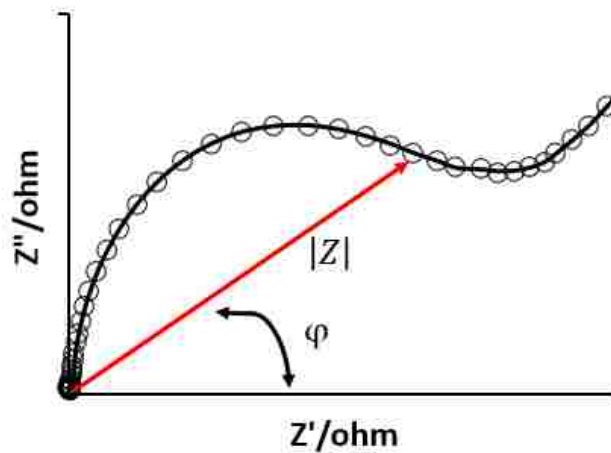


**Figure 2.8** Impedance spectrum (Nyquist plot) in the complex plane (each point on the spectrum represents the impedance vector at one frequency).

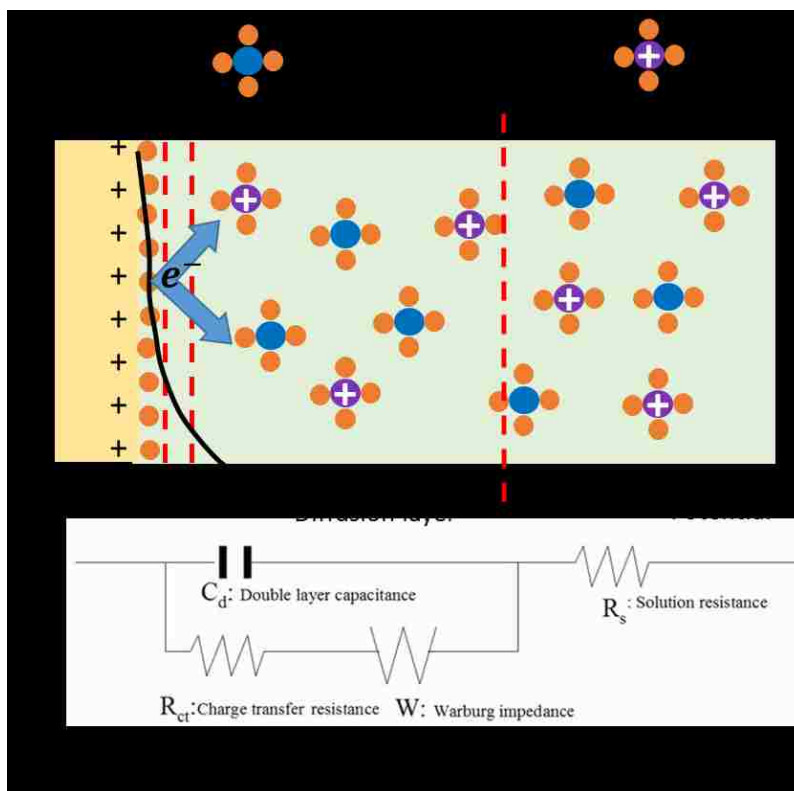


**Figure 2.9** Interface of electrode with redox probes and corresponding circuit model.

Adapted from Park and Park. [65]

## 2.4.2 Grazing-incidence small angle X-ray scattering

The pore orientation of the mesoporous silica thin films is further characterized by grazing-incidence small angle X-ray scattering (GISAXS) to support the EIS results in **Chapter 4**. In GISAXS, the X-ray incident to the sample at an angle smaller than critical angle for total external reflection of substrate. [75] In this case, the X-ray only penetrates a depth of a few nanometer from the top surface without penetrating into the substrate supporting the thin film, which eliminates noise and increases the surface sensitivity.[76] The total external reflection also ensures highly intense scattering signal. Furthermore, the use of an area detector allows the capture of the 2-D scattering in all directions, which

reflects the geometry of the film.[77] Thus, the GISAXS have been widely applied to characterize the nanoporous structure and orientation of block copolymers,[76] and metal oxides (silica and titania) nanoscale thin films.[75, 78, 79] Smarsly et al.[78] used GISAXS to confirm the orthogonal orientation of mesoporous thin film with 2D HCP structure template using Brij surfactant and the lattice parameter obtained was found to be consistent with TEM measurements. Furthermore, in-situ GISAXS can be used to investigate the formation of nanostructure in real time and identify the factors that affect the morphology and orientation of the mesoporous thin film. Nagpure et al.[80] applied GISAXS to monitor the growth of mesostructure of titania thin films during aging and found aging temperature, relative humidity and substrate chemistry has significant effect on the final orientation of pore, which guides the successful preparation of ordered titania thin film with orthogonally oriented 2D HCP using chemical neutral surface. Thus, the GISAXS is applied in **Chapter 4** to characterize the structure of different mesoporous silica, which provides supporting information for the EIS measurement.

### **2.4.3 Confocal laser scanning microscopy**

In order to visualize the incorporation of boronic carriers into the synthetic lipid membranes, confocal laser scanning microscopy (CLSM) is utilized in **Chapter 3**. CLSM is powerful tool for optical sectioning to examine thick sample structures at different depths with high resolution.[63] Unlike fluorescence microscopy, which captures the fluorescence emission from the whole fluorescent sample, CLSM uses point laser illumination to excite only one sample point at a time while the out of focus emission from rest of the sample is filtered by a pinhole placed at the focal plane before it gets to the detector.[81] This ensures high resolution as only the fluorescence emission from the targeted point is detected. The

laser point is then scanning across the whole sample surface at the depth of interest and the point-by-point light signals collected are integrated by computer to reconstruct the 2-D image. The depth of targeting surface can be controlled by moving the sample up and down. Thus, the 3-D reconstructions of the sample then can be achieved based on depth profile.[82] The high resolution depth profiling of CLSM enables us to examine the molecules distribution inside the sample. Most important of all, biomolecules diffusivity at different positions inside the sample can be characterized using fluorescence recovery after photobleaching (FRAP) in CLSM.

FRAP is a common technique for measuring the lateral mobility of fluorescently tagged molecules.[83] In CLMS, high intensity excitation light is illuminated on a small area of a surface containing a fluorescent probe, inducing photochemical destruction of the fluorescent molecules, which result in permanent loss of fluorescence.[84] The photobleached area is then monitored for fluorescence intensity recovery over a period of time as the unbleached fluorescent molecules transport laterally from the surrounding region and replace the bleached molecules. [83] For further analysis, fluorescence recovery kinetics which describe the lateral diffusion can be fit to give the diffusivity of the biomolecules. The mobility of dsRNA in the mesoporous silica cargos measured by FRAP, which is important for effective dsRNA delivery for RNA interference, is extensive discussed in **Chapter 6**.

The diffusion model was adapted from Kangs and A. Kenworth [85] with the assumptions of full fluorescence recovery to pre-bleach values and known half time fluorescence recovery: [63]

$$\frac{F(t) - F_o}{F_{inf} - F_o} = \exp\left(-\frac{2 \tau_D}{t}\right) \left[ \mathbf{I}_0\left(\frac{2 \tau_D}{t}\right) + \mathbf{I}_1\left(\frac{2 \tau_D}{t}\right) \right] \quad (2.2)$$

where  $F(t)$  is the measured fluorescence intensity as a function of time ( $t$ ),  $F_o$  is fluorescence intensity before bleaching ( $t = 0$ ),  $F_{inf}$  is the fully recovered fluorescence intensity ( $t = \infty$ ), and  $\mathbf{I}_0$  and  $\mathbf{I}_1$  are modified Bessel functions, and  $\tau_D$  is the characteristic diffusion time, which is correlated to the diffusivity,  $D$ , as described by **Eq. 2.3**, where  $r$  is the bleach spot radius.

$$D = \frac{r^2}{4 * \tau_D} \quad (2.3)$$

The diffusivity,  $D$ , and the fully recovered fluorescence intensity ( $F_{inf}$ ) were determined by fitting model to the time-dependent fluorescence recovery curve by nonlinear regression using the `lsqcurvefit` function in MATLAB.

#### 2.4.4 Transport in a diffusion cell

In **Chapter 3 and 5**, in order to examine the solute transport through the silica membrane in the presence of boronic acid immobilized lipid bilayer, a horizontal static diffusion cell is employed (**Figure 2.10**). This diffusion cell has two separate chambers, and the composite membrane is placed in between the chambers. The testing solution is placed on the donor chamber. Under constant stirring, the solute is then transported across the membrane and to the receptor chamber, which is initially loaded with blank solution. The solute concentration on either side of the membrane is tested as a function time to quantify the solute flux across the membrane. Furthermore, permeability ( $P$ ) of the membrane to the solute then can be defined from the concentrate profile of the solute in the two chambers.[28]

One-dimensional steady state diffusion is assumed across the membrane in the continuous stirring static diffusion cell, which has constant flux (J) across the membrane and can be expressed as (Eq. 2.4), [86] where L is the thickness of the membrane,  $C_D, C_R$  are solute concentration on the donor and receptor side at sampling time (t) and  $D_e$  is the solute diffusion coefficient.

$$J = -D_e \frac{dC}{dx} = \frac{D_e}{L} (C_D - C_R) = P * (C_D - C_R) \quad (2.4)$$

Based on mass balance, where the solute mass reduction rate in donor side is equals to the mass transfer rate across the membrane :

$$V_D * \frac{dC_D}{dt} = -A * J = -A * P * (C_D - C_R) \quad (2.5)$$

$$V_R * \frac{dC_R}{dt} = A * J = A * P * (C_D - C_R) \quad (2.6)$$

The above equations can be transformed as

$$\frac{d(C_D - C_R)}{dt} = -A * P * (C_D - C_R) \left[ \frac{1}{V_D} + \frac{1}{V_R} \right] \quad (2.7)$$

After the integration, the following equation can be yield for calculating the solute permeability (P) as function of time:

$$\ln \left( \frac{C_{D0} - C_{R0}}{C_D - C_R} \right) = P * t * A * \left[ \frac{1}{V_D} + \frac{1}{V_R} \right] \quad (2.8)$$

where  $C_{D0}, C_{R0}$  are solute concentration on the donor and receptor side at t=0; A is the membrane area exposed to the solution;  $V_D, V_R$  are the volume of donor and receptor chamber.

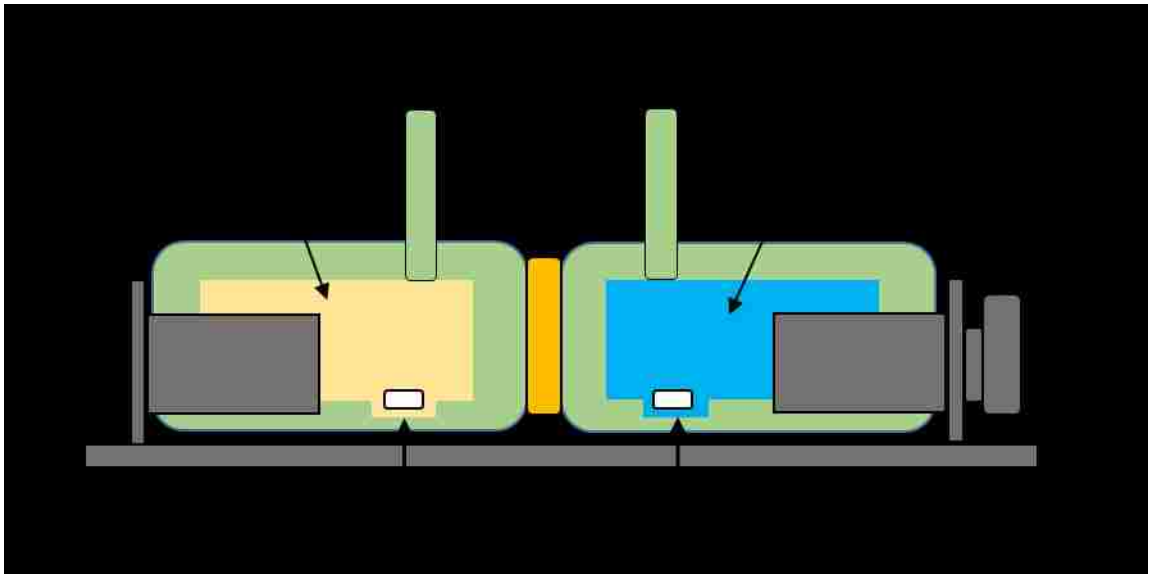


**Figure 2.10** Diffusion cell for characterizing membrane transport properties. Adapted from Wooten,[28]

## **Chapter 3: Lipid Pore-Filled Silica Thin Film Membranes for Biomimetic Recovery of Dilute Carbohydrates**

### **3.1 Abstract**

Selectively permeable biological membranes comprising lipophilic barriers inspire the design of biomimetic carrier-mediated membranes for aqueous solute separation. The recovery of glucose, which can reversibly bound by boronic acid carriers, is examined in lipid pore-filled silica thin film composite membranes with accessible mesopores. The successful incorporation of lipids (1, 2-dipalmitoyl-sn-glycero-3-phosphocholine (DPPC)) and boronic acid carriers in the pores of a mesoporous silica thin (~200 nm film thickness, 10 nm pores) through evaporation deposition is verified by confocal microscopy and differential scanning calorimetry (DSC). In the absence of the boronic acid carrier, lipids confined inside the pores of silica provide a factor of 14 increase in transport resistance to glucose relative to traditional supported lipid bilayers formed by vesicle fusion on the porous surface. The addition of a lipid-immobilized boronic acid carrier (4-(N-Boc-aminomethyl) phenylboronic acid (BA), 59 mol% in DPPC/BA mixture) facilitates the transport of glucose through the membrane (glucose flux increases from  $45 \times 10^{-8} \text{ mol/m}^2/\text{s}$  to  $225 \times 10^{-8} \text{ mol/m}^2/\text{s}$  in the presence of boronic acid). Furthermore, the transportation can be improved by environment factors like pH gradient (related to binding of glucose) and temperature (related to the lipid bilayer diffusivity). The successful development of biomimetic nanocomposite membranes can provide for the efficient dilute aqueous solute upgrading or separations, such as the processing of carbohydrates from hydrolase mixtures of lignocellulose, using engineered carrier/catalyst/support systems.



### 3.2 Introduction

The recovery of aqueous sugars is a model separation that highlights the need for the development of alternative affinity-based separations. The chemical affinity of sugars to some compounds such as zinc porphyrins, resorcinarenes, alkaline earth metals and boronic acid derivatives is attractive for selective separation of different sugars.[87] Among these sugar receptors, the boronic acid derivatives are of particular interest as the boronate ligand can reversibly interact with the 1, 2-diols or 1, 3-diols of saccharides to form cyclic esters with five or six member rings.[42, 43, 45] Furthermore, the association strength is largely depends on the type of sugars (catechol > fructose > glucose),[88] which makes this reversible reaction with specific complexation very attractive for sugar sensing[89] and selective separation. Consequently, boronic acids have been used to functionalize nanoparticles for sugar recovery.[42, 43] Besides adsorption, boronic acids are commonly used as carbohydrate carriers in ion exchange membranes[90] and liquid membranes[10, 91] to facilitate the separation of sugars. The selective transport of sugar through liposomes by boronic acid has also been demonstrated. [92]

The ability of biological membranes to facilitate the selective transport of ions or hydrophilic molecules using carriers inspired the design of carrier-mediated biomimetic membrane for highly separations in dilute aqueous solute systems in this work. High surface area mesoporous silica thin films with tunable pore structure are promising separation platforms for the construction of an artificial membrane supports. Composite silica thin films with ordered perpendicularly oriented hexagonally close packed (HCP) pore structure on a macroporous support have recently been synthesized by our laboratory and demonstrated as size-exclusion membranes.[33] The composite thin film membranes

are mechanically robust and the hydrophilic surface of the silica allows easy surface functionalization and formation of lipid bilayers. The perpendicular orientation of the 10 nm pores, formed by surfactant templating on a neutral surface, provides for efficient transport. Thus, incorporating the carrier immobilized lipid bilayers with the silica thin film brings opportunities for designing composite membrane for highly selective separation of molecules. Specifically, the recovery of aqueous glucose, which is transported through the lipid bilayer by complexing with boronic acid carriers on the donor side of the membrane and released on the receiving phase, has been chosen as model separation, representing the recovery of dilute carbohydrates from the depolymerization of biomass (**Figure 3.1**). The incorporation of carrier in the membrane allows for high permeability and high selectivity that can't be achieved simultaneously in conventional membrane process.[37, 87]

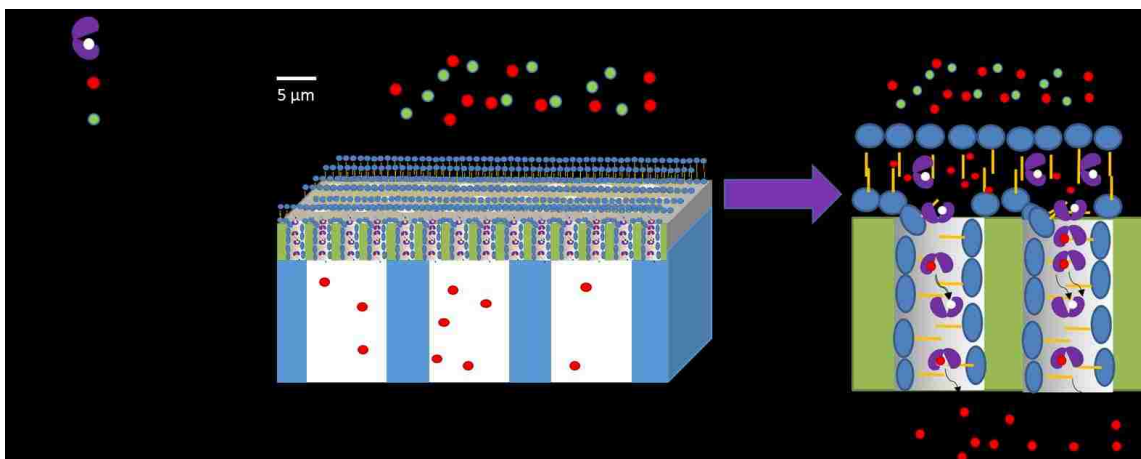


**Figure 3.1** Glucose transport through lipid pore-filled silica thin film supported by macroporous support (anodic aluminum oxide) using boronic acid carrier.

Preparing a defect-free membrane to provide high background transport resistance is important for effective carrier-mediated transport.[62] Generally, supported lipid layers (SLBs) can be prepared using Langmuir-Blodgett (LB) deposition or vesicle fusion.[49] In

the LB method, a single layer of lipids is formed by pulling the solid support through a Langmuir trough which has a lipid monolayer spread at the air-water interface. The LB technique is unable to embedded carrier into the bilayer.[93] Vesicle fusion, where pre-formed small unilamellar vesicles (SUVs, 20 -100 nm) lipid vesicles spread on the hydrophilic support through electrostatic interaction, is a simpler method to prepare supported lipid bilayers (SLBs).[50] For mesoporous surfaces, vesicle fusion produce lipid bilayers that span pore sizes up to 20 nm, [64, 94, 95] as the SUVs are too large to rupture in the pores. [94] However, completely defect-free bilayers are difficult to achieve through vesicle fusion. The existence of hole defects can be revealed by AFM.[96] Aspects like composition and concentration of lipid, preparation method of liposomes, temperature, solution conditions (pH, presence of divalent cations) and physicochemical properties of the support strongly affect the interaction between lipid vesicles and the surface, and final quality of lipid bilayers.[96, 97]

Here we propose a robust lipid pore-filled system as barrier for biomimetic separation (**Figure 3.1**). By dissolving lipid molecules in organic solvent to avoid the formation of vesicle, which are far larger than available pore size, lipid assemblies can be infiltrated into the pores.[64] After removing the organic solvent and rehydration, lipid bilayers is then formed inside the pores through rehydration. Schlipf et al.[64] have successfully demonstrated the confinement of lipid assemblies (1, 2-dipalmitoyl-sn-glycero-3-phosphocholine (DPPC)) into pores of mesoporous silica particles (5.4 nm and 9.1 pores). Furthermore, it is found that the lipid mobility at different locations of lipid filled particles (at the core, mid core or surface of the particle) is similar, suggesting lipid self-assemblies are continuous through the pores, which is necessary for the incorporation and proper

function of small lipophilic carriers and membrane proteins. This suggests the potential application of lipid pore-confinement on a membrane support to mimic the biological membrane for separation and biosensing applications.

In this work, the ability of the lipid assemblies (1, 2-dipalmitoyl-sn-glycero-3-phosphocholine (DPPC)) confined in mesopores of a membrane platform to provide robust barriers to transport is examined and compared to traditional lipid coated mesoporous thin films. The enhanced transport in carrier-mediated biomimetic membranes was confirmed by measuring the permeability of glucose through the composite membrane before and after the immobilization of boronic acid (4-(N-Boc-aminomethyl) phenylboronic acid) into lipid bilayers. The environmental factors like pH gradient (related to carrier-solute association) and temperature (related to the lipid bilayer diffusivity) were explored to improve the glucose permeability. This work presents a versatile method for carbohydrates recovery. In addition to the boronic acid carrier for sugar separation, the combination of high surface area silica materials and selectively permeable lipid bilayers suggests potential applications for efficient, selective dilute aqueous solute separations if a specific carrier for the solute is incorporated.

### **3.3 Experimental sections**

#### **3.3.1 Material**

Anodic aluminum oxide (AAO) membranes (Whatman, 25 mm in diameter) with pores of approximately 200 nm in diameter, a porosity of 0.25-0.5, and a nominal thickness of 60  $\mu\text{m}$  was purchased from Fisher Scientific and served as the macroporous support for the silica thin film. Tetraethyl orthosilicate (TEOS, 98%), polyethylene oxide (PEO)-polypropylene oxide (PPO)-PEO triblock copolymer (P123, average  $M_n \sim 5,800$ ),

cetyltrimethylammonium bromide (CTAB,  $\geq 99\%$ ) glycerol ( $\geq 99\%$ ), potassium phosphate buffer tablets, chloroform ( $\geq 99\%$ ), 1, 6-Diisocyanatohexane (DH, 98%), sodium hydroxide (NaOH,  $\geq 98\%$ ) and glucose ( $\geq 99.5\%$ ) were supplied by Sigma Aldrich. Ethanol (anhydrous) was purchased from DLI and hydrogen chloride (HCl, 6N), acetone ( $\geq 99.5\%$ ), and potassium chloride (KCl,  $\geq 99.0\%$ ) were purchased from Fisher Scientific. Vybrant® DiO cell-labeling solution was purchased from Thermo Fisher scientific. Alizarin red S (ARS, certifiable grade) was supplied by Amresco. 4-(N-Boc-aminomethyl) phenylboronic acid (BA, 97%) was purchased from Frontier scientific. 1,2-dipalmitoyl-sn-glycero-3-phosphocholine (DPPC,  $>99\%$ ) was purchased from Avanti lipid.

### **3.3.2 Synthesis of thin film silica supported by anodic aluminum oxide (AAO) membrane**

Thin film silica membranes with perpendicularly oriented pore array were synthesized on macroporous AAO supports using a neutral chemical surface method as previously reported by Wooten et al [33] and Koganti et al.[98] To block the pores of AAO support for silica thin film deposition, cross-linked P123 was used as a temporary pore blocking film. A 0.696 mmol/L P123 in acetone was under continuous stirring while an equimolar amount of 1, 6-diisocyanatohexane was added in a nitrogen bag. Three drop of glycerol was then added and constant stirred for 10 minutes. The solution was used to dip coat the AAO support and to modify the glass slides to create chemically neutral surface for sandwiching the membranes. The dip coated supports were aged at 100°C for 24 hours.

The mesoporous silica coating solution was prepared by addition of a solution of P123 to a prehydrolyzed silica sol following the procedure of Brinker et al.[99] TEOS, anhydrous ethanol, deionized ultra-filtered water and HCl were added together in a mole ratio of 1:

3.8: 1: 5 x 10<sup>-5</sup>. This solution was refluxed at a temperature of 70°C for 90 minutes. A final amount of HCl and water were added yielding a concentration of 7.34 mM HCl. The mixture was stirred at room temperature for 15 minutes. The mixture was then aged at 50°C for 15 minutes. A solution of P123 and ethanol in a mole ratio of 0.01: 18.7 was then added to the TEOS mixture and stirred for 10 minutes. The final mole ratio was 1 TEOS: 22 C<sub>2</sub>H<sub>5</sub>OH: 5 H<sub>2</sub>O: 0.004 HCl: 0.01 P123. The copolymer modified AAO supports were dip coated in the final solution at a speed of 7.6 cm/min. The silica thin films coated AAO support were then sandwiched between two chemically neutral surfaces. The thin films of silica on AAO supports were aged and dried at 50°C for 24 hours and then 100°C for 24 hours. The films were then calcined 500°C for 4 hrs with temperature ramping from room temperature at 1°C/min to remove the pore template and crosslinked pore blocking polymer.

### **3.3.3 Membrane characterization**

FIB/SEM instrument (FEI Helios Nanolab 660) was used to characterize the membrane surface morphology. The samples (bare AAO support and thin film silica membrane) were prepared by attaching them to double sided carbon tape on 15 mm aluminum mounts. Transmission electron microscopy (JEOL 2010F TEM) was used to characterize the pore structure of the silica thin film. To prepare a TEM sample, the composite membrane was placed in a 5 M HCl solution under constant stirring for 24 hours to dissolve the AAO support membrane. The resulting material was deposited onto a lacy carbon grid after being dispersed in ethanol.

The pore accessibility of the thin film silica membrane was demonstrated by pressure driven ethanol flux through the membrane. The membrane was placed on a vacuum

filtration holder (Cole Parmer) and secured to an Erlenmeyer flask. A chemical duty vacuum/pressure pump (Millipore) was used to control the vacuum pressure. The volume of ethanol through the membrane under pressure drop of 16, 26, 34 and 40 kPa in 5 minutes was recorded. The ethanol flux through the bare AAO support was also measured to compare with the thin film silica membrane. Each measurement were conducted in triplicates.

### **3.3.4 Synthesis of spherical mesoporous silica particles**

Spherical mesoporous silica particles SBAS (Santa Barbara Amorphous Batch) materials were prepared using the procedure of Schlipf et al. [100] Initially, 0.465 g of CTAB dissolved in 20 mL of deionized water was added to 3.10 g P123. This solution was placed in a water bath at 30°C and stirred vigorously while 7.8 mL of 200 proof ethanol and 45.9 mL of 1.5 M HCl were added. After the P123 completely dissolved, 10 mL of TEOS was slowly added drop wise. This solution was mixed for 2 h. At the end of 2 h, the solution was poured into a Parr 4748 Teflon lined bomb, which had been acclimated to the hydrothermal aging temperature, between 60°C and 120°C, prior to use. The sample was kept at the desired hydrothermal aging temperature in an oven for 3 days. At the end of the 3 day period, the sample was removed from the bomb and mixed in a high speed mixer to homogenize the solution. After homogenization, the sample was filtered and rinsed with deionized water. After filtration, the sample was placed into a single walled Whatmann cellulose extraction thimble, and the surfactants were removed using Soxhlet extraction with 200 mL of 200 proof ethanol over 24 h. The pore dimension (5 – 12 nm) increases as the hydrothermal aging temperature (60 -120°C) increase as measured by nitrogen adsorption.

### **3.3.5 Boronic acid (BA) immobilized lipid filled silica membrane/particle preparation through evaporation deposition**

To make a mixture of DPPC/BA in a molar ratio of 6.9: 10, 5 mg of DPPC and 2.5 mg 4-(N-Boc-aminomethyl) phenylboronic acid (BA) were dissolved with 1 mL CHCl<sub>3</sub> and sonicated for 5 minutes. A silica membrane or 10 mg silica particles was then immersed in the DPPC solution and sonicated for 25 minutes in a shell vial (25mm x 95mm). The above mixture was then blow-dried with nitrogen and was further dried under high vacuum for at least 2 hrs. To form bilayers, the dried lipid inside the silica membrane was rehydrated in 1 mL PBS solution and sonicated at 47°C for 1 hr. The sample was sonicated for another 15 minutes while cooling to 30°C. The excess lipid was removed by washing the membrane with PBS three times.

### **3.3.6 Boronic acid immobilized lipid enveloped silica membrane/particle preparation through vesicle fusion**

To make a mixture of DPPC/BA in a molar ratio of 6.9: 10, 5 mg of DPPC and 2.5 mg BA was dissolved in 1 mL CHCl<sub>3</sub>, then the lipid was blow-dried with air for 1 hr and was further dried under high vacuum for at least 2 hrs. Then the dried lipid was rehydrated in 1 mL PBS solution to form multilamellar vesicles. The resulting mixture was then extruded at 45 °C through a polycarbonate filter with 200 nm diameter pores 21 times, which produces small unilamellar vesicles with a mean diameter of 200 nm. The lipid solution was then mixed a silica membrane or 10 mg silica particles for 1 hr to facilitate vesicle fusion. The excess lipid was removed by washing the membrane with PBS three times.



### **3.3.7 Attenuated total reflectance Fourier transform infrared spectroscopy (ATR-FTIR)**

To confirm the existence of lipid assemblies in the pores of lipid filled membranes (silica and AAO) were characterized using a ThermoNicolet Nexus 470 spectrometer equipped with a narrowband liquid nitrogen cooled mercury cadmium telluride (MCT) detector and ATR with single-reflection 45° ZnSe crystal (VeeMAX III, PIKE Inc., Madison, WI). Each spectrum was collected at a resolution of 4 cm<sup>-1</sup> and 250 scans with IR beam incident at 45°.

### **3.3.8 Confocal laser scanning microscopy**

To label the lipid and boronic acid, 1mL of lipid bilayer coated particles were mixed with 10uL of 1 mM fluorescent dye DiO and 1mL of boronic acid immobilized lipid bilayer coated particles were mixed with 1mL of 1 mM Alizarin red S (ARS) on a shaker for 30 min. The samples were then washed with PBS three times and imaged within 2 hours of preparation using a Leica TSP SP5 confocal microscope. Experiments were performed at 28°C using a 63x/1.4 oil immersion objective. DiO was excited at 488 nm with an argon laser at 6% laser power for imaging and emission was collected between 490 nm and 510 nm. ARS-BA complex was excited at 514 nm for imaging and emission was collected between 580 nm and 620 nm.

### **3.3.9 Differential Scanning Calorimetry**

DSC was used to confirm the formation of lipid bilayers on silica particles by measuring the gel to fluid phase transition temperature of supported DPPC bilayers. Following the preparation of supported lipid bilayers on particles, particle suspensions were centrifuged at 1,000 x g to form a soft pellet. After formation of a soft pellet, 10 uL

of the pellet was hermetically sealed in a DSC sample pan. Thermograms were run on a TA Instruments Q600 DSC between 20°C and 70°C at a ramp rate of 10°C/min and returned to 20°C at a cooling rate of 10°C/min.

### **3.3.10 Glucose affinity to boronic acid at different pH**

To measure the relative glucose affinity to boronic acid at different pH, 1 mL of 5 mg/mL BA immobilized liposome solution was mixed with 1 mL of 1 mM ARS to yield fluorescent ARS-BA complex. The fluorescent emission at 600 nm of ARS-BA immobilized liposome solution before and after addition of 92.8 mM glucose at various pH were measured using plate reader (Synergy Mx, BioTek, Winooski, VT) as excited at 490 nm. The fluorescent intensity reduction of the solution after addition of glucose was reported with normalization to the original intensity at experimental pH. Each measurement were conducted in triplicate.

### **3.3.11 Glucose diffusion through membranes as a function of temperature and pH**

Glucose diffusion through the silica thin film membranes was measured in a side by side diffusion cell (PermeGear, Hellertown, PA). The membrane was held into place between the chambers, which each side holding 7 mL, being secured tightly together by a clamp allowing a 2 cm<sup>2</sup> cross sectional area of the membrane to be exposed. The donor side of the cell was loaded with 7 mL of 5.6 mM glucose solution in PBS buffer (0.9 M, pH 7.4 or adjusted to 10 by NaOH). The receptor side was initially loaded with 7 mL of PBS buffer (pH 7.4 or adjusted to 5 by HCl) with no solute. The diffusion cell was then placed on a heater plate with temperature controlled at 23°C or 45°C. The concentration of solute in the receptor side and donor sides were both sampled as a function of time. At sampling time, 200 uL sample from each side was taken and the concentration was test

using high performance liquid chromatography with a Bio-Rad Aminex HPX-87H and a Shodex R01 refractive index detector. The mobile phase was degassed 5 mM H<sub>2</sub>SO<sub>4</sub> fed at a rate of 0.4 mL/min, and the temperature of the column was at 50°C.

### **3.4 Results and discussion**

#### **3.4.1 Synthesis of mesoporous silica thin film on porous support as separation platform**

Silica thin films with accessible 2-D hexagonally close packed (HCP) pore structure on porous support were utilized as separation platform and a support for lipid assemblies. The HCP pore structure formed from cylindrical micelles by surfactant templating is considered to be superior for membrane applications due to their continuous channels, which do not offer alternate pathway for the diffusion, compared to interconnected cubic structure.[16] However, HCP pores naturally tend to align with the substrate during surfactant templating.[29] This parallel orientation make the pores inaccessible, and not suitable for membrane applications.[30] Recently, we have successfully demonstrated the synthesis of silica thin film with perpendicularly oriented HCP pore on a porous support and its ability to act as nanofiltration membrane.[33] The same technique was employed here to prepare the composite membrane as lipid bilayer support.

Porous anodic aluminum oxide (AAO) substrate was used as support for the silica thin film. To provide a neutral surface for perpendicular pore alignment and simultaneously prevent the penetration of silica into the pore of the support, the AAO was dip coated with cross-linked copolymer to block the pores prior to the subsequent silica thin film deposition. The copolymer layer also served as a chemically neutral layer to align the pore perpendicularly.[32] After a stable pore structure was obtain through aging, calcination

was performed to remove the pore template and the blocking copolymer layer. To confirm that pore-accessible silica thin film was successfully deposited on the porous support, the SEM images of bare AAO support and silica thin film coated AAO support after calcination were compared. As shown on **Figure 3.2b**, a continuous silica thin film with opening pores is formed on the top of porous support, which results in greater electron scattering and decrease in contrast comparing to the bare AAO support (**Figure 3.2a**). Characterization of the silica thin film by TEM (**Figure A.1**) shows that the pores of the silica thin film are highly ordered HCP structure with pore dimension of approximate 10 nm. Therefore, porous substrate supported silica thin films with accessible continuous cylindrical channels is successfully synthesized. However, it is hard to determine whether the deposited silica thin film is defect free or not by SEM imaging since the electron beam can destroy the thin film and cause defects. Additional ethanol flux measurement through the composite membrane at given pressure drop (**Figure A.2**), shows measurable flux which is proportional to the pressure drop, suggesting uniform coating of defect free silica thin film with accessible pores on the support.

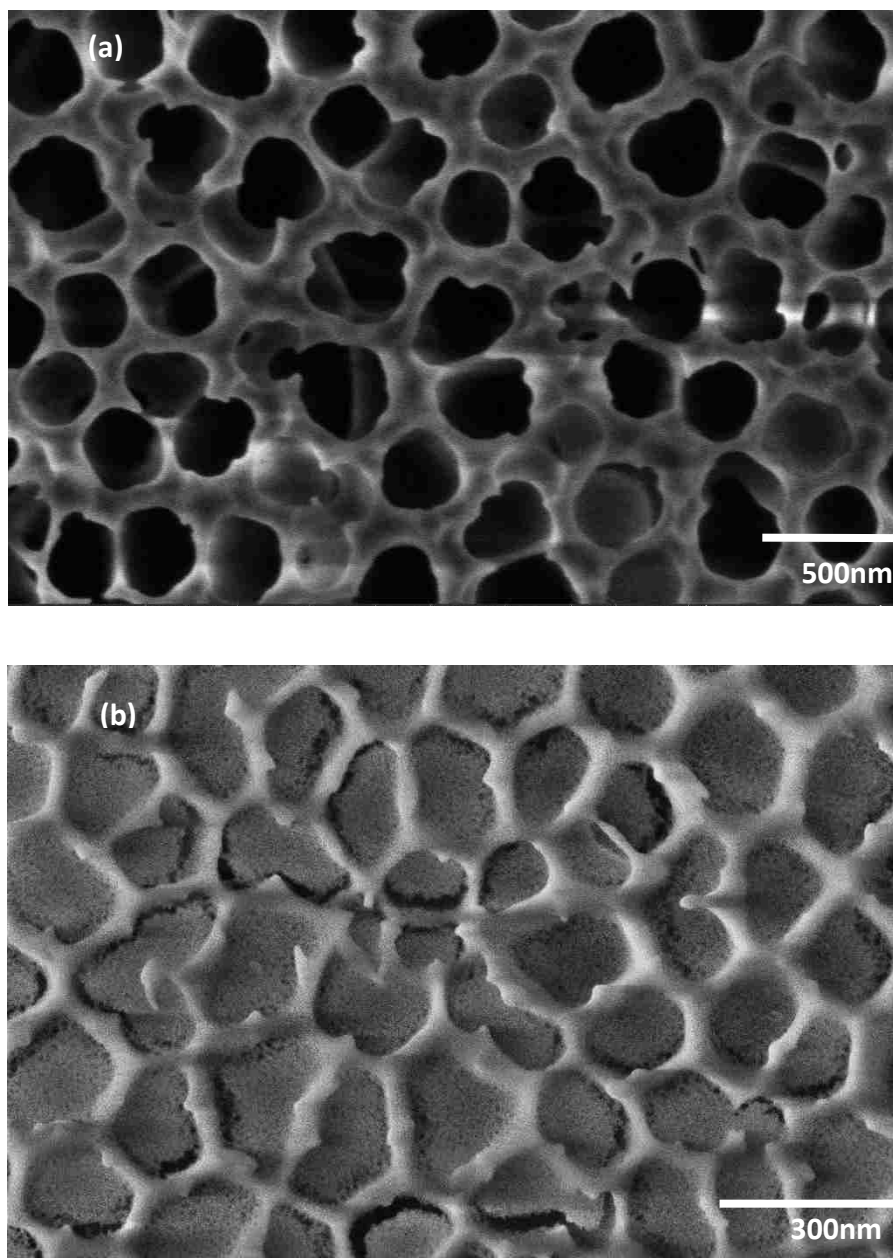


**Figure 3.2** Plane-view SEM images of (a) AAO support and (b) silica thin film coated AAO.

### **3.4.2 Lipid Pore-Filled Silica Thin Film Membranes as a Transport Barrier**

In order to examine the location of DPPC lipid assemblies on porous supports, spherical mesoporous silica particles with pore size of 11.8 nm, which is close to that of the silica thin film was chosen as a model platform to allow direct visualization of lipid

bilayer location on porous support using confocal scanning laser microscopy.[64] As shown, the lipid enveloped particles prepared by vesicle fusion have a continuous, single layer of lipid bilayer (tagged with green fluorescent dye DiO) surrounding the spherical particle surface (**Figure 3.3a**). Alternatively, the confocal images of the lipid pore-filled particles (**Figure 3.3b**) suggest that the lipid bilayers are confined inside the pores through evaporation deposition. Typically, the lipid bilayer of DPPC has a thickness of 3-5 nm.[101] Limited by the thickness of lipid bilayers, this evaporation deposition method for packing the lipid inside the pores can only apply for particles with pores larger than lipid bilayer thickness. If the pore size is too small, lipid bilayers can only form on the particles surface, which results in a lipid enveloped particles.[64]

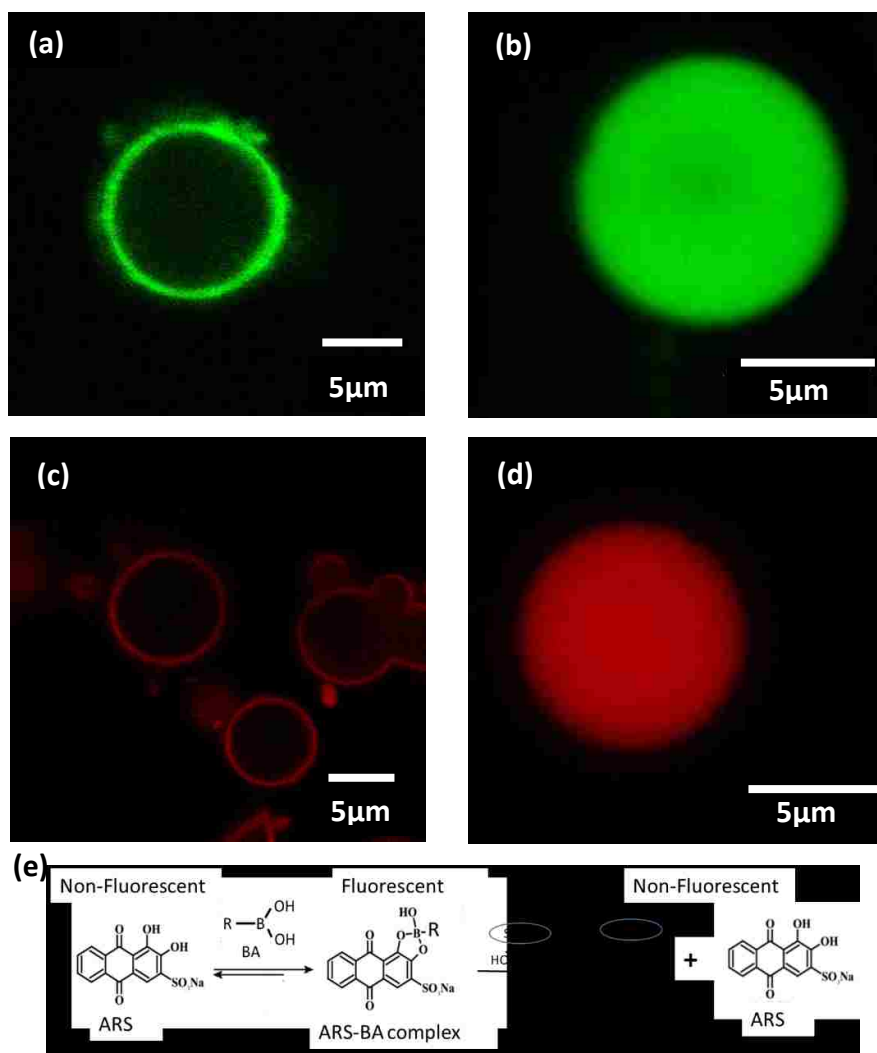


**Figure 3.3** Confocal microscopy image of (a) lipid enveloped silica particle; (b) lipid filled silica particles; (c) lipid-BA enveloped silica particle; (d) lipid-BA filled silica particles; (e) scheme of competitive complexation between Alizarin Red S (ARS) and glucose to boronic acid. Lipid is tagged with green fluorescent DiO and boronic acid (BA) is complexed with ARS to give red fluorescence. All confocal images showed the cross-section of the core of the particle (pore diameter: 11.8 nm).

The ability of supported lipid bilayers to effectively prevent the nonselective transport of sugar in the absence of carrier is critical for providing subsequent selective membrane transport using the lipid-embedded boronic acid carrier. To quantify the effect of lipid

location (lipid filled pores versus traditional lipid enveloped-pores) on membrane performance, glucose flux through the two types of supported lipid bilayers was measured and compared with the bare support (silica thin film membrane). As shown in **Figure 3.4**, the glucose flux of lipid enveloped membrane prepared by vesicle fusion is the similar to that of the silica membrane and AAO support, which indicates that it is not an effect barrier for glucose transport. Meanwhile, lipid filled membrane, where lipid are confined inside the membrane pores show a 14-fold decrease in glucose flux , suggesting that lipid filling is a more efficient barrier than lipid enveloping. Therefore, defects common to lipid bilayers prepared from vesicle fusion reported in literatures,[96] is not negligible in the preparation of thin film supported membranes. The high flux of glucose may be due to defects in the supported lipid bilayer defect, which can be reduced through the the optimization of the surface chemistry of the support, lipid composition and deposition methods to make better solute rejecting bilayer on silica thin film surface. For example, the hydraulic permeability of commercial nanofiltration membrane NTR-7450 (sulfonated polyethersulfone) with sulfonic surface charge was significantly reduced (by about 12-fold) after vesicle fusion of 1,2-dimyristoyl-sn-glycero-3-phosphocholine (DMPC), while the deposition of DMPC vesicles on NF-270 membrane (polyamide) with carboxylic surface charge didn't alter the membrane permeability significantly.[102] Changing the DMPC to DMPC/DMTAP (1, 2-Dimyristoyl-3-trimethylammonium propane) lipid mixture for vesicle fusion on NTR-7450 further reduced the hydraulic permeability by 2-fold. Alternatively, the transport of glucose, which is more permeable in lipid bilayers, may present a more stringent test of the integrity of the supported lipid bilayer than the transport of ions; the permeability coefficient of ions ( $K^+$ ,  $Na^+$ ,  $Cl^-$ ) through the liposome



is around the scale of  $10^{-10}$  -  $10^{-12}$  cm/s , while that of glucose is about  $10^{-7}$  cm/s.[34] The lipid enveloped silica thin film membrane may be better suited to applications involving biomimetic ion transport rather than uncharged hydrophilic molecules, for which it does not have significant barrier properties.

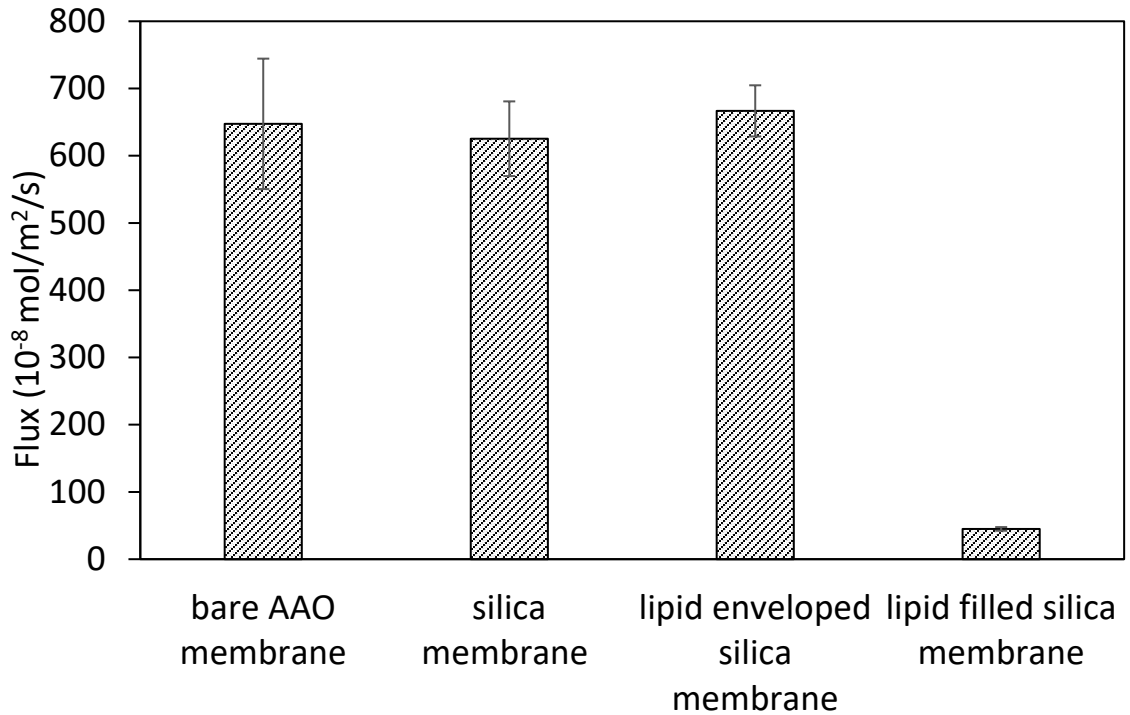


**Figure 3.4** Glucose flux through different membrane (5.6 mM initial glucose solutions in donor side of diffusion cell). The error bars are based on the sampling times at 1 h, 1.5 h, 3 h of diffusion).

In the case of the lipid-filled pores, the thickness of a lipid bilayer is about 4 nm, and pore dimension of silica thin film is about 10 nm, allowing for the inclusion of lipid self-assemblies. This is consistent with the observation of Schlipf et al.,[64] where the evaporation deposition methods was used to prepare DPPC lipid filled mesoporous silica particles with different pore sizes (3.0 nm, 5.4 nm and 9.1 nm). They found that lipid only

exists on the surface of particle with 3.0 nm pores, while it assembled in the pores of 5.4 nm and 9.1 nm particles. The observation that lipid can't exist in pores smaller than its bilayer dimension (about 4 nm) indicates that the lipid may form a variety of assemblies like bilayer or micelle inside the nanopores of silica. They also reported that the lipid diffusivity remind consistent regardless of lipid location (at the core, mid core or surface of the particle), suggesting uniform distribution of lipid assemblies inside the pores. Similarly, dissipative particle dynamics simulations of DMPC confined in hydrophilic pores revealed that the morphology of pore confined lipids were dependent on the pore radius (R) relative to the lipid length (L) and lipid concentration in the pores.[103] When the lipid concentration gradually increased, the lipid first formed micelles of distinct morphologies, then nucleation and growth into cylindrical bilayers. [103, 104] The larger the ratio of pore radius to lipid length, the lower the concentration at which the cylindrical bilayer formed. [103] The effect of pore size and nonionic concentration has also been studied for nonionic surfactant bilayers in confined pores. Cylindrical bilayers of n-dodecyl-penta (ethylene glycol) (C12E5, 4.2 nm thick bilayer on flat surface) were formed in 8 nm cylindrical nanopores of silica particles when the bulk concentration was above the CMC, as characterized by grazing incidence small-angle neutron scattering (GISANS). Considering the pore size of silica thin film membrane (~10 nm), and the lipid concentration (6.9 nM, CMC= 0.46 nM), the lipid most likely forms two layers of cylindrical bilayer that line the inner pore surface of the silica membrane to act as barrier to aqueous solute.

ATR-FITR was also performed to characterize the location of lipid assemblies in the composite membranes (consist of silica thin film and AAO support). ATR-FITR (**Figure**

**3.5**) shows the existence of C-H stretch ( $2915, 2846\text{ cm}^{-1}$ ),  $\text{PO}_2^-$  stretch ( $1222, 1087\text{ cm}^{-1}$ ) and C-O-C stretch ( $1052\text{ cm}^{-1}$ ) for DPPC on AAO and silica membrane after lipid filling, which indicates that the lipid not only exists inside the silica layer but also inside the AAO support. However, Karp et al. [105] reported that the DMPC or DPPC bilayers formed on the inner pore of AAO (200 nm) were normal to the magnetic field, which is parallel to the long axis of AAO pore as characterized by solid state NMR, suggesting that lipid exist as multiple cylindrical bilayers in the pores of an AAO support.[106] Comparing to the 200 nm pore of AAO, the multilayer of lipid bilayers are not sufficient to block the pores, therefore the barrier behavior of this composite membrane is primarily result from the lipid pore-filled silica thin film.

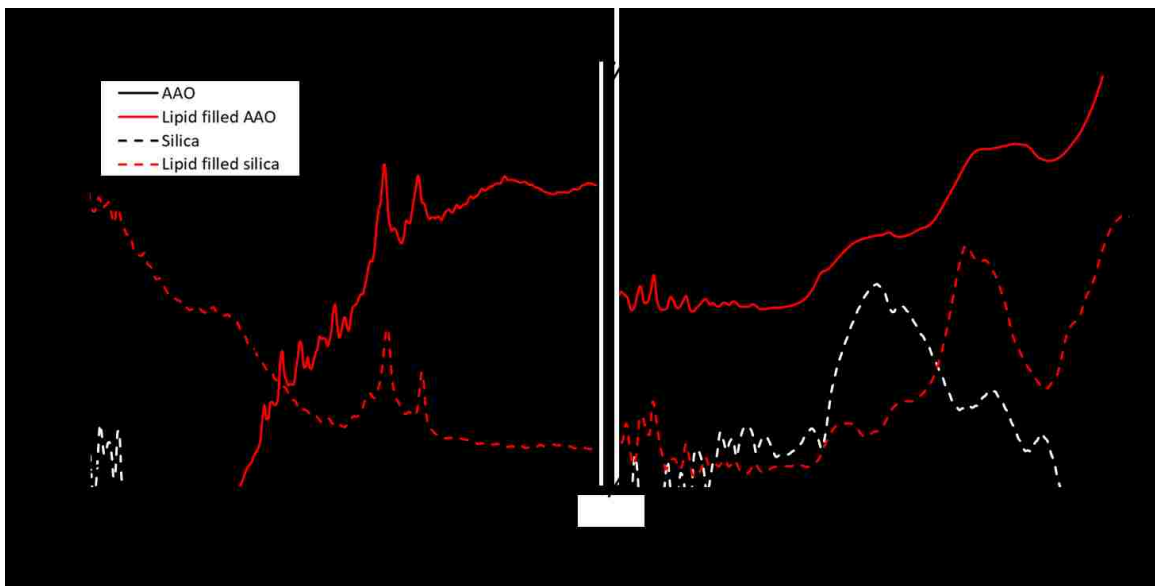


**Figure 3.5** ATR-FTIR spectra of bare AAO, silica, lipid filled AAO and lipid filled silica membrane.

### 3.4.3 Incorporation of boronic acid carrier into lipid bilayers

The lipophilicity of the boronic acid is an important factor for immobilizing the carrier into the lipid bilayer to ensure sugar transport efficiency. Westmark et al.[92] encapsulated different types of boronic acids and glucose into liposome and found that the glucose efflux from the liposome, as facilitated by boronic acid, was largely dependent on the lipophilicity of the carrier. Thus a lipophilic boronic acid, 4-(N-Boc-aminomethyl) phenylboronic acid (partition coefficient,  $P=2.53$ ), is chosen for its ability to reside in the lipid bilayer. A mixture of DPPC/BA in a molar ratio of 6.9:10 (59 mol% BA) was dissolved in chloroform prior to lipid rehydration to incorporate boronic acid into lipid assemblies. To further confirm that boronic acid is successfully immobilized into lipid bilayers, the dye Alizarin red S (ARS), which is not fluorescent itself but becomes fluorescent once complexed with boronic acid, was utilized (**Figure 3.2e**). ARS was added to the boronic acid immobilized lipid system and indicates that boronic acid presents on silica particles surface in lipid enveloping system (**Figure 3.3c**), while boronic acid is distributed inside the particles in lipid pore-filling system (**Figure 3.3d**). The location of boronic acid and lipid bilayers in particles (either at the surface of lipid-enveloped particles or throughout lipid pore-filled particles) are identical, which confirms that boronic acid is confined in the lipid bilayers.

In order to test if the addition of boronic acid alters the structure of lipid bilayers, the gel to fluid phase transition temperature of the lipid bilayers, before and after the immobilization of boronic acid was compared. This gel to fluid phase transition temperature of the bilayer represents is associated with disorder of the acyl chains of lipid molecules as the bilayer becomes more fluid with increasing temperature.,[35] . As measured by differential scanning calorimetry (DSC) , in the absence of boronic acid, the

lipid in the lipid filled particles have the same phase transition of 41.3°C ( **Figure 3.6**) as DPPC liposomes.[107] For boronic acid immobilized lipid filled particles, the transition temperature decreases to 39.3°C, with a corresponding decrease in the enthalpy of the gel to fluid phase transition. This is consistent with the incorporation of boronic acid in the DPPC bilayer, increasing the membrane fluidity. The phase transition temperature and enthalpy change of the phase transition gradually decrease as the additive concentration increases in the bilayer, potentially disordering the bilayer structure so this transition becomes negligible at a critical concentration which depends on the type of additives and lipid.[108-110] In DPPC, 50 mol% cholesterol was reported to completely eliminate the phase transition.[111, 112] Because the bilayer structure could affect the transport properties in the biomimetic membrane, knowledge of the effect of boronic acid on the gel to fluid phase transition is important in interpreting the effect of carrier type and concentration on membrane performance.

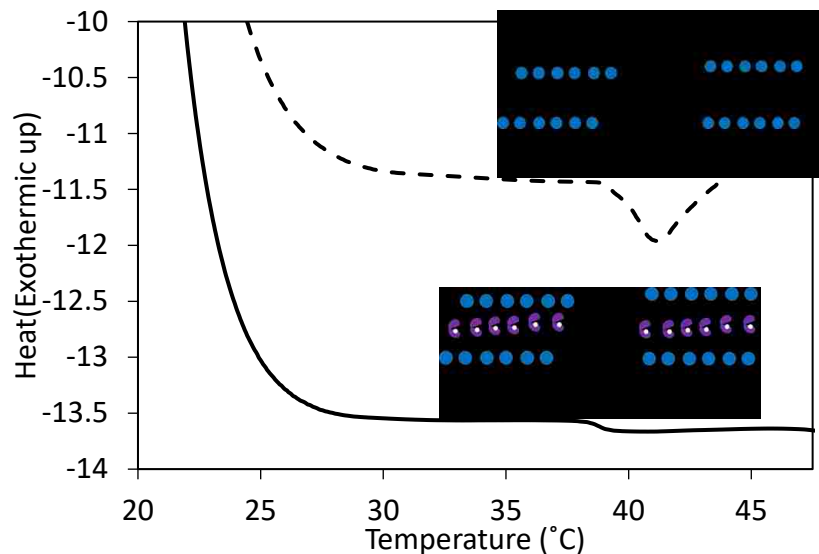


**Figure 3.6** Gel to fluid phase behavior of lipid filled silica particle (dash line) and boronic acid immobilized lipid filled silica particle (solid line) as measured by DSC (59 mol% boronic acid, pore diameter: 11.8 nm).

#### 3.4.4 Glucose transport through supported lipid bilayers with boronic acid carrier

Transport of glucose through the lipid-filled composite silica thin film membrane was compared with and without boronic acid carrier in the lipid phase using a static diffusion cell. Glucose transport with boronic acid was only measured in the lipid-filled pores because lipid enveloping did not provide sufficient barrier to transport. As shown in **Figure 3.7**, glucose flux is enhanced by a factor of four after the immobilization of boronic acid at room temperature (RT), which suggests that boronic acid is carrying glucose through the membrane. The transport mechanism of glucose through the lipid filled silica membrane utilized is hypothesized as described in **Figure 3.1**. On the glucose concentrated side, glucose combines with boronic acid which is immobilized in lipid bilayers then transported through the lipid bilayers. Due to the low glucose concentration on the receiving side, the glucose-boronic acid complex dissociates and releases glucose and boronic acid. The free

boronic acid then can go back to facilitate transport of another glucose molecule. Its combination of passive transport and facilitated transport in a single membrane overcomes the trade-off between high permeability and high selectivity that can't be achieved simultaneously in conventional membrane processes. Meanwhile, the incorporation of carrier into membrane allows the reuse of the carrier which largely reduces the cost of transport catalyst and eliminates the recovery step of carrier from the product or the aqueous solution.

Opportunities to control the glucose flux in the boronic acid carrier system include a) tuning the glucose-boronic acid interaction via choice of boronic acid or environmental conditions; b) altering the transport properties in the lipid assemblies; and c) adjusting the relative concentrations of the glucose and the boronic acid carrier. For a 5.6 mM (dilute) glucose solution, 13 mol%, 59 mol% and 74% boronic acid in the lipid solution deposited by evaporation deposition resulted in glucose flux of 142, 412 and 294 x 10<sup>-8</sup>mol/m<sup>2</sup>/s at 45°C (neutral pH), respectively. At 74 mol% BA, boronic acid precipitation was apparent in lipid mixture, thus the carrier was not effective. Increasing the glucose concentration in the donor phase to 28 mM resulted in a flux of 1700 x 10<sup>-8</sup>mol/m<sup>2</sup>/s. These glucose concentrations were chosen to represent dilute sugar concentrations consistent with biomass hydrolysates (1~20 g/L) [7, 8]. However, the concept of boronic acid carriers in liquid membranes has been examined in liquid membranes at sugar concentrations of 100, 300, 500 mM,[10] which suggests that the range of operation with respect to glucose operation concentration can be extended.

The ability to operate above and below the gel-fluid transition of lipid bilayers suggests a potential temperature dependence of the flux based on differences in mobility

of the carrier due to changes in membrane structure. After incorporating about 59 mol% boronic acid, the lipid bilayers still retains a gel-fluid phase transition at approximately 39°C. Glucose diffusion studies conducted above the transition temperature (at 45 °C) after carrier immobilization show an increase in glucose flux by a factor of two from  $225 \times 10^{-8} \text{ mol/m}^2/\text{s}$  to  $412 \times 10^{-8} \text{ mol/m}^2/\text{s}$  (**Figure 3.7**). While the glucose flux in the absence of boronic acid also increases with increasing operation to 45°C (a factor of 1.4), the effect is more significant for the boronic acid immobilized lipid assemblies (**Figure 3.7**). This dramatic temperature effect on solute flux is attributed to changes in the fluidity of the lipid bilayers. Below the transition temperature, the lipid bilayers is in a “solid” gel phase, where the lateral diffusion is very slow so the lipid bilayers is more rigid and less permeable, which limited the mobility of immobilized boronic acid. Above the transition temperature, the bilayers are in a “fluid” liquid phase.[35] In this state, the lipid bilayers shows rapid lateral diffusion and more favorable for compound exchange with the environment,[113] which allows the carrier to move fast and improve transport efficiency.

In order to test membrane stability when switching below and above the phase transition temperature, multiple temperature-switch cycles were performed. **Figure 3.8** shows that the glucose flux reduced by 35% (cycle 3) and 15% (cycle 4) after two cycles between room temperature and 45°C. However, no boronic acid carrier leakage into the aqueous phase was detected as determined by fluorescence spectroscopy during the cycles. The reduction of glucose flux may have been caused by the annealing above the phase transition temperature, which melt the lipid bilayers to reconstruct a better barrier,[114] and reduces the background flux. In addition to temperature, lipid composition and support surface chemistry are well documented factors that will affect lipid bilayer fluidity.[115,



116] Thus, factors that affect lipid bilayer fluidity its permeability need to be carefully examined to improving the transport efficiency and selectivity of the solute.

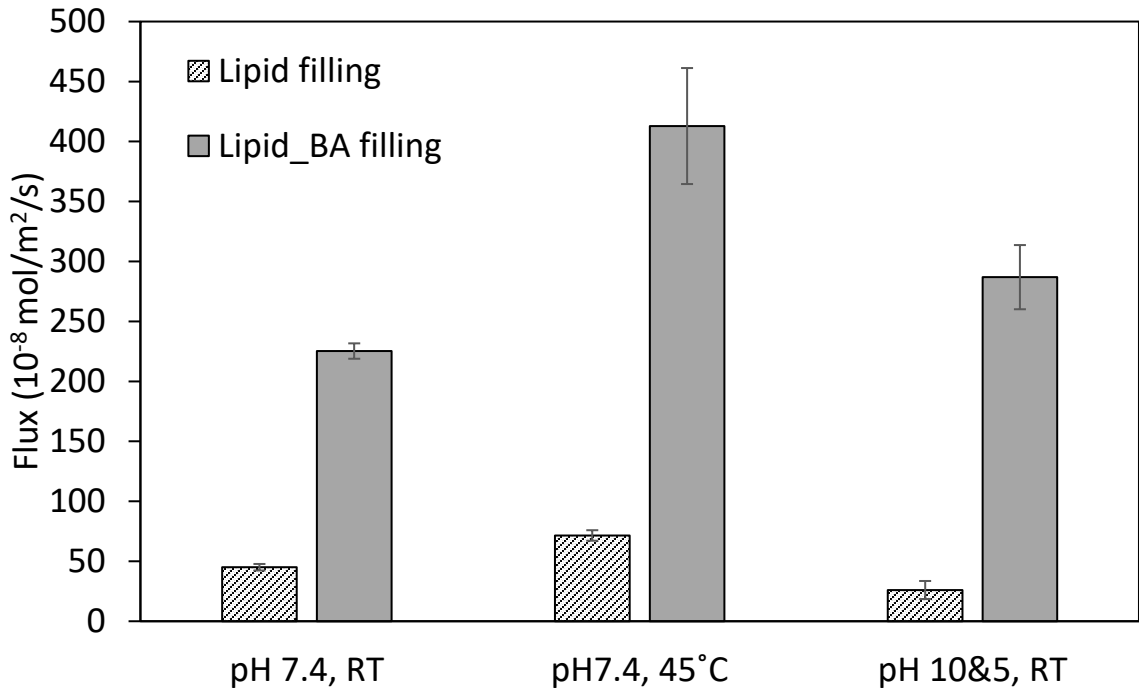


**Figure 3.7** Glucose flux through lipid filled membrane with or without boronic acid carriers as a function of temperature (room temperature versus 45°C) and pH (pH 7.4 versus a pH 10 (donor)/pH 5 (receptor) gradient), (5.6 mM initial glucose solutions, 59 mol% BA and error based the sampling at 2 h, 3 h, 4 h of diffusion ).

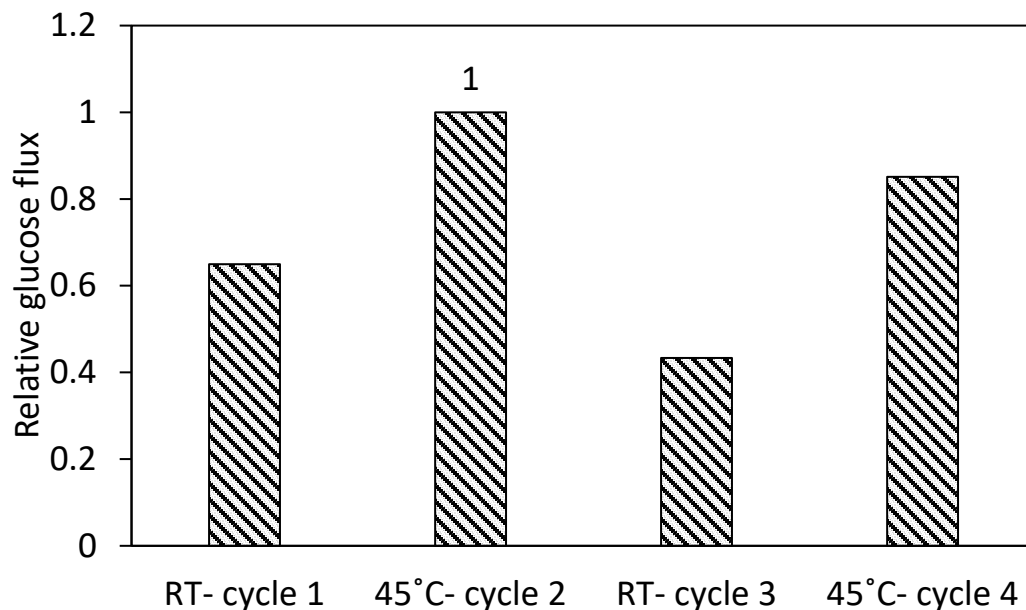


**Figure 3.8** Relative glucose flux through boronic acid immobilized lipid filled membrane during multiple temperature-switch cycles (At each cycle, the same membrane started with 5.6 mM initial glucose solutions and sampling at 2 h of diffusion. Flux reported was normalized to flux measured on cycle 2).

An alternative approach to changing the glucose flux through the membrane is to change the interactions of the solute-carrier system. The formation and dissociation of glucose-boronic acid complex is pH dependent.[117] The competitive binding between the dye Alizarin red S (ARS) and glucose to 4-(N-Boc-aminomethyl) phenylboronic acid was used to quantify the interaction of the glucose-boronic acid as a function of pH. As the ARS-boronic acid complex is fluorescent, the addition of glucose results in the dissociation of this complex and decrease in fluorescent intensity (**Figure 3.3e**). The relative reduced fluorescent intensity of the ARS-BA complex as a function of pH at constant glucose concentration is shown in **Figure 3.9**. Glucose binds to boronic acid strongly at basic conditions and minimally at acidic conditions.

Based on this observation, glucose flux was measured across the lipid-filled silica thin film membranes while maintaining the donor side of the diffusion cell at pH 10 (to enhance glucose and boronic acid association), and the receptor side at pH 5 (promoting dissociation of the glucose-boronic acid complex). The lipid-filled silica thin film membrane acts as an ion barrier, allowing this pH gradient to be maintained across the membrane. Applying the pH gradient on donor and receptor phases improves glucose diffusion from  $225 \times 10^{-8} \text{ mol/m}^2/\text{s}$  to  $287 \times 10^{-8} \text{ mol/m}^2/\text{s}$  relative to neutral pH experiments when facilitated by boronic acid (**Figure 3.7**). No significant change in glucose diffusion is observed relative to the neutral pH in the absence of boronic acid. This observation further supports the mechanism of boronic acid-mediated transport of glucose in the lipid-filled pores. Most importantly, it demonstrates that tuning the strength of the saccharide-boronic acid interaction can be used to alter transport through the lipid-filled pores. This tuning can be achieved through operating conditions (as in the case of pH), or the choice of boronic acid.

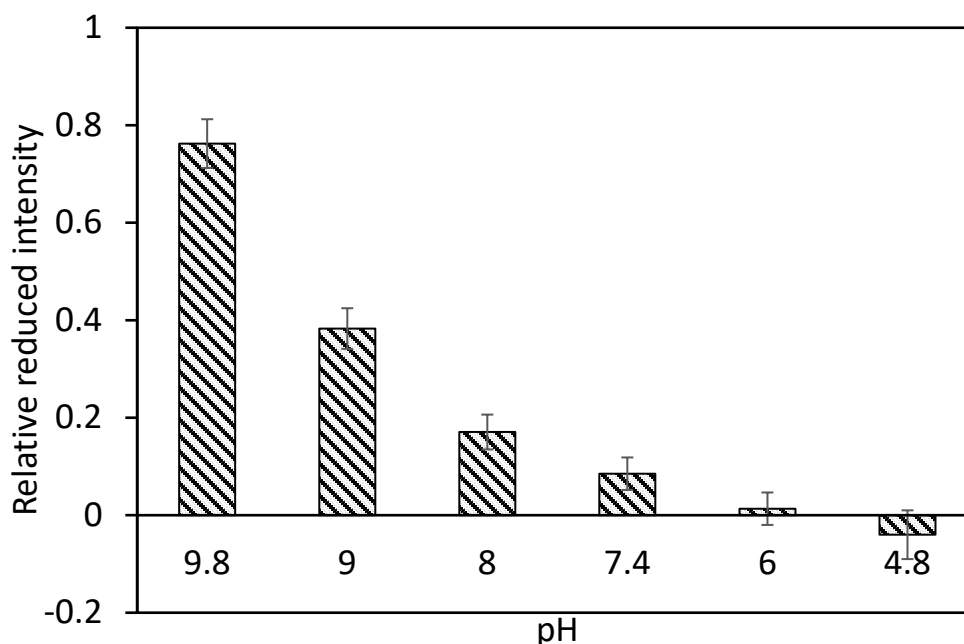


**Figure 3.9** Relative reduced fluorescent intensity after adding glucose to ARS-BA complex (fluorescent) to competitively form ARS-glucose (no fluorescent) as a function of pH. (Fluorescence intensity change was normalized to the original intensity at experimental pH. Error based on three replicates).

Boronic acid as carbohydrate carrier has previously been incorporated into liquid membranes consisting of 2-nitrophenyl octyl ester supported by flat sheet of porous polypropylene for sugar separation. Duggan, Houston [91] reported a glucose flux of  $0.54 \times 10^{-8} \text{ mol/m}^2/\text{s}$  using 50 mM 2-(aminomethyl)-phenylboronic acid through supported liquid membrane at neutral pH, when the feed concentration of glucose was 300mM. Glucose flux increased more than ten-fold when pH gradient was applied (pH of 11.3 on donor side and pH of 6.0 on receptor side), which is consistent with the pH effect seen in this work. Compared to the supported liquid membrane, the boronic acid immobilized in lipid filled silica membrane present a glucose flux of  $225 \times 10^{-8} \text{ mol/m}^2/\text{s}$  at normal condition (neutral pH and room temperature), which is almost 400 times greater than that

of liquid membrane. In addition to the significant glucose flux difference, the liquid membrane has stability problems as the organic phase is held in the support pores by capillary force.[87] Besides, Luccia, Smith [10] reported that glucose flux reduced about half times after 48 hours of transport due to the hydrophobicity difference between organic solvent and carrier, causing carrier to leach out the membrane during the transport.[10] As a result, quaternary ammonium salt is often added to improve the boronic acid solubility in the liquid membrane. It was found that the addition of Aliquat 336 (trioctylmethylammonium chloride) to the liquid membrane increased the glucose flux by two to ten-folds depending on the pH of solution, which was attributed to the better sugar-boronic acid complex solubility in the liquid membrane due to its stronger association with the Aliquat.[118] Meanwhile, the DSC result already showed that the boronic acid used is compatible with the lipid bilayers without introducing other additives to the sugar solution.

To demonstrate potential of the boronic acid immobilized lipid filled silica membrane to selectively separate carbohydrates representative of biomass hydrolysates, the flux of three carbohydrate is compared: glucose (six-carbon sugar), xylose (five-carbon sugars) and cellobiose (disaccharide of glucose) were measured (**Figure 3.10**). The effect of temperature (room temperature and 45°C) and pH gradient (pH 7.4 and a pH 10 (donor)/pH 5 (receptor) gradient) on the flux were also evaluated. As shown, xylose has the highest flux through the membrane while the flux of cellobiose is the lowest. The observation is consistent with the reported relative carbohydrate association constant ( $K_{eq}$ ) to the phenylboronic acid at neutral pH, which favors the complexation with xylose: xylose > glucose > cellobiose. [117] As expected, the flux of three sugars significantly increase as the temperature increases above phase transition temperature, while the permeability of

xylose and glucose over cellobiose are reduced slightly. The temperature change increases the overall fluidity of the lipid bilayers, which enhances the solute permeability regardless of their association constant difference and results in lower selectivity. In contrast, applying pH gradient results in the improvement of solute permeability and selectivity at the same time. Because the pH gradient directly changes the association constant which is specific to different type of carbohydrates, both the permeability and selectivity increases. The results demonstrate that the proposed boronic acid-mediated biomimetic membrane has potential for selective recovery of monosaccharides from the biomass hydrolysate.

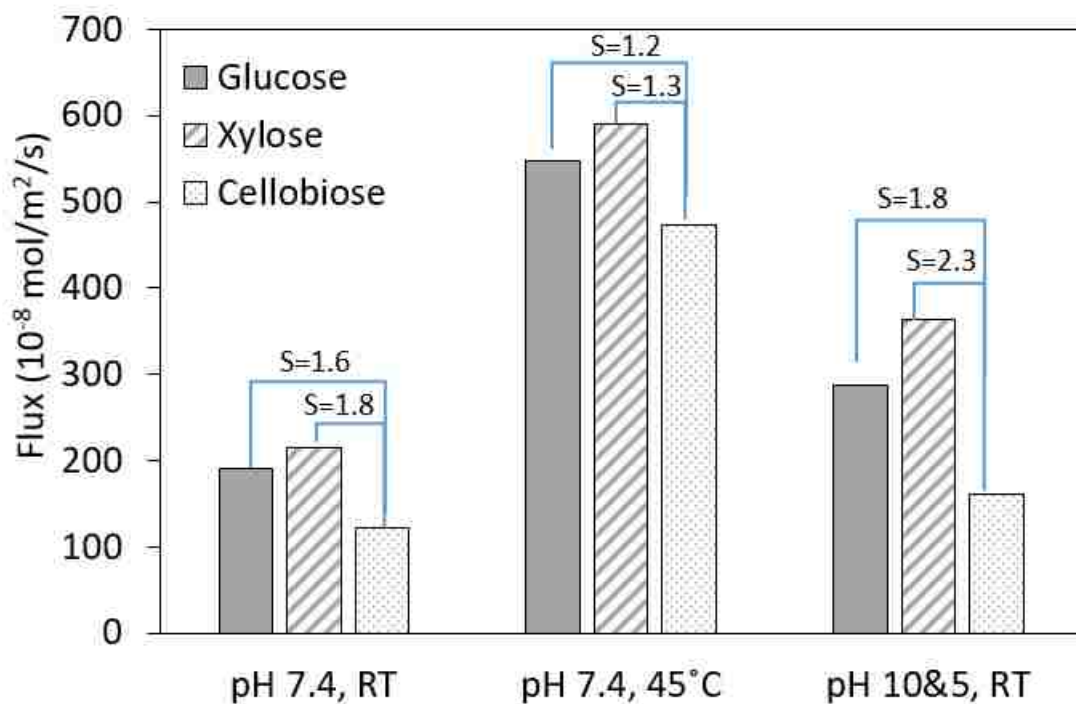


**Figure 3.10** Selective separation of carbohydrate mixture (5.6mM glucose, 5.6mM xylose, 5.6mM cellobiose) through boronic acid immobilized lipid filled membrane at as a function of temperature (room temperature versus 45oC) and pH (pH 7.4 versus a pH 10 (donor)/pH 5 (receptor) gradient. (Sampling time: 2 h, S=Selectivity).

### 3.5 Conclusion

Lipid pore-filled silica thin film membrane with a lipid-immobilized carrier is successfully demonstrated to facilitate the transport of hydrophilic molecules. These robust lipid-filled mesoporous membranes act as barriers to ions and small hydrophilic solutes that can be matched with biomimetic carriers to provide selective transport as a separation and sensing platform. Relative to traditional supported lipid bilayers that reside on the external surface of the porous film, the lipid pore-filled membrane provides a better barrier which is critical for the carrier function in the membrane. A unique aspect of lipid-filled pore membranes is the temperature dependence of flux due to the gel to fluid lipid bilayer phase transition, which can be used as a temperature switch to increase or decrease mobility through the membrane. Opportunities to tune transport through the solute-carrier interactions can be used to manipulate the flux and achieve selective separations. In the case of carbohydrate-boronic acid mediated transport, the affinity-dependent transport suggests potential for separating sugars from dilute aqueous mixtures of processed biomass for the improvement of lignocellulose conversion to chemicals. More broadly, the biomimetic membrane which combines high surface area silica thin film membrane with selective permeable lipid bilayers has potential as an efficient aqueous-based separation technology through the selection of lipid-based carrier molecules.

## **Chapter 4: Impedance Analysis of Ion Transport through Supported Lipid Bilayers on Accessible Mesoporous Silica Thin Films**

### **4.1 Abstract**

Ion transport through supported lipid bilayers and lipid-confined pores on silica thin films is examined using Electrochemical Impedance Spectroscopy (EIS). The ability to quantify the accessibility of the pore structure of the mesoporous silica thin films, which is essential for the incorporation of proteins and small hydrophilic carriers for separation application and the transport of solute through a silica thin film membrane, is demonstrated. While EIS has previously been used to investigate the transport of ions through supported lipid bilayers on nonporous and microporous supports, limited investigations quantify ion transport through supported lipid bilayers that span mesoporous thin films and no previous investigations examine ion transport through lipid-filled mesoporous thin films. The choice of redox probe molecule is demonstrated to be critical to extending EIS ion transport through lipid enveloped and lipid filled mesoporous silica thin film with accessible, orthogonally oriented cylindrical pores, where pore structure was confirmed by grazing-incidence small-angle scattering (GISAXS). The system with pores filled lipid (1,2-dipalmitoyl-sn-glycero-3-phosphocholine, DPPC) is showed to be a superior barrier (18-fold higher resistance) compared to one with a bilayer deposited at the pore openings by vesicle fusion. The latter may have defects in the pore spanning bilayer as indicated by the EIS measurement using a neutral hydrophilic redox probe (1, 1'-ferrocenedimethanol, FDM), which is prevent by the lipid membrane. Meanwhile, the pore-confined lipid is found to provide a pathway for the diffusion of a hydrophobic redox probe (1, 1'-



dioctadecyl-4, 4'-bipyridinium dibromide, DBD) across the membrane, which provides a basis for study of the function of incorporated lipophilic carriers. The EIS is demonstrated to be a powerful technique for characterizing the configuration and ion transport through mesoporous silica thin film-supported lipid membranes, which provide insights for making better barriers on mesoporous supports for carrier-mediated membrane separation processes.

## 4.2 Introduction

As the barriers between cells and their external environment, biological membranes exhibit highly selective permeability that is maintained by its main component, amphipathic lipid molecules.[119] Because they have a cylindrical shape, lipid molecules tend to assemble into bilayers where the hydrophilic head is exposed to water and hydrophobic tail resides in a hydrophobic layer. The lipid bilayer allows hydrophobic molecules to pass through but is relatively impermeable to hydrophilic molecules (ions, charged macromolecules, carbohydrates, etc.).[120] Small and uncharged molecules (water, glycerol, urea etc.), although they are hydrophilic, can pass through fairly quickly.[34] Due to their selective permeability, artificial lipid bilayers that mimic biological membranes have great potential for applications in biosensing and selective separations.

In this context, porous supports which can provide reservoirs under the lipid bilayer to limit interactions between proteins and solid substrates become attractive.[56] Porous materials including alumina (55-280 nm pores), [69, 121, 122] silicon nitride (200-700 nm), [55] Teflon filters (5  $\mu\text{m}$ ), [123] silicon (0.2-2  $\mu\text{m}$ ), [121] and mesoporous silica (3-

12 nm)[56, 64] have been reported as lipid bilayer supports.[124] Among these, mesoporous silica thin films are highly biocompatible, and thus provide advantageous platforms to explore the functionality of protein or smaller lipophilic biomolecules incorporated in supported lipid bilayers for selective separations or biosensing. The surfactant templating technique provides the opportunity for synthesis of highly ordered mesoporous thin films with tunable nanopores, [11, 12] which can match the size of lipid bilayers[64] or transmembrane proteins.[56] In our previous work (**Chapter 3**), we successfully demonstrated the feasibility of lipid pore-confinement in silica thin film membranes with orthogonally oriented cylindrical pores (~10 nm) on a macroporous support to act as highly selective barrier. Furthermore, the functionality of a small model lipophilic carrier (boronic acid) incorporated in the pore-confined lipid barrier was confirmed. Isaksson et al.[56] also reported the successful deposition of a transmembrane protein (human aquaporin 4) supported in lipid bilayers deposited onto the surface of mesoporous silica thin film with cylindrical 6 nm diameter pores. This pore size accommodates the hydrophilic domain of the protein within the pores of the solid substrate.

While mesoporous silica thin films are a promising biomimetic platform for studying the function of proteins or small lipophilic carriers confined in lipid bilayers, systematic characterization of transport processes in this composite synthetic biomimetic membrane system is rarely reported. Electrochemical impedance spectroscopy (EIS) is a non-invasive and label-free technique permitting such an investigation of ion transport through membranes.[125] EIS is measured by applying an AC potential to the system of interest, where the resulting current perturbation reflects a series of transport processes happening between the aqueous phase and the electrode surface such as electron transfer, mass

transport and chemical reaction.[65, 73, 120] EIS has been widely applied in assessing the porous structure and ion diffusion within the pores of filtration membranes [66, 126] and ordered nanoporous thin films.[67] Also and perhaps more importantly, EIS has been used extensively to study the structure, stability, electrical insulating properties of lipid bilayers with or without incorporated ion channels on bare or surface modified gold electrodes [41, 59, 68] and porous materials.[69, 121, 122]

Here, silica thin films with orthogonally aligned hexagonal pore arrays, which offer continuous channels for molecule transport, were prepared on electrically conductive fluorine doped tin oxide (FTO) glass slides as lipid bilayer supports. The thin film pore accessibility, which is critical for transport applications, was characterized by electrochemical impedance spectroscopy (EIS). Furthermore, the effect of lipid bilayer preparation methods on the mass transport through lipid coated silica thin film (in the form of a bilayer deposited at the pore openings, which we refer to as “pore enveloping”, or pore filling) was explored, as a highly insulating lipid bilayer is essential for detecting activity of proteins or biomimetic carriers in the bilayer. To further examine the diffusion of charged carriers in the lipid membrane, the transport of hydrophobic probes through the two different types of supported lipid assemblies were compared. This study provides insights for the design of a robust biomimetic membrane platform for investigating the function of membrane proteins or peptides and small lipophilic carriers for biosensing and selective separation applications.

## **4.3 Experimental sections**

### **4.3.1 Material**

Tetraethyl orthosilicate (TEOS, 98%), fluorine doped tin oxide (FTO) coated glass, polyethylene oxide (PEO)-polypropylene oxide (PPO)-PEO triblock copolymer (P123, average  $M_n \sim 5,800$ ), glycerol ( $\geq 99\%$ ), 1,1'-ferrocenedimethanol (FDM, 97%), 1,1'-dioctadecyl-4,4'-bipyridinium dibromide (DBD, 97%), potassium phosphate buffer (PBS) tablets, chloroform ( $\geq 99\%$ ), and 1,6-diisocyanatohexane (DH, 98%) were supplied by Sigma Aldrich. Ethanol (anhydrous) was purchased from DLI and hydrogen chloride (HCl, 6N), acetone ( $\geq 99.5\%$ ), and potassium chloride (KCl,  $\geq 99.0\%$ ) were purchased from Fisher Scientific. 1,2-dipalmitoyl-sn-glycero-3-phosphocholine (DPPC,  $>99\%$ ) was purchased from Avanti Polar Lipids. Nochromix powder was purchased from Godax Laboratories, Inc.

### **4.3.2 Synthesis of mesoporous silica thin film supported by fluorine doped tin oxide (FTO) coated glass**

For electrochemical measurements, mesoporous silica thin films were prepared on electrically conductive FTO coated glass slides. Prior to deposition of silica thin films, FTO slides were cleaned with DIUF water, acetone, and isopropanol followed by UV-ozone treatment for 20 min to remove any organic contaminants. Thin film silica membranes with orthogonally oriented pore array were synthesized using a neutral chemical surface method as previously reported by Wooten et al. [33] and Koganti et al.[98] To make a neutral chemical surface, a solution was prepared using 0.696 mmol/L P123 in acetone, to which an equimolar amount of 1, 6-diisocyanatohexane was added with continuous stirring in a nitrogen bag. Three drops of glycerol were then added and stirred for 10 minutes. The

resulting solution was used to dip coat clean FTO slides or borosilicate glass slides (cleaned with Nochromix solution) to create chemically neutral surfaces for sandwiching the membranes. The dip coated supports were aged at 100°C for 24 hours to cure the modifying layers.

The mesoporous silica coating solution was prepared by addition of a solution of P123 to a prehydrolyzed silica sol following the procedure of Brinker et al.[99] TEOS, anhydrous ethanol, deionized ultra-filtered water and HCl were added together in a mole ratio of 1: 3.8: 1:  $5 \times 10^{-5}$ . This solution was refluxed at a temperature of 70°C for 90 minutes. A final amount of HCl and water were added yielding a concentration of 7.34 mM HCl. The mixture was stirred at room temperature for 15 minutes. The mixture was then aged at 50°C for 15 minutes. A solution of P123 and ethanol in a mole ratio of 0.01: 18.7 was then added to the TEOS mixture and stirred for 10 minutes. The final mole ratio was 1 TEOS: 22 C<sub>2</sub>H<sub>5</sub>OH: 5 H<sub>2</sub>O: 0.004 HCl: 0.01 P123. The copolymer modified FTO slides were dip coated using the final solution at a speed of 7.6 cm/min. To prepare orthogonally oriented pores, the silica thin film-coated modified FTO slides were then sandwiched between two chemically modified glass surfaces. The thin films of silica on FTO slides were aged and dried at 50°C for 24 hours and then 100°C for 24 hours. The films were then calcined 500°C for 4 hrs with temperature ramping from room temperature at 1°C/min to remove the pore template and crosslinked pore blocking polymer. Thin film silica membranes with parallel oriented pore were also prepared by dip coating the sol-gel solution on FTO slides that were not modified with the copolymer/DH film. Nonporous silica thin films were prepared by dip coating the sol-gel solution without surfactant P123 onto unmodified FTO slides.

### **4.3.3 Silica thin film characterization**

Grazing-incidence small-angle scattering (GISAXS) was used to characterize the pore orientation of the silica thin film after calcination. GISAXS experiments were done at the Advanced Photon Source (APS) at Argonne National Laboratory on beamline 8-ID-E using a X-ray beam size of 100  $\mu\text{m}$  x 50  $\mu\text{m}$  (H x V) with wavelength of 1.687 Å and a sample-detector distance of 1474 mm. The GISAXS pattern was collected at room temperature with a Pilatus 1M pixel array detector using a 6 s exposure time at an incidence angle of 0.17°. The corrected data were analyzed using the GIXSGUI package for MATLAB.

### **4.3.4 Lipid filled silica thin film preparation through evaporation deposition**

First, 10 mg of DPPC were dissolved in 7 mL  $\text{CHCl}_3$ . A silica thin film-coated FTO slide was then immersed in the DPPC solution and sonicated for 25 minutes in a cylindrical vial (25 mm  $\times$  95 mm). The above mixture was then blow-dried with flowing nitrogen and was further dried under high vacuum at room temperature for at least 2 hrs. To form bilayers, the dried lipid inside the silica membrane was rehydrated in 7 mL PBS solution and sonicated at 47 °C for 1 hr. The sample was sonicated for another 15 minutes while cooling to 30 °C. The excess lipid was removed by washing the membrane with PBS three times.

### **4.3.5 Lipid enveloped silica thin film preparation through vesicle fusion**

10 mg of DPPC was dissolved in 1 mL  $\text{CHCl}_3$ , placed in a glass vial, and the solvent was removed under flowing air for 1 hr. The deposited DPPC was further dried under high vacuum at room temperature for at least 2 hrs. Then the dried lipid was rehydrated in 1 mL PBS solution to form multilamellar vesicles. The resulting mixture was extruded at 45 °C

through a polycarbonate filter with 200 nm diameter pores 21 times, which produces small unilamellar vesicles with a mean diameter of 200 nm. The lipid solution was diluted to 7 mL, and then mixed with a silica thin film-coated FTO slide for 30 mins to facilitate vesicle fusion. The excess lipid was removed by washing the membrane with PBS three times.

#### **4.3.6 Electrochemical measurement**

The silica thin film pore accessibility and ion transport through lipid coated silica thin film were characterized by electrochemical impedance spectroscopy (EIS), according to the procedure of Wei and Hillhouse.[67] The measurements were conducted in an electrochemical cell (**Figure 4.1a**) with three electrodes, which were connected to a potentiostat (CHI 660D, CH Instruments, Inc.). Bare or lipid-coated silica thin films on FTO slides were used as working electrodes, while a platinum wire and an Ag/AgCl electrode were used as counter and reference electrodes, respectively. Ion transport of a hydrophilic probe 0.01 mM 1,1'-ferrocenedimethanol (FDM) or a hydrophobic probe 1,1'-dioctadecyl-4, 4'-bipyridinium dibromide (DBD) was measured in 0.5 M KCl in PBS buffer (pH 7.4) as the electrolyte. The area of the silica thin film exposed to the electrolyte solution was 4 cm<sup>2</sup>. The formal reduction potential of FDM<sup>+</sup>/FDM redox couple for EIS measurement was determined to be 0.21 V by cyclic voltammetry applying a potential between -0.1 and 0.6 V at a scan rate of 50 mV/s to the sample. The EIS was measured over a frequency range of 0.1 Hz to 100 kHz with a dc potential of 0.21 V and an ac perturbation signal of 10 mV at room temperature. The data obtained were fitted to an equivalent circuit model (**Figure 4.1b**) using software Z-view.

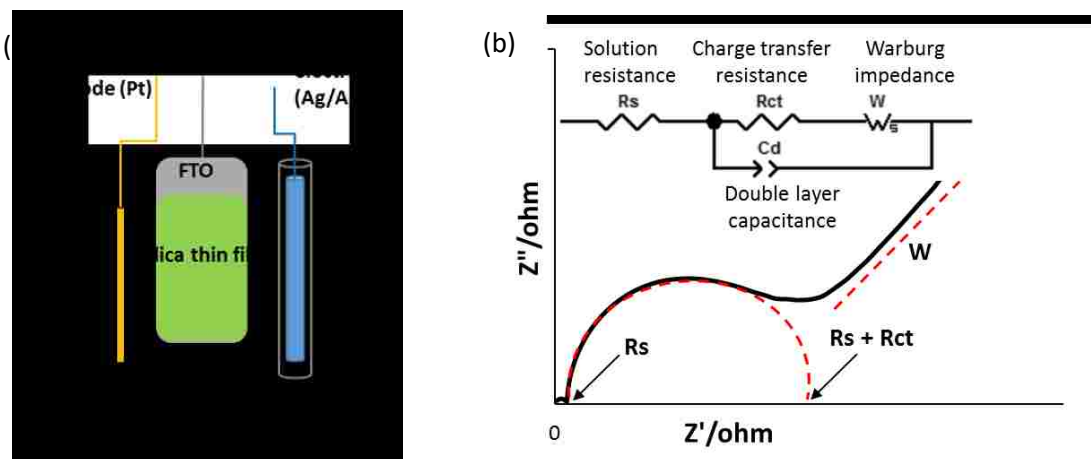


**Figure 4.1** (a) Electrochemical cell setup for EIS measurement; (b) Impedance spectrum and corresponding equivalent circuit model for silica thin film.

## 4.4 Results and discussion

### 4.4.1 Electrochemical analysis of the mesoporous silica thin film structure

Before evaluating pore accessibility of silica thin films by electrochemical impedance spectroscopy (EIS), the pore morphology of the films was first characterized by grazing-incidence small-angle scattering (GISAXS). **Figure 4.2** shows representative 2D GISAXS patterns of silica thin films with parallel oriented (p-HCP) and orthogonally oriented (o-HCP) hexagonal close packed pores after calcination to remove the surfactant template. For the silica thin film prepared on an unmodified surface, two out-of-plane diffraction spots of low intensity are observed on both sides of the beam stop, which are indexed to the  $(\bar{1}1)$  and  $(11)$  reflections of a distorted 2D hexagonal mesostructured with  $c2mm$  space group oriented parallel to the glass slide.[78] The intense spot right above the beamstop ( $q_z \sim 0.2 \text{ \AA}^{-1}$ ) corresponds to the  $(02)$  reflection. On the other hand, two intense in-plane rods parallel to the x-ray beam and no out-of-plane diffraction spots are seen for the silica thin film prepared on a chemically neutral surface, which is consistent with an orthogonal pore orientation.[80, 127] From the GISAXS patterns, the diffraction spots for parallel



oriented and orthogonally oriented silica thin film are observed at  $q_y$  of  $0.13 \text{ \AA}^{-1}$  and  $0.063 \text{ \AA}^{-1}$ , respectively, which corresponds to d-spacing of 4.82 nm and 9.95 nm. [128]

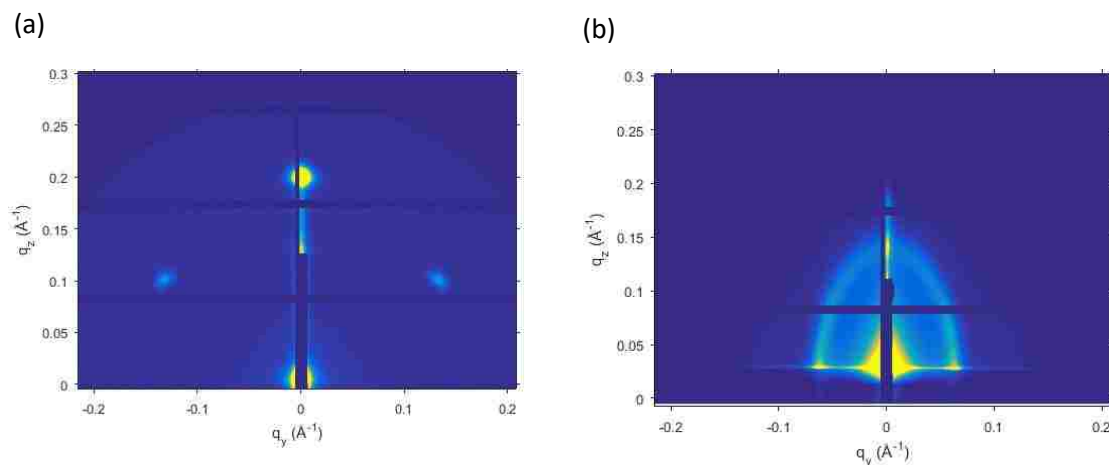


**Figure 4.2** 2D GISAXS patterns of (a) parallel oriented; (d) orthogonal oriented mesoporous silica thin film after calcination.

The effect of mesoporous structure on mass transport through the silica thin film was investigated with EIS. Due to the negative charge of the silica surface, the transport of anionic redox species in mesoporous silica thin films is restricted by electrostatic repulsion in the addition to the influence from the film structure itself.[129] To eliminate the electrostatic repulsion, the positively charged/neutral redox species  $\text{FDM}^+/\text{FDM}$  was chosen as the probe molecule while controlling the system pH at 7.4.[67] After applying a small amplitude ac potential to the system, the complex impedance ( $Z(\omega) = Z' + j Z''$ ) can be extracted from the resulting ac current and presented in the complex plane (giving a Nyquist plot or impedance spectrum, **Figure 4.1b**). The impedance spectrum can be analyzed using the simple equivalent circuit model  $R(\text{RCW})$ , which contains four elements: an electrolyte solution resistance ( $R_s$ ), which is ideally given by the intercept of the small leftmost semicircle with the x-axis; charge transfer resistance ( $R_{ct}$ ) representing

the electron transfer rate between the redox species and the electrode at the interface, which can be estimated from the diameter of the larger semicircle; mass transfer impedance ( $W$ ) representing the 1D semi-infinite diffusion of electrolyte in the bulk phase, which appears as a straight line following the semicircle ; and electrical double layer capacitance ( $C_d$ ) at the electrolyte-sample interface.[73, 74]

**Figure 4.3** presents the Nyquist plots of the bare FTO electrode, o-HCP silica, p-HCP silica and nonporous silica thin film on FTO. The corresponding parameters obtained by fitting the spectra to the equivalent circuit model using *Z-view* software are shown in **Table 4.1**. All samples present a typical spectrum profile, with the straight line following the semicircle gradually becomes shorter as the electrode accessibility is reduced, due to the limited range of frequencies probed. The solution resistance  $R_s$ , which represents resistance associated with ion migration in the solution, is similar for different substrates measured in the same electrolyte solution. The charge transfer resistance  $R_{ct}$  is directly related to the electrode area accessible to the electrolyte.[130] As shown,  $R_{ct}$  is the lowest for the bare FTO electrode, which is consistent with the full accessibility to the electrolyte. At the opposite extreme,  $R_{ct}$  is highest for the nonporous silica membrane because the electrode is completely covered by the silica, thus preventing electron exchange between the redox probe and electrode. The charge transfer resistance for mesoporous silica with orthogonal or parallel orientation is significantly reduced compared to nonporous silica, indicating the existence of accessible pores. The o-HCP silica film shows much smaller  $R_{ct}$  than the p-HCP film, which is consistent with the orthogonally oriented cylindrical pore offering a direct pathway to transport redox probes to the electrode surface. Although, the pores of p-HCP silica are buried under silica membrane surface, the existence of micropores in the

silica walls and defects in the mesopore structure most likely permit some charge carrier transport, giving  $R_{ct}$  between that of o-HCP silica and nonporous silica. Thus, EIS provides results consistent with the morphology of the mesoporous silica thin films inferred from GISAXS.

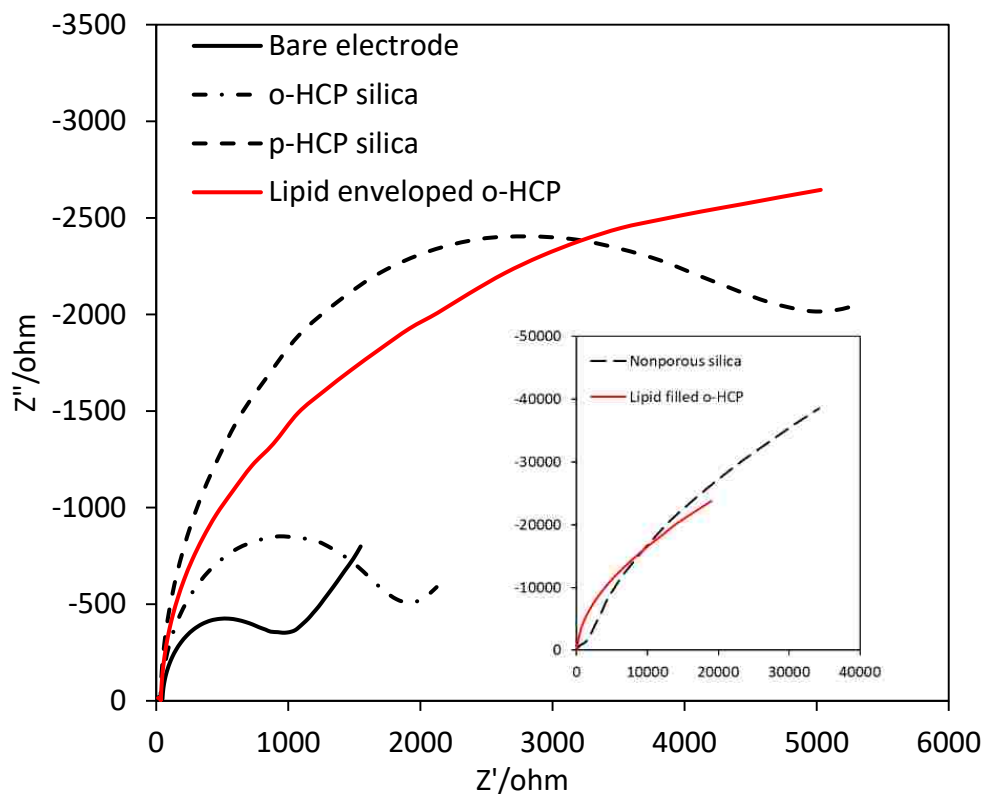


**Figure 4.3** Nyquist plots of silica thin films with different pore structures and lipid enveloped o-HCP silica on FTO electrodes measured using the hydrophilic redox probe (FDM). The insert presents the Nyquist plots for the nonporous silica and lipid filled o-HCP silica on FTO.

**Table 4.1** Resistance and active electrode areas of silica thin films with varying structures and lipid supported by o-HCP silica estimated by an equivalent circuit model R (RCW) for EIS measurements with hydrophilic probe FDM. (Error based on three samples).

Substrate	Bare FTO	o-HCP	p-HCP	Nonporous	Lipid enveloped	Lipid filled
$R_s(\Omega \cdot \text{cm}^2)$	$144 \pm 3$	$152 \pm 1$	$140 \pm 10$	$130 \pm 30$	$125 \pm 2$	$140 \pm 20$
$C_d(\mu\text{F}/\text{cm}^2)$	$12 \pm 3.2$	$9.6 \pm 0.1$	$9.0 \pm 0.0$	$8.0 \pm 2.7$	$8.9 \pm 0.2$	$8.2 \pm 1.3$
$R_{ct}(\Omega \cdot \text{cm}^2)$	$2500 \pm 960$	$7200 \pm 1100$	$23000 \pm 1900$	$681000 \pm 120000$	$20700 \pm 2600$	$137000 \pm 25000$
Active electrode area (1- $\theta$ )	1	$0.36 \pm 0.06$	$0.11 \pm 0.01$	$0.004 \pm 0.007$	---	---

According to Wei and Hillhouse, [67] the effective unblocked electrode area of mesoporous silica thin film coated FTO electrode is inversely proportional to  $R_{ct}$  for a given electrolyte concentration and sample area. Thus, the active electrode coverage can be estimated by dividing the bare electrode resistance by the resistance of a silica thin film when measured under identical conditions. The active electrode coverage (1- $\theta$ ) of p-HCP silica and nonporous silica thin film coated FTO were calculated to be 0.11 and 0.004, respectively (**Table 4.1**), values which are close to those reported for parallel oriented silica templated by P123 and dense silica.[67] For o-HCP silica, which hasn't been examined in existing literatures using EIS, the active electrode coverage is about 0.36, falling between that of a body centered cubic (BCC) silica film (0.55) and double-gyroid silica film (0.33).

However, the large pore accessibility doesn't necessary result in faster diffusion. It was found that the double-gyroid structure had a diffusion coefficient one order of magnitude higher than the BCC structure, which has a more torturous structure that impedes diffusion.[67] Thus, the active electrode coverage needs to be considered in

combination with the actual structure of the silica thin film to gain a full understanding of the silica thin film. The o-HCP silica with orthogonal oriented channels is expected to provide a continuous pathway for probe molecules to easily transport to the electrode surface, while providing significant pore accessibility. Shunsuke et al.[130] also found the charge transfer resistance decreased with increasing degree of order and length of the hexagonally ordered mesoporous carbon channels as assessed by EIS. Therefore, the mass transport through the mesoporous thin film are dependent on pore size, length and tortuosity, which can be reflected in the EIS measurement.

#### **4.4.2 Electrochemical analysis of lipid supported by mesoporous silica thin film**

To examine the effect of lipid bilayer preparation methods (in the form of pore enveloping, or pore filling) on mass transport through biomimetic membranes with accessible pores, impedance spectra were compared for bare, lipid enveloped, and lipid filled o-HCP silica using the hydrophilic redox probe (FDM) (**Figure 4.3**). For direct comparison, the same equivalent circuit model was also used to analyze EIS spectra both bare and lipid-coated silica thin films. The resulting resistances reflect the effects of lipid bilayer in relation to the accessible pores of the bare silica thin film (**Table 4.1**). As expected, both lipid enveloped and lipid filled silica have a greater charge transfer resistance,  $R_{ct}$ , compared to the bare o-HCP silica (2-fold and 18-fold higher, respectively), indicating the successful formation of a lipid assembly that shields accessible pores from the redox groups. Furthermore, the resistance of lipid filled silica is six-fold higher than that of lipid enveloped silica, and falls between that of p-HCP and nonporous silica.

In addition, the phase angle profile (**Figure 4.4**) shows a dramatic increase in the phase angle at low frequencies (0.1-10 Hz) after lipid deposition onto the silica support (lipid

filled>lipid enveloped). This increase corresponds to a decrease of the membrane capacitance and better electrically insulating behavior due to addition of lipids.[55, 70] These observations suggest that confining the lipid inside the pores could have resulted in a more cohesive, defect free lipid structure than an “enveloped” lipid bilayer suspended on the pore surface via vesicle fusion. Although the resistance of lipid enveloped silica was not as great as lipid filled silica, its resistance is still comparable to that of p-HCP silica, suggesting the lipid bilayers suspending on the pore are able to block most of the pores. However, there may be defects on the bilayer, which makes the electrode partially accessible to the redox probes.

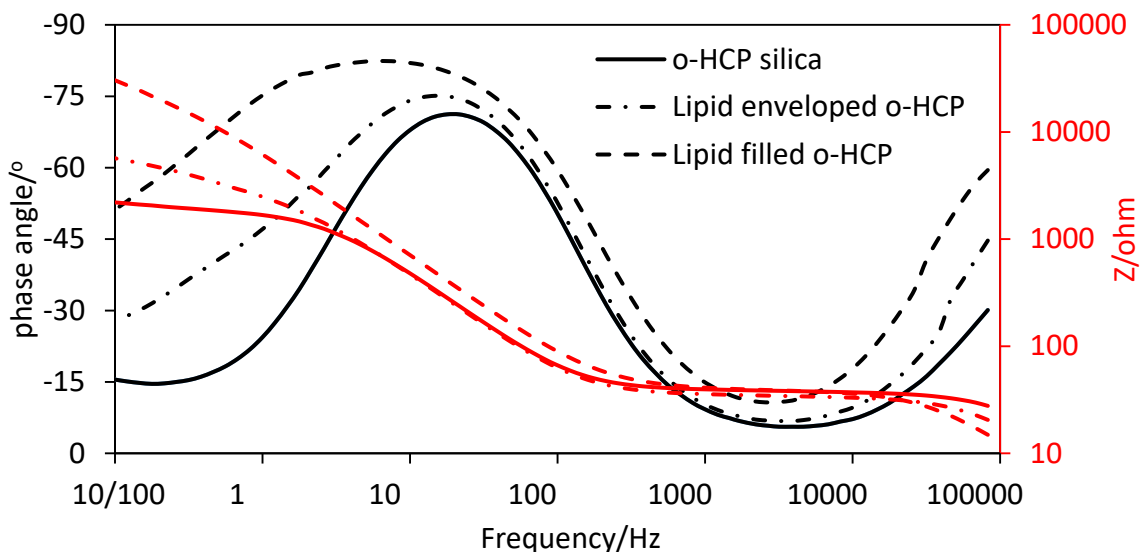


**Figure 4.4** Phase angle (black) and absolute impedance (Z, red) profile with experimental frequency for bare, lipid enveloped, lipid filled o-HCP silica on FTO electrode. The probe for this measurement was FDM.

In a previous study,[131] the capacitance from EIS of a lipid bilayer supported on gold electrode was reported to be about  $0.5 \mu F/cm^2$ . The bilayer structure was then confirmed by modeling the bilayer as a plate condenser and calculating the corresponding thickness

( $\delta$ ) with **Eq. 4.1** to be 3.62 nm (where the vacuum permittivity  $\epsilon_0=8.85\times 10^{-14} F/cm$  and the dielectric constant was assumed to be  $\epsilon =2.05$ ).[132] This thickness is consistent with the bilayer thickness measured by AFM.[133] However, the capacitance estimated here for the lipid bilayer suspended on the mesoporous silica surface (about  $50 \mu F/cm^2$ ) is much higher than the theoretical value. This can be attributed to the small pore size of the support. Pantoja et al.[134] found that the capacitance of lipid bilayers suspended on microporous silicon wafers increased from  $0.4 \mu F/cm^2$  to  $1 \mu F/cm^2$  when the pore size decreased from  $200 \mu m$  to  $50 \mu m$ . The increase of capacitance was attributed to the increase of bilayer area for small pores.[134] Zhu et al.[55] also reported an average capacitance of  $5.9 \mu F/cm^2$  for lipid bilayers suspended on silicon nitride with pore sizes of 200 nm, 400 nm and 700 nm. Thus, the silica thin film with pores an order of magnitude smaller ( $\sim 10$  nm) could have result 10-fold higher capacitance.

$$C_m = \frac{\epsilon \cdot \epsilon_0}{\delta} \quad (4.1)$$

The high capacitance could also result from the incomplete fusion of ruptured bilayer patches, leading to the defects in the bilayer.[122] The existence of pinhole defects in supported lipid bilayers have been revealed by AFM.[96] These defects increases the water occupancy in the bilayer, which has a much higher dielectric constant than lipid and results in higher capacitance.[57] In fact, the surface coverage of the lipid bilayer may be estimated from the overall capacitance ( $C_m$ ) of lipid bilayer with defect, assuming the bilayer capacitor and the defect (water) capacitor act in parallel.[122] Similarly, the incorporation of proteins in bilayers, which also have a higher dielectric constant than lipids, also was reported to give higher capacitance by Giess et al.[135] And the approximate concentration of incorporated proteins can be estimated based on the

measured capacitance. Despite the structure defects, pore-suspending lipid bilayer supported by mesoporous silica thin film is still promising for providing a reservoir for examining the function of transmembrane protein. Strategies to eliminate defects include surface modification and using charged lipids, changing the lipid composite, or changing the deposition method.[96, 97]

Tantawi et al.[121, 136] reported that the resistance of 3  $\mu\text{m}$  thick porous silicon membranes with mean pore diameters of 0.50-2  $\mu\text{m}$  increased from 40  $\text{k}\Omega \text{ cm}^2$  to 250  $\text{k}\Omega \text{ cm}^2$  after Langmuir-Blodgett deposition of lipid bilayers consisting of 1,2-diphytanoyl-sn-glycero-3-phosphoserine (DPPS) and 1,2-diphytanoyl-sn-glycero-3-phosphoethanolamine (DPPE). The composite system proved to be insulating enough to detect the function of epithelial sodium channel (ENaC) proteins.[124] In addition to porous supports, tethered bilayer lipid membrane (tBLM) prepared on metal electrode surfaces are commonly used as model systems to provide good barrier properties for examining the functional incorporation of proteins.[62] tBLMs are reported have resistances ranging from 0.5~10  $\text{M}\Omega \text{ cm}^2$  with varying lipid composition, while the resistance of a tethered monolayer spacer is about 1  $\text{M}\Omega \text{ cm}^2$ .[59, 62, 137] Although many tBLMs are superior barriers compared to porous substrate-supported bilayers, the tethering significantly reduces the lateral mobility of the lipid membrane and incorporated proteins.[58] Meanwhile, the lipid confined in nanopores of silica was found to have same mobility as the lipid at the external surface of a support.[64] Thus, the confinement of lipid in the pores of the mesoporous silica thin film appears to be a robust method to make defect-free lipid structure, while maintaining sufficient mobility for studying the function of incorporated proteins or small lipophilic carriers for separation application.



The movement of small-molecule hydrophobic carriers after complexing with targeted solutes in the lipid bilayer is a dominating factor to separation efficiency, which is affected by the lipid configuration on the support. Thus, to further examine the diffusion of the hydrophobic carrier in the lipid membrane (lipid enveloping and lipid filling), the electron transfer between a redox-active lipophilic molecule (1,1'-Dioctadecyl-4, 4'-bipyridinium dibromide, DBD) used by previous study[138] and the lipid coated o-HCP silica thin film supported by FTO electrodes was measured. **Figure 4.5** illustrates the impedance spectra of bare FTO, o-HCP, lipid enveloped o-HCP and lipid filled o-HCP silica films. In contrast to the hydrophilic redox probes FDM<sup>+</sup>/FDM, which are kept from away from the electrode surface after the formation of lipid bilayer resulting in increasing resistance increase (**Figure 4.3**), the lipophilic redox groups can partition into the lipid bilayer from the aqueous solution and favor electron transfer on the electrode surface. For the lipid filled o-HCP, the porous pathway are filled with lipid, which is more favorable for the transport of DBD across the composite membrane to reach the electrode surface than the water. Thus, a 3-fold reduction in resistance is seen for the lipid filled o-HCP comparing the bare o-HCP. Meanwhile, its resistance is still 2-fold higher than that of bare electrode surface, which is attributed to a thin water layer between the lipid and the electrode surface and to partial coverage of the surface by the o-HCP silica films. However, for the lipid enveloped o-HCP, no significant resistance reduction is seen compared to the bare o-HCP, which is consistent with the existence of a thin lipid bilayer suspending on the mesoporous silica thin film filled with water.

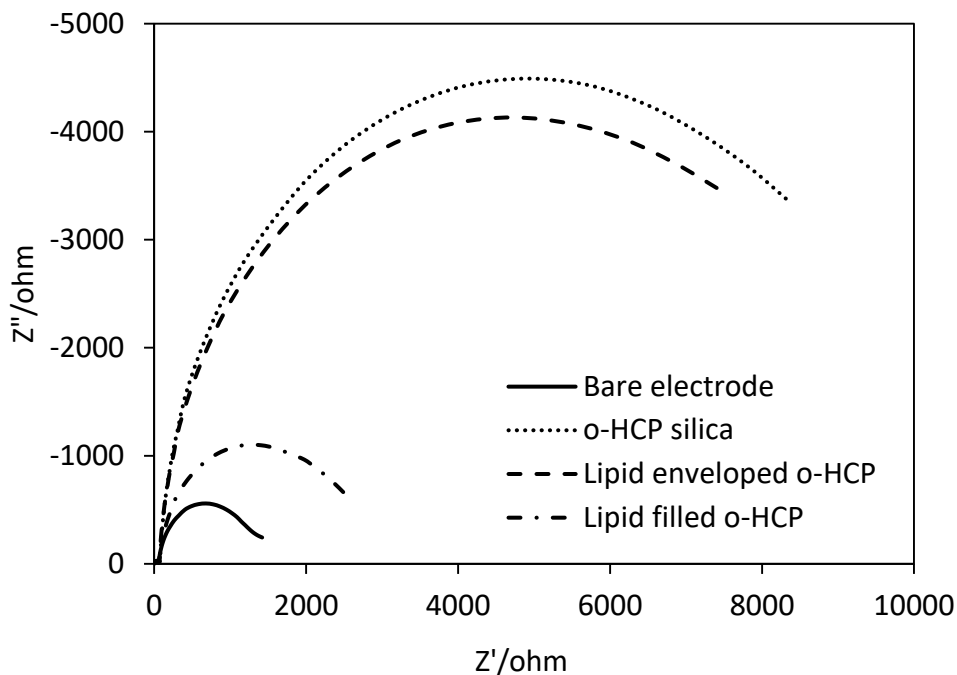


**Figure 4.5** Impedance spectra of FTO electrode, bare, lipid enveloped and lipid filled o-HCP silica using hydrophobic redox probes (DBD).

Prior studies of lipid-based biomimetic synthetic membranes focused primarily on lipid bilayers on a solid supports, black lipid membranes, tBLMs or polymer cushioned bilayers.[60, 62] Relative to the single lipid bilayer common to these studies, the pore confinement of lipid in the mesoporous thin film is demonstrated here to be an effective barrier. Significantly, lipid assemblies in pores provide a larger hydrophobic reservoir for the incorporation of small lipophilic carriers. In addition, the distribution of lipid throughout the mesoporous support creates a hydrophobic pathway for the fast transport of hydrophobic carrier-target complexes rather than an aqueous environment. This non-tortuous pathway for hydrophobic complexes is expected to be critical for many types of biomimetic separation. Furthermore, Schlipf et al.[64] found that the diffusivity of lipid confined in the pores of mesoporous silica particles at different locations (on the surface,

core, middle core of the particles) were identical. This suggest that the lipids are mobile throughout pores, which is important for the movement and reusability of carriers inside the lipid membrane.

#### **4.5 Conclusion**

Electrochemical impedance spectroscopy (EIS), a non-invasive and label-free technique, was successfully applied to examine the ion transport through mesoporous silica thin films and lipid assemblies supported on those films. Mass transport through mesoporous silica thin films with different pore morphologies could be readily distinguished by EIS, which is critical for screening separation platforms for constructing biomimetic membranes. The lipid deposition method (in the form of lipid enveloping or lipid filling), which results in different lipid membrane configurations, was found to have significant effects on the mass transport across the lipid membrane, as probed using EIS. Most significantly the lipid filled system, which is a new type of supported lipid architecture, is demonstrated to be a superior barrier while providing effective mobility for functioning small lipophilic carriers. The application of EIS to mesoporous silica thin film-supported lipid membranes enables the study of the fundamental properties of biomimetic membranes, which sets the stage for exploring the application of these confined lipid assemblies in biosensing, selective separations and drug delivery.

## **Chapter 5: Enzyme Immobilization on Synthetic Biomimetic Membranes for Dilute Aqueous Solute Upgrading and Recovery**

### **5.1 Abstract**

Biomimetic inspired synthetic membranes have been developed which employ carriers in lipid bilayers to control the permeability of hydrophilic solutes through nanoporous supports. To further enhance the selectivity of these composite membranes and add catalytic functionality, this work explores covalent bonding of enzymes onto orthogonally oriented hexagonally close packed (HCP) silica films on macroporous membrane supports. Transport of the product through the silica thin film membrane is then facilitated by the carrier immobilized in the lipid bilayer, with a goal of achieving upgrading and recovery of aqueous solutes in a one-step process. In this study, the conversion of glucose to fructose using glucose isomerase (GI) was used as a model system. FTIR analysis confirmed the immobilization of the enzyme on the epoxy group modified silica membranes, which demonstrated higher stability compared to physical enzyme adsorption. The integration of immobilized enzyme with the biomimetic separation membrane effectively enhanced the initial reaction rate of enzyme from 0.06 mM/h to 0.16 mM/h, comparing to enzyme immobilized on bare silica membrane. Fructose, a desirable starting point for the catalytic upgrading of biomass hydrolysate solutions, was transported through the membrane by the boronic acid carrier. However, product with high purity cannot be achieved in the lab scale static diffusion study. To evaluate the ability of enzyme immobilized synthetic biomimetic membranes to achieve high selectivity and productivity through further optimization of the performance parameters, a general mathematical model was developed to describe

the reaction and mass transfer through the biocatalyst and carrier-mediated separation integrated membrane. The model was parameterized using Thiele modulus which describes the reaction and diffusion process in the enzyme layer and relative permeability between the product and substrate in the selectivity separation membrane. The model is proven to give a precise prediction of the reaction and separation process and factoring dominating the process can be identified and manipulated to achieve better performance.

## **5.2 Introduction**

In pharmaceutical and food industries, biocatalytic processing is used to achieve efficient production using low value added or dilute products as a starting point. These feed streams are particularly challenging for commercialization. A promising technology for low cost and high yield and purity product yield is to combine the reaction and selective separation in a single membrane operation.[139] Integrated reaction-separation membranes are easy to scale up, are low energy consumption and are cost effective due to the continuous process and reusability of immobilized enzyme, which reduces capital investment, maintenance and operation. In addition, the combination of biocatalysis with selective separation membranes (i.e., enzymatic membrane reactors) allows selective removal of products in real time, resulting in low product concentration at the reaction site.[140-142] This low product concentration drives equilibrium-based reactions forward and reduces inhibition of the biocatalyst due to product formation, thus achieving higher reaction efficiency.[143] Furthermore, immobilization of enzyme onto the membrane support enhances the operational stability and reusability of enzyme, with potentially

improved activity, temperature and pH tolerance, and recovery efficiency , compared to the free enzyme.[144]

In this work, we are proposing continuous recovery and upgrading of dilute aqueous solutes utilizing a biocatalyst integrated biomimetic separation membrane, which is critical to the development of biotechnology applications. The biomimetic separation membrane is detailed described in **Chapter 3**, which utilized the pore confined lipid assemblies as barrier to exclude the solution and embedded carriers with specific binding to selectively separate the targeted solute. To integrate the biocatalyst and selective separation process, high surface area mesoporous silica thin films with ordered perpendicularly oriented hexagonally close packed (HCP) pore structure on a macroporous support is identified as potential upgrading and separation platform. The composite thin film membranes are chemically and mechanically robust, thermally stable, and the easy surface functionalization of silica surface provides various covalent coupling strategies for immobilizing the biocatalyst. Meanwhile, the hydrophilic surface of silica and large pore dimensions (~10 nm) allows the assembly of the lipid barrier inside the pores without interfering with immobilized enzyme on the surface.[64] Specifically, the upgrading and recovery of carbohydrates has been chosen to prove the concept of proposed biocatalyst-selective separation integrated membrane (**Figure 5.1**). Isomerization of glucose, which is the main hydrolysis product of cellulose, to fructose is important for producing value added chemicals. The HMF (5-hydroxymethyl-furfural) is a potential dehydration product of carbohydrates using a metal oxide catalyst, and its production is mainly limited by the fructose yield converting from glucose [145]. The isomerization of glucose to fructose, which is catalyzed by glucose isomerase enzyme, a reversible reaction commonly

employed to produce high fructose syrup in food industry. [146] The buildup of product will slow down the reaction rate and limit the glucose conversion.[147] In the case of dilute aqueous systems, immobilization of the glucose isomerase to the selective separation membrane allows the continuous removal the fructose from enzyme immobilized layer of the membrane by the boronic acid carrier, which has a higher affinity for fructose than glucose, thus improving the glucose conversion. The one-step production of fructose is a novel method to make use of membrane technologies to upgrade dilute aqueous solutions, applied specifically to improve biofuel production efficiency.

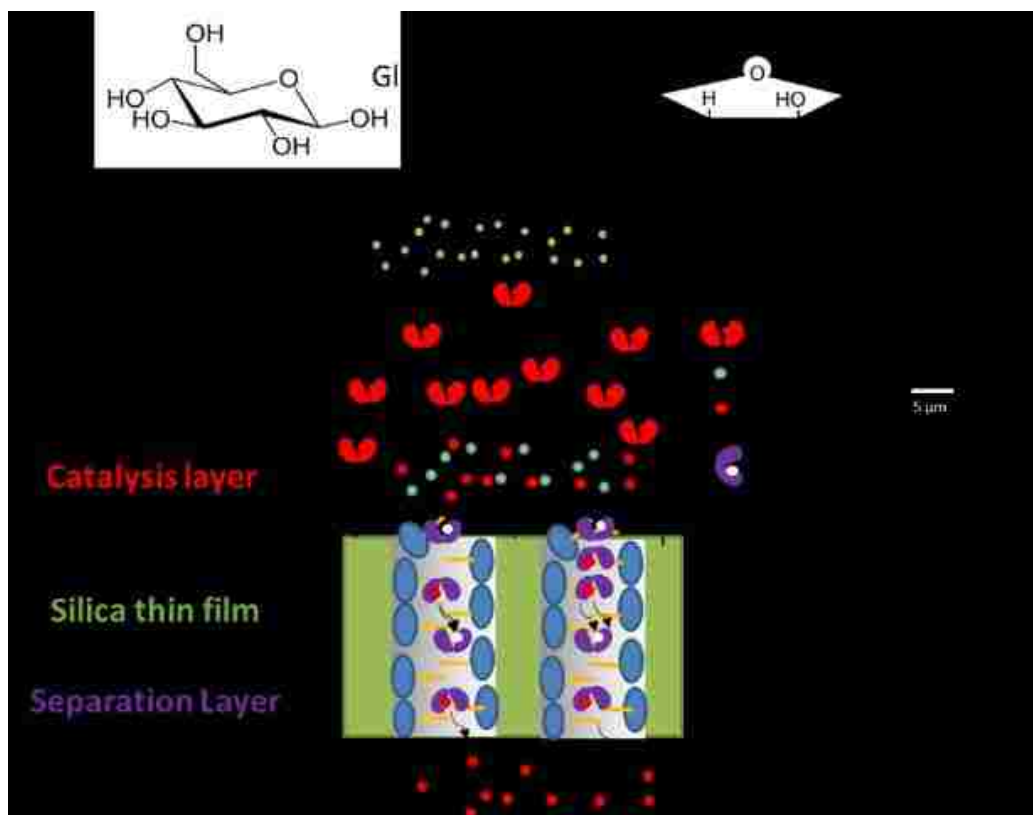


**Figure 5.1** Scheme for recovery and upgrading of the fructose from glucose using an enzyme-immobilized biomimetic integrated membrane.

Due to the high complexity of the reaction-separation integrated process, parameters involved in either the reaction or transport steps through the membrane will impact the other process. For example, Xu et al.[148] found that the initial hydrolysis activity of immobilized lipase on CA (cellulose acetate)/PTFE (polytetrafluoroethylene membrane) first increased then decreased with the increasing of enzyme loading. This was attributed to the blocking of membrane pores by the high enzyme loading, which limited the diffusion of the product through membrane. Concurrently, the slow diffusion increased the enzyme inhibition due to increased product concentration in the immobilized enzyme layer. In addition, although high reaction temperature is favorable for diffusion, the thermal denaturation of immobilized enzyme may need to be considered in this context. Thus, the factors like membrane structure, membrane pores relative to the enzyme size, enzyme immobilization method and loading concentration, and operation conditions (initial substrate concentration, pH, temperature, and flow rate) must be optimized to adjust the relationship between the enzyme activity and the product transport through the separation membrane to ensure the productivity of the composite membrane.[140]

In this work, the effectiveness of an enzymatic membrane reactor with integrated biomimetic separation for one-step upgrading and separation of dilute aqueous solutes is demonstrated. Glucose isomerase is covalently bound to the thin film silica through the epoxy group grafted silica surface. The stability of the covalently immobilized enzyme is compared to physical adsorption is characterized by FTIR. The glucose conversion and transport through the enzyme immobilized selective separation membrane (boronic acid immobilized lipid filled membrane) is quantified using a static diffusion cell. Additionally, a mathematical model is proposed to describe the chemical reaction and selective mass



transfer through the composite membrane for evaluating the effect of particular parameters on the two processes and identifying the dominant factors in membrane performance. The model will serve as a useful tool for predicting the purity and yield of the desired product and optimizing operation conditions between the reaction and selectivity of the carrier-mediated separation membrane. The model, parameterized using Thiele modulus which describes the reaction and diffusion process in the enzyme layer and the relative permeability between the product and substrate in the selectivity separation membrane, is not limited to this model enzyme/biomimetic carrier system, and is broadly applicable to the design of reactive membranes.

## **5.3 Experimental methods**

### **5.3.1 Material**

Anodic aluminum oxide (AAO) membranes (Whatman, 25 mm in diameter) with pores of approximately 200 nm in diameter, a porosity of 0.25-0.5, and a nominal thickness of 60  $\mu\text{m}$  was purchased from Fisher Scientific and served as the macroporous support for the silica thin film. Tetraethyl orthosilicate (TEOS, 98%), polyethylene oxide (PEO)-polypropylene oxide (PPO)-PEO triblock copolymer (P123, average  $M_n \sim 5,800$ ), glycerol ( $\geq 99\%$ ), potassium phosphate buffer (PBS) tablets, chloroform ( $\geq 99\%$ ), 1, 6-Diisocyanatohexane (DH, 98%), and glucose ( $\geq 99.5\%$ ) were purchased from Sigma Aldrich. Ethanol (anhydrous) was purchased from DLI and acetone ( $\geq 99.5\%$ ) was purchased from Fisher Scientific. 4-(N-Boc-aminomethyl) phenylboronic acid (BA, 97%) was purchased from Frontier Scientific. 1, 2-dipalmitoyl-sn-glycero-3-phosphocholine (DPPC,  $>99\%$ ) was purchased from Avanti Lipid. The epoxy silane 3- glycidoxypropyl)-trimethoxysilane was purchased from Gelest, Inc.

### **5.3.2 Epoxy silane modification of mesoporous silica thin film**

The silica membrane was first lightly functionalized with 3- glycidoxypropyl)-trimethoxysilane (GPTS) to help with the grafting of GI without blocking the pore. The thin film silica supported by anodic aluminum oxide (AAO) membrane for enzyme immobilization was prepared as described in **Chapter 3**. In a nitrogen purged bag, 10.8  $\mu\text{L}$  of GPTS was added to 6 mL of chloroform to produce a 0.0018 v/v % solution then sonicated for 10 minutes. A solution containing 10  $\mu\text{L}$  of the GPTS mixture, 4 mL chloroform and a silica membrane were added to a cylindrical vial ((25mm x 95mm), then sonicated for 30 minutes while GPTS reacted with the silica surface. After the reaction, the excess chloroform/silane solution was poured off while in the nitrogen purged bag. The excess GPTS was removed from the functionalized silica membrane by sonicating the membrane in ethanol for 10 mins three times. After washing, the membrane was dried in the oven overnight at 80°C. The surface functionalization of silica membrane with epoxy silane GPTS was confirmed using Fourier transform infrared (FTIR) spectroscopy. Each spectrum was collected at a resolution of 4  $\text{cm}^{-1}$  and 250 scans using a ThermoNicolet Nexus 470 spectrometer equipped with a (deuterated triglycine sulphate) DTGS detector.

### **5.3.3 Glucose isomerase (GI) immobilization on the synthetic biomimetic membrane (boronic acid immobilized lipid filled silica membrane)**

To add the immobilized enzyme and lipid carrier functionality to the composite membrane, the epoxy modified silica membrane was incubated in a solution of 10 mg of DPPC and 5 mg 4-(N-Boc-aminomethyl) phenylboronic acid (BA) which were dissolved in  $\text{CHCl}_3$ , and sonicated for 25 minutes in a cylindrical vial (25mm x 95mm). The above mixture was then blow-dried with nitrogen and was further dried under high vacuum for at

least 2 hrs. 2 mL of GI enzyme and 2 mL of PBS were then added to each membrane and sonicated at 47 °C for 1 hour to allow for the rehydration of lipid and immobilization of the GI. The sample was sonicated for another 15 minutes while cooling to 25°C. The excess lipid and GI were removed by washing the membrane with PBS three times. The morphology of the silica membrane before and after the immobilization of GI were characterized using FIB/SEM instrument (FEI Helios Nanolab 660). The samples were prepared by attaching them to double sided carbon tape on 15 mm aluminum mounts. The GI was also physically attached to the silica membrane by sonicating the unmodified silica membrane with 2 mL of GI enzyme and 2 mL of PBS for 1 hour.

#### **5.3.4 Glucose upgrading through composite membranes**

The conversion of glucose to fructose by immobilized GI through the silica thin film membranes was measured in a side by side diffusion cell (PermeGear, Hellertown, PA). The membrane was held into place by the chambers, which each hold 7 mL, being secured tightly together by a clamp allowing a 2 cm<sup>2</sup> cross sectional area of the membrane to be exposed. The donor side of the cell was loaded with 7 mL of 2 g/L glucose solution in PBS buffer (0.9 M, pH 7.4). The receptor side was initially loaded with 7 mL of PBS buffer with no solute. The diffusion cell was then placed on a heater plate with temperature controlled at 50°C. The concentration of glucose and fructose in the receptor side and donor sides were both sampled as a function of time. At sampling time, 200 uL sample from each side was taken and the concentration was test using high performance liquid chromatography (HPLC) with a Bio-Rad Aminex HPX-87H and a Shodex R01 refractive index detector. The mobile phase was degassed 5 mM H<sub>2</sub>SO<sub>4</sub> fed at a rate of 0.4 mL/min, and the temperature of the column was at 50°C.

## 5.4 Result and discussion

### 5.4.1 Characterization of glucose isomerase immobilized thin film silica membrane

Silica thin films with accessible 2-D hexagonally close packed (HCP) pore structure on porous support (AAO), which allows fast diffusion through the cylindrical pores,[33] were utilized as separation platform and glucose isomerase (GI) immobilization support. To graft GI on to the silica surface, silica membrane was modified with 3-(glycidoxypropyl)-trimethoxysilane (GPTS) to produce a terminal epoxy group, which can covalently bind with the amine group of enzymes (**Figure 5.1**). **Figure 5.2** presents the membrane morphology before and after the immobilization of GI. As shown, the bare AAO support (**Figure 5.2a**) has a pore size of around 200 nm, which is an ideal support for silica thin film as it contributes minimal resistance to diffusion. A continuous silica thin film with 10 nm pores was then formed on the surface of porous support (**Figure 5.2b**), which resulted in greater electron scattering in the SEM image and decrease in contrast. As reported in **Chapter 3**, porous substrate supported silica thin films with accessible continuous cylindrical channels were successfully synthesized. While the bare silica membrane showed a uniform clear surface, epoxy modified silica membrane with bound enzyme had many globular structures (**Figure 5.2c**), which confirmed the successful immobilization of GI to the silica surface.

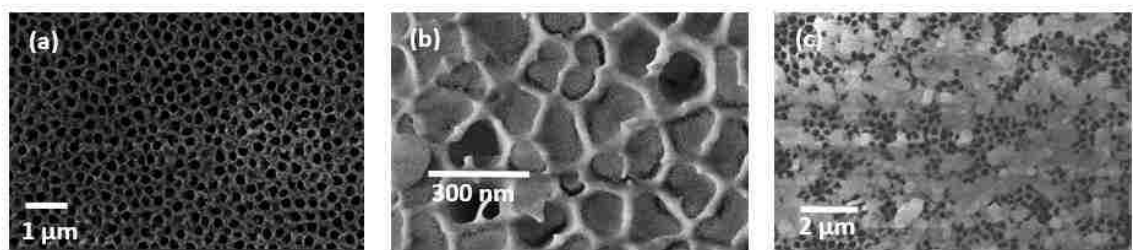


**Figure 5.2** SEM images of (a) AAO support; (b) silica thin film coated AAO; (c) glucose isomerase immobilized membrane.

The grafting of functional groups to the thin film silica membrane was verified by Fourier transform infrared (FTIR) spectroscopy. **Figure 5.3** shows the FTIR spectra of bare silica, epoxy modified silica, covalently-bound GI silica and GI adsorbed silica (in the absence of epoxy modification for covalent binding of GI). As expected, for bare silica, a broad signal between  $3000\text{ cm}^{-1}$  and  $3600\text{ cm}^{-1}$  appeared due to existent of O-H vibration on silica surface, comprising Si-OH. After the epoxy functionalization, two bands at  $2858\text{ cm}^{-1}$  and  $2930\text{ cm}^{-1}$  are due to the alkyl C-H stretching of propyl chain from GPTS.[149] The C-H bending also caused the signal at  $1477\text{ cm}^{-1}$  and  $1538\text{ cm}^{-1}$ . Furthermore, the O-H signal between  $3000\text{ cm}^{-1}$  and  $3600\text{ cm}^{-1}$  increased after epoxy modification, since the hydrolyzed epoxy also contributed to the O-H stretching in addition to Si-OH. After covalent binding of GI to the epoxy modified silica membrane, a band at  $1640\text{ cm}^{-1}$  appeared, which was attributed to the C=O stretching in amide group.[150] An additional band at  $3317\text{ cm}^{-1}$ , representing the N-H vibration of amine appeared and overlapped with O-H stretching. This observations indicates that GI is immobilized to the silica membrane. For comparison, GI was also physical adsorbed to silica membrane, which resulted in the appearance of the band of C-H stretch on  $2858\text{ cm}^{-1}$  and  $2930\text{ cm}^{-1}$ . However, after incubating the silica membrane with adsorbed GI in the water bath of  $50^{\circ}\text{C}$  (optimum

reaction temperature for GI is 60-70 °C) for 6 h, the C-H stretch disappeared, which suggested desorption of GI from the composite membrane (data not shown). Meanwhile, the characteristic peaks for GI were still presented for covalent bound GI silica membrane after the same water bath treatment (data not shown). Thus, physical adsorption is too weak to retain the enzyme during desired operation conditions, while covalent binding stabilizes the immobilized enzyme and increases the reusability.[149] In order to quantify the enzyme amount immobilized on to silica membrane, the enzyme concentration change before and after the reaction with the membrane was measurement using protein assay. However, nearly no concentration change was seen, suggesting the immobilized enzyme amount is very small to detect. Effective method for quantifying small enzyme concentration is still under examination and it is necessary for comparing the activity of immobilized enzyme to the free enzyme.

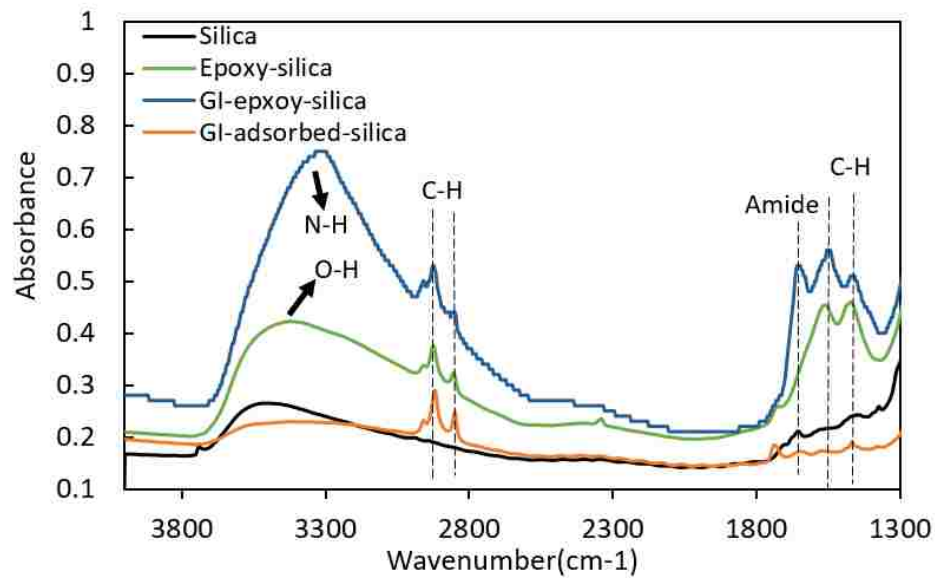


**Figure 5.3** FTIR spectra of silica, epoxy modified silica, GI immobilized silica through covalent coupling with epoxy or physical adsorption.

To examine the effect of epoxy modification and GI immobilization on the transport property of the separation membrane, fructose permeability through the unmodified and modified membranes were measured. As shown in **Figure 5.4**, the epoxy modified and GI bound silica membrane presented similar fructose permeability compared to the bare silica thin film membrane. This observation suggests that the pore of silica membrane is not blocked by the epoxy group or the bound GI, which ensures the fast diffusion through the composite membrane.

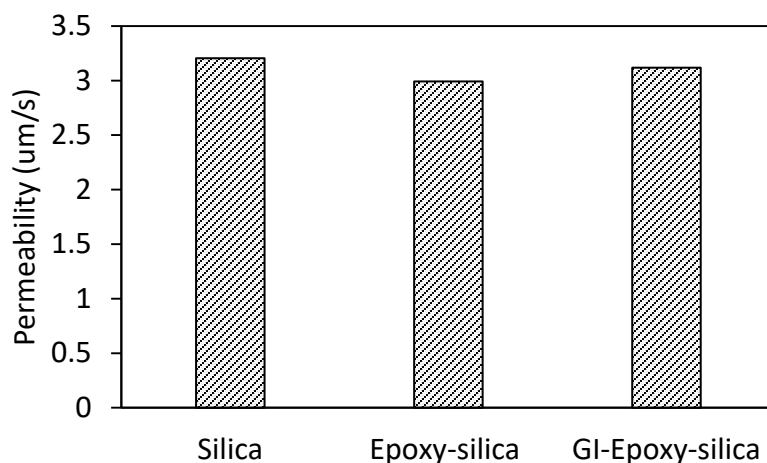


**Figure 5.4** Fructose permeability through the bare, epoxy modified, and GI epoxy-modified silica membrane at 50°C.

#### **5.4.2 Glucose conversion through glucose isomerase immobilized silica composite membranes**

The effect of immobilized GI on fructose yield and sugar transport was evaluated by analyzing the glucose and fructose concentration in the donor phase and receptor phase of the static diffusion cell for an initial solution concentration of 2 g/L glucose solution in the donor phase at 50°C. The glucose and fructose concentrations were measured as a function of time for GI immobilized membranes for the silica composite membrane, the lipid-filled

silica composite membranes, and the lipid-filled silica composite membrane with immobilized boronic acid as a sugar carrier. **Figure 5.5** illustrates the total fructose yield (sum of fructose on donor and receptor phase) as a function of time when glucose reacted with three different types of glucose isomerase immobilized membranes. The fructose production over time showed a linear relationship, which indicates that the reversible reaction can be neglected in a short reaction period due to the low product concentration .[148, 151] Thus, the immobilized enzyme activity was determined by linear regression of the product concentration profile. For lipid-BA filled silica, lipid filled silica and bare silica, the initial reaction rate of the immobilized GI were calculated to be 0.16, 0.13, 0.06 mM/h respectively, for the first order reaction. This observation indicates that the glucose isomerase immobilized membrane showed significant activity and the combination of biocatalyst with separation membrane further improved the enzyme activity.



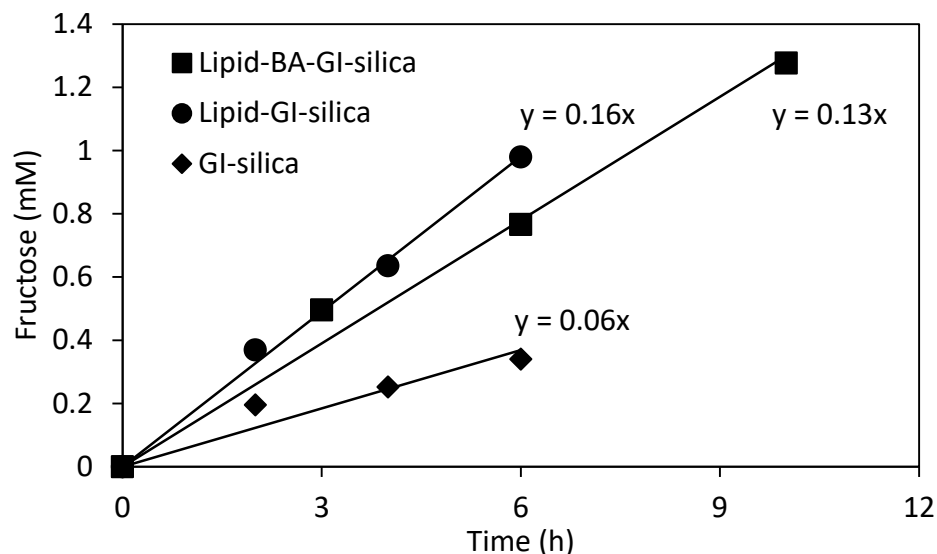


**Figure 5.5** Fructose concentration in the static diffusion cell as a function of time through the GI immobilized membranes for the silica composite membrane (GI-silica), the lipid-filled silica composite membrane, (lipid-GI-silica) and the lipid-filled silica composite membrane with immobilized boronic acid as a sugar carrier (Lipid-BA-GI-silica). The initial glucose concentration was on the donor side is 2g/L or 11.1mM.

Glucose and fructose concentrations on the donor phase and receptor phase at 6 hour of reaction and diffusion are presented on **Table 5.1**. For the bare silica membrane without lipid barrier, less glucose conversion was seen due to the more rapid transport of sugar between the donor and receptor phase, which results in a significant reduction of glucose concentration that can react with the enzyme on the donor phase. Meanwhile, the addition of lipid barrier significantly decreased the diffusion of glucose to the receptor phase, thus the fructose yield is enhanced by about two times. However, the fructose production reduced slightly due to the addition of boronic acid carrier, which facilitate the transport of both glucose and fructose. Therefore more glucose is transported through the membrane by boronic acid than the new produced fructose due to the low isomerization rate which

result in much higher amount of glucose than fructose on the donor phase. Thus, a tradeoff between the enzyme activity and the transport rate of the separation membrane need to find to improve the selectivity and product yield of the biocatalyst-separation integrated membrane.

**Table 5.1** Glucose and fructose concentrations in the donor and receptor sides of the static diffusion cell separated by the GI immobilized separation membrane at 6 hrs. (The initial glucose concentration was on the donor side is 2g/L or 11.1mM.)

		<b>Lipid-BA-GI-silica</b>	<b>Lipid-GI-silica</b>	<b>GI-silica</b>
Donor side (mg/L)	Glucose	1643	1811	1026
	Fructose	130	165	31
Receptor side (mg/L)	Glucose	218	106	953
	Fructose	7	11	30
Total Fructose yield		137	176	61

#### **5.4.3 Transport model development for biocatalyst and carrier-mediated separation integrated membrane at continuous flowing system**

The static diffusion cell results demonstrate the successful synthesis of the enzymatic membrane reactors with biomimetic separation, using the isomerization of glucose as a model system. However, to optimize the performance of the enzymatic membrane reactor, the relationship between the enzyme activity and the product transport through the separation membrane on product yield and selectivity needs to be described. A mathematical model is developed to predict the purity and yield of the desired product under various conditions using a biocatalyst and carrier-mediated separation integrated

membrane. This model can be used to focus further research efforts by identifying the most relevant transport and kinetic variables to achieve a high performance enzymatic membrane reactor using data acquired from static diffusion cell experiments and estimated from a model membrane reactor operating under continuous flowing system. Thus, the effect of the rate of reaction (dictated by enzyme kinetics, extent of functionalization, immobilization method, etc)) and the effect of the relative permeability and overall flux through the membrane can be analyzed.

The model presents a general case where two aqueous phases are separated by selective membrane with an immobilized enzyme layer on the membrane surface (**Figure 5.6**). The substrate flows continuously through a well-stirred donor phase of the reactor. During the flowing, the reaction of the substrate is catalyzed by the enzyme that are located at the interface of the composite membrane. Thus the transport process can be divided into a reaction zone and a diffusion zone. In the reaction zone, the substrate is catalyzed by the immobilized enzyme while diffusing through the enzyme layer toward the membrane. After it reaches the interface between enzyme layer and separation membrane, the substrate and product diffuse into receiving phase. A continuous feed stream is also feed to the well-stirred receiving phase to continuously remove the product. Thus the concentration of substrate (A) and product (P) in the reactor is the same as that of the outlet stream.

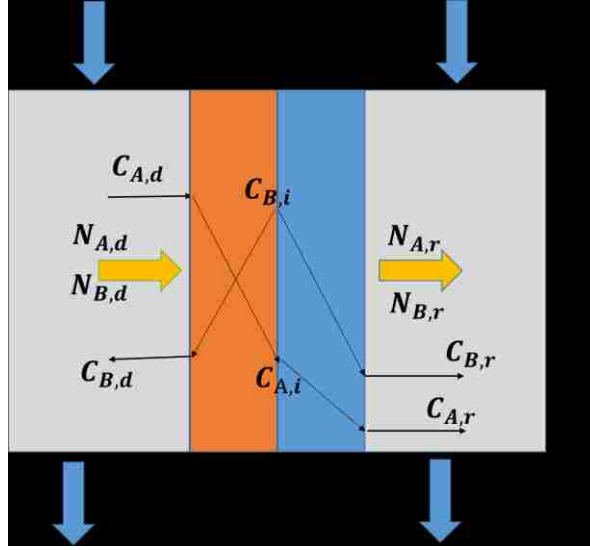


**Figure 5.6** Concentration profile through the reaction-diffusion membrane ( $v$ : flow rate;  $C$ : concentration;  $N$ : species flux;  $A$ : substrate;  $B$ : product;  $d$ : donor phase;  $r$ : receiving phase;  $i$ : interface between enzyme layer and the membrane).

In the bio-catalysis layer, the substrate is catalyzed by the immobilized enzyme while diffusing. Based on the mass balance in a differential element ( $\Delta V$ ) (**Eq.5.1**), where  $N = -D_A * \frac{dC_A}{dz}$  is the substrate flux across the enzyme layer at position  $Z$ ,  $A$  is the membrane area and  $r_A = k_1 C_A - k_{-1} C_B$  is the reaction rate. The reaction-diffusion equation (**Eq.5.2** and **Eq.5.3**) for the enzyme layer can be derived for the substrate ( $A$ ) and product ( $B$ ):

$$(N * A)_Z - (N * A)_{Z+\Delta z} - r_A * \Delta V = 0 \quad (5.1)$$

$$D_A * \frac{d^2(C_A)}{dz^2} - k_1 C_A + k_{-1} C_B = 0 \quad (5.2)$$

$$D_B * \frac{d^2(C_B)}{dz^2} + k_1 C_A - k_{-1} C_B = 0 \quad (5.3)$$

where  $D_A, D_B$  is the diffusion coefficient of the substrate and product in the enzyme layer,  $k_1$  and  $k_{-1}$  is the forward and reverse reaction rate constant.

At the interface between the donor phase and enzyme layer ( $Z=0$ ), the partition coefficient between the aqueous phase and enzyme layer is assumed to be 1, thus following boundary conditions can be obtained, and the  $C_{A,d}$  and  $C_{B,d}$  are the substrate and product concentration on the donor phase.

$$C_A(0) = C_{A,d}; C_B(0) = C_{B,d} \quad (5.4)$$

At the interface between the enzyme layer and the separation membrane ( $Z=d$ ), the mass flux leaves the enzyme layer should be the same as the mass flux enter the separation membrane, which is assumed as a one-dimensional steady state diffusion with constant flux across the separation membrane. Thus the boundary conditions at  $Z=d$  can be expressed as:

$$D_A * \left(\frac{dC_A}{dz}\right)_{z=d} = -P_A * (C_A(d) - C_{Ar}); D_B * \left(\frac{dC_B}{dz}\right)_{z=d} = P_B * (C_B(d) - C_{Br}) \quad (5.5)$$

where  $P_A$  and  $P_B$  are the mass transfer coefficient in the separation membrane,  $C_{Ar}$ ,  $C_{Br}$  are the substrate and product concentration at the receptor phase.

Besides, the whole system need to satisfy the following mass balance for the donor phase (**Eq.5.6** and **Eq.5.7**) and receptor phase (**Eq.5.8** and **Eq.5.9**):

$$v_1 * C_{A,0} - v_1 * C_{A,d} - N_{A,d} * A = v_1 * C_{A,0} - v_1 * C_{A,d} + D_A * \left(\frac{dC_A}{dz}\right)_{z=0} * A = 0 \quad (5.6)$$

$$0 - v_1 * C_{B,d} - N_{B,d} * A = -v_1 * C_{B,d} + D_B * \left(\frac{dC_B}{dz}\right)_{z=0} * A = 0 \quad (5.7)$$

$$0 - v_2 * C_{A,r} + N_{A,r} * A = 0 - v_2 * C_{A,r} + P_A * (C_A(d) - C_{Ar}) * A = 0 \quad (5.8)$$

$$0 - v_2 * C_{B,r} + N_{B,r} * A = 0 - v_2 * C_{B,r} + P_B * (C_B(d) - C_{Br}) * A = 0 \quad (5.9)$$

Above mass balance are utilized to solve for the unknown parameters in the boundary conditions. **Eq.5.6 – 5.9** can be transformed to **Eq.5.10 – 5.13** correspondingly:

$$C_{A,d} = (v_1 * C_{A,0} + D_A * \left(\frac{dC_A}{dz}\right)_{z=0} * A) / v_1 \quad (5.10)$$

$$C_{B,d} = D_B * \left(\frac{dC_B}{dz}\right)_{z=0} * A / v_1 \quad (5.11)$$

$$C_{A,r} = \frac{P_A * A}{v_2 + P_A * A} * C_A(d) \quad (5.12)$$

$$C_{B,r} = \frac{P_B * A}{v_2 + P_B * A} * C_B(d) \quad (5.13)$$

Substitutes **Eq.5.10 – 5.11** to **Eq.5.4** and **Eq.5.5** correspondingly, the boundary conditions as a function of dependent variables can be derived:

$$C_A(0) = (v_1 * C_{A,0} + D_A * \left(\frac{dC_A}{dz}\right)_{z=0} * A) / v_1 \quad (5.14)$$

$$C_B(0) = D_B * \left(\frac{dC_B}{dz}\right)_{z=0} * A / v_1 \quad (5.15)$$

$$D_A * \left(\frac{dC_A}{dz}\right)_{z=d} = -P_A * \frac{v_2}{v_2 + P_A * A} * C_A(d) \quad (5.16)$$

$$D_B * \left(\frac{dC_B}{dz}\right)_{z=d} = P_B * \frac{v_2}{v_2 + P_B * A} * C_B(d) \quad (5.17)$$

Finally, **Eq. 5.2, 5.3** and **Eq.5.14 – 5.17** were utilized to solve for the profiles of substrate ( $C_A$ ) and product ( $C_B$ ) concentration, and the derivative of substrate ( $\frac{dC_A}{dz}$ ) and product ( $\frac{dC_B}{dz}$ ) across the membrane using MATLAB solver (bvp4c) for the one-dimensional boundary value problems of ordinary differential equation (ODE). Then the substrate and product concentration on the donor and receptor side can be calculated using **Eq.5.10 – 5.13** to evaluate the membrane performance The MATLAB coding is included in **Appendix B**.

In the model discussed above, parameters  $k_1, k_{-1}, D_A, D_B, d, P_A, P_B, C_{A,0}, v_1, v_2, A$  is involved. Among them  $C_{A,0}, v_1, v_2, A$  are the operating parameters of the system, which can be manipulated independently as needed. And the rest is related to the properties of composite membrane, which depends on who the membrane is prepared. First of all, the mass transfer coefficient ( $P_A, P_B$ ) across the selective separation membrane (boronic acid immobilized lipid filled membrane ) for the substrate (A, glucose ) and product (B, fructose) is obtained by measuring their diffusion through the separation membrane without enzyme layer in the a static diffusion cell which is discussed in **Chapter 3**, and values are calculated to be 0.21  $\mu\text{m/s}$  for both glucose and fructose. The enzyme layer thickness (reaction-diffusion zone),  $d$ , can be estimated by assuming the immobilized enzyme (glucose isomerase )molecules are sphere shape, which has a molecular weight of 120,000 g/mol and diameter of 5.1 nm.[152] The layers or thickness of enzyme immobilized then can be calculated from the enzyme loading amount on the membrane ( $C_E$ ), assuming a porosity of 0.5 for the enzyme layer.[153, 154]. The the enzyme layer thickness is estimated to be 200 nm, based on the average value reported in literature, [153, 154] in the absence of experimental data for this system. The species diffusion coefficient ( $D_A, D_B$ ) in the enzyme layer is assume to be the same as in the water, because the glucose isomerase is water soluble and the pores of the enzyme should be filled with water. So the diffusion coefficient of fructose and glucose are  $6.7 \times 10^{-6} \text{ cm}^2/\text{s}$ . The reaction rate ( $k_1, k_{-1}$ ) of enzyme immobilized membrane is quantified by the measuring fructose production as a function of time by incubating the membrane in a glucose solution , and  $k_1, k_{-1}$  are both calculated to be  $0.015 \text{ h}^{-1}$  for the first order reversible reaction.

First of all, the proposed model is verified by predicting the glucose and fructose profile on the donor and receptor side for a static diffusion cell and is compared to experimental data discussed previously in this chapter. **Figure 5.7** shows the model prediction of glucose and fructose concentration profile on the donor side and receptor in a static diffusion cell through the lipid-filled silica composite membrane with immobilized boronic acid as a sugar carrier (Lipid-BA-GI-silica) is consistent with experimental measurement. Thus, the model proposed and the assumption made are reasonable and can be further applied to a continuous flowing system and examine the effect of membrane properties (enzyme layer and membrane permeability) on the separation efficiency of the membrane.

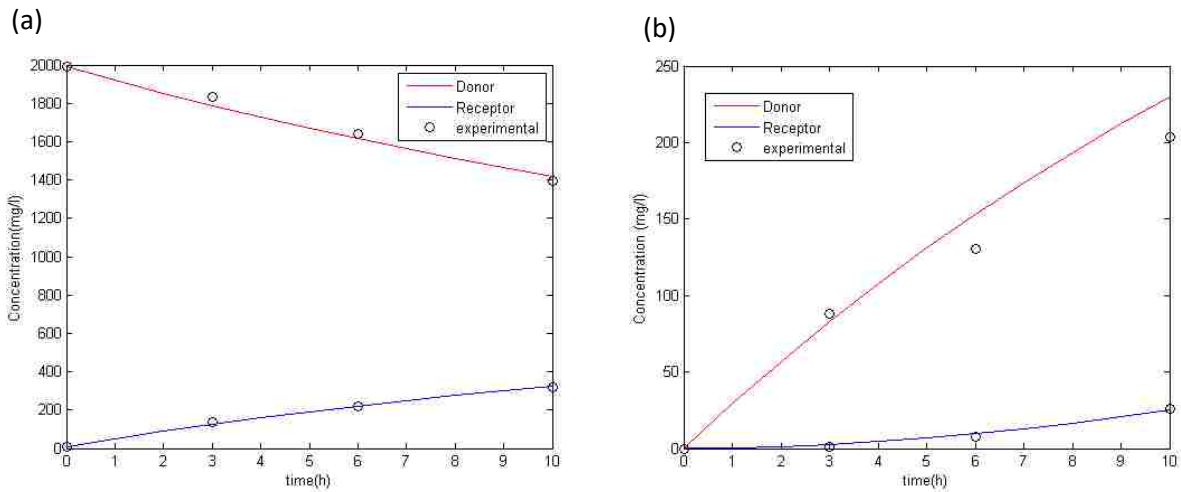


**Figure 5.7** Model prediction and experimental measurement of glucose (a) and fructose (b) concentration in the static diffusion cell as a function of time through the lipid-filled silica composite membrane with immobilized boronic acid as a sugar carrier (Lipid-BA-GI-silica). The initial glucose concentration was on the donor side is 2000 mg/L.



To estimate investigate the role of enzyme reactivity and permeability on the productivity and selectivity for the membrane operated in a continuous flowing system. Following dimensionless numbers are defined:

$$\text{Thiele modulus} = \frac{\text{Reaction rate}}{\text{Diffusion rate}} = \varphi^2 = \frac{k_1 * d^2}{D} \quad (5.10)$$

$$\text{Relative permeability} = \alpha = \frac{\text{Permeability of product}}{\text{Permeability of substrate}} = \frac{P_B}{P_A} \quad (5.11)$$

The Thiele modulus (**Eq.5.10**) defines the relative relation between the reaction rate and diffusion rate in a reaction-diffusion zone (enzyme layer), thus this parameter describes the whole processes happened in the enzyme layer, which important for quantifying the effect of properties change in the enzyme layer on the whole membrane performance. **Figure 5.8a** presents the predicted selectivity (fructose over glucose) on the receptor phase as a function of the value of Thiele modulus. The selectivity increases as the values of Thiele modulus increases. Besides, the increase of selectivity is less significant, when the value of Thiele modulus is below  $10^{-6}$ , where the diffusion is dominating. Meanwhile, selectivity dramatically increases to about 30 when the value of Thiele modulus is increased to 0.00025, where the reaction rate is becoming dominating. **Figure 5.8b** presents the fructose profiles in the enzyme layer when the value of Thiele modulus is  $2.5 \times 10^{-5}$ . As shown, the fructose concentration first increases then decreases, suggesting the reaction and diffusion are competing. Thus, the model result here suggest that is important to achieve a trade-off between the enzyme activity and diffusion in the enzyme layer to achieve desired membrane performance. Factors like enzyme immobilization amount, thickness of enzyme layer, porosity of the enzyme layer are all related physical parameters that will affect the enzyme activity and diffusion, thus the membrane selectivity.

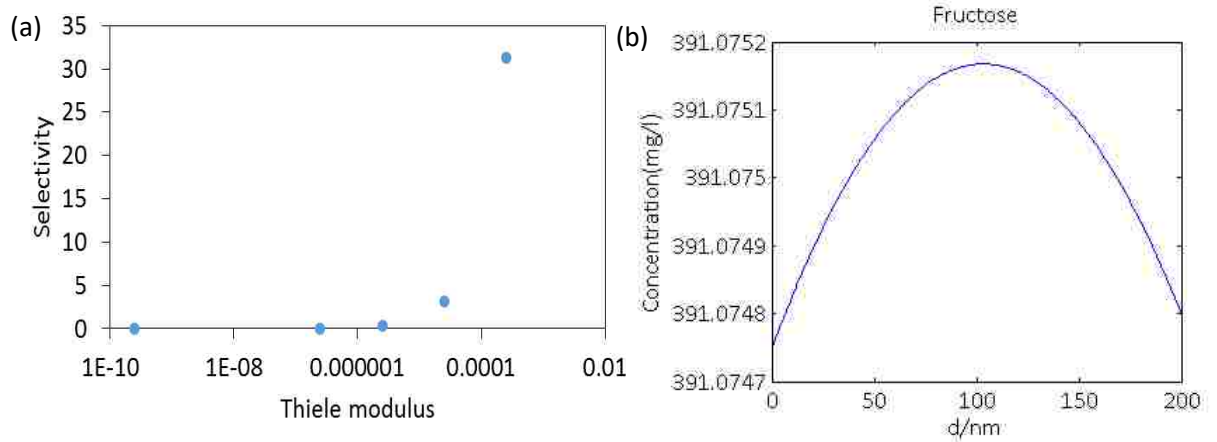


**Figure 5.8** (a) Model prediction of selectivity (fructose over glucose) on the receptor phase as a function of the value of Thiele modulus. (b) Fructose profiles in the enzyme layer when the value of Thiele modulus is  $2.5 \times 10^{-5}$ .

The relative permeability (**Eq.5.11**) defines the relative diffusion rate of product (B) and the substrate (A), which is critical for membrane selectivity to the product over the substrate. **Figure 5.9** illustrates the model prediction of selectivity (fructose over glucose) on the receptor phase as a function of relative permeability under given Thiele modulus. As shown, for a given Thiele modulus value ( $2.5 \times 10^{-5}$  or  $2.5 \times 10^{-4}$ ), the selectivity increases as the relative permeability increases which is consistent with more fast transport of product than substrate and results in increasing selectivity. Furthermore, for high Thiele modulus value ( $2.5 \times 10^{-4}$ ), the effect of the relative permeability is more significant, suggesting the reaction and diffusion in the enzyme is dominating the separation process. Although, the enzyme layer has more significant effect on the membrane performance, the role of the selective separation membrane cannot be neglected. Since the enzyme layer is dominating, it may be better to investigate the selective separation membrane separately to observe sensitive change for different factors specific to affect the separation membrane such the barrier structure, affinity to the carrier, and carrier concentration etc.

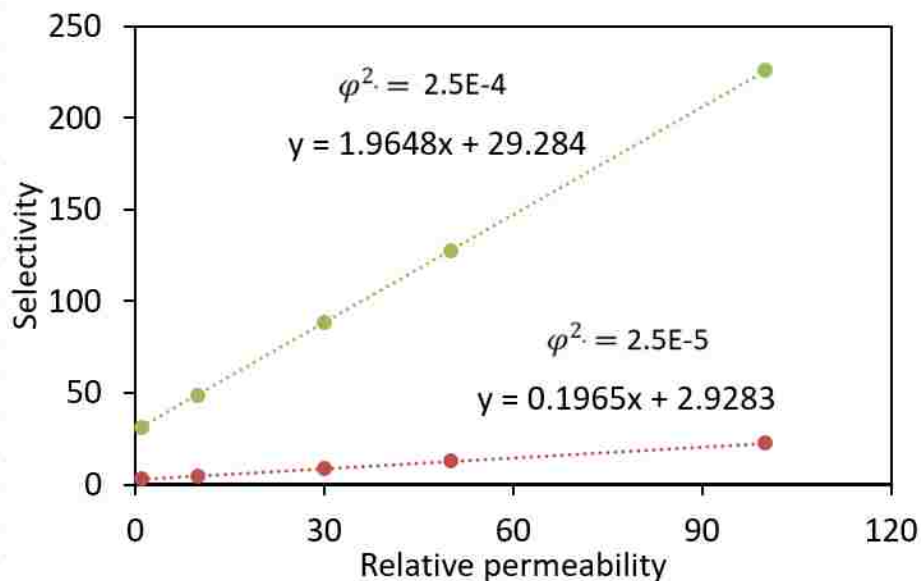


**Figure 5.9** Model predication of selectivity (fructose over glucose) on the receptor phase as a function of relative permeability under given Thiele modulus.

## 5.5 Conclusion

In this work, biocatalyst is successfully immobilized on carrier-mediated separation membrane for the upgrading and recovery of dilute aqueous solute. Using glucose isomerase (GI) as a model enzyme and boronic acid as carrier, the conversion of glucose to fructose and separation was demonstrated, which indicates that it is feasible to achieve low cost and high purity product yield by combining the reaction and selective separation in one single membrane process. However, due to the high complexity of the reaction-separation integrated process, parameters involved in two processes need analysis to achieve high selectivity and production. A mathematical model that describes the chemical reaction and selective mass transfer through the composite membrane is proposed. The revealed that the Thiele modulus which decries the reaction and diffusion process is a dominating factor for the membrane performance. Also the relative permeability between

the product and substrate is shown to affect the selectivity. Thus, the model is expected to be a useful tool for predicting the purity and yield of the desired product and optimizing operation conditions for the biocatalyst and carrier-mediated separation integrated membrane.

## Chapter 6: Size-Dependent Loading and Mobility of RNA in Porous Silica

### Nanoparticles

#### 6.1 Abstract

Porous silica nanoparticles (pSNPs) are promising carriers for the delivery of nucleic acids to cells due to their tunable pore morphology, high loading capacity, biocompatibility and ease of surface functionalization. For example, the delivery of double-stranded (ds)RNA to insects to achieve effective RNA interference (RNAi) is proposed as an effective and highly specific pest management strategy. With the advent of nanoparticle synthesis techniques that provide pore sizes sufficient for the loading of RNA in the pores (and not simply on the external surface of the particle), knowledge of the effect of pore confinement on RNA loading and release is required for the design of effective delivery vehicles. The loading behavior of dsRNA (84 bp and 282 bp dsRNA of *Spodoptera frugiperda*) with the pSNP of varying pore size (nonporous, 3.6 nm, 7.4 nm and 11.8 nm) and diffusivity (mobility) of the dsRNA in RNA-loaded pSNPs were investigated. Large diameter amine-functionalized silica nanoparticles (~10  $\mu\text{m}$ ) were used to provide directly visualize of fluorescently labeled dsRNA loading and exchange by confocal laser scanning microscopy. It was found that the 282 bp dsRNA can't be loaded to 3.6 nm pores while 84 bp dsRNA can, revealing that the relative dimension of dsRNA length to the pore size affected the dsRNA encapsulation efficiency. Fluorescence Recovery after Photobleaching (FRAP) indicated that the dsRNA mobility at the surface and in the core of dsRNA-loaded pSNPs was similar and increased from 0.0002 to 0.001  $\mu\text{m}^2/\text{s}$  as pore size increased from 3.6 nm to 11.8 nm for 84 bp dsRNA. The mobility at same pore size furthered reduced for

282 bp dsRNA However, the mobility of dsRNA with varying lengths on nonporous materials was not detectable, which suggest that it is important to have porous structure to serve as a “sink” in providing a mobile network of dsRNA on the surface of the particle. This work successfully demonstrates the loading of RNA on functionalized pSNPs and identified factors that affects RNA loading and releasing, which provides basis for the delivery of RNA-loaded silica particles to insects. Besides, the pSNPs saturated with dsRNA can exchange dsRNA with the surrounding solution, suggesting, the mobility of dsRNA in the pores have a functional effect on delivery of dsRNA to insects.

## **6.2 Introduction**

The development of gene therapy technology, which delivers foreign nucleotides (oligonucleotides, siRNA, and DNA) to the targeted sites in the living cells to inhibit the expression of gene of interest to achieve the treatment of diseases,[155] has bring numerous opportunities for life science. Among them, RNA interference (RNAi) one of the popular branches. For example, insect pest management can be improved by delivering the specifically designed small interfering RNA (siRNA) to the cell to suppress the targeted genes which is related to the insect fitness or mortality.[156] However, the application of RNAi is often limited by the delivery efficiency of the nucleic acids to the targeted sites for therapy. Because the nucleic acid itself are easily degraded by nuclease and cannot directly pass through the cell membrane, as they both have negative charge.[155] Therefore, identifying efficient carrier to protect and deliver the nucleotides to the targeted sites of insect cells has become the key challenge to achieve effective gene therapy.

Porous silica nanoparticles (pSNPs) have been investigated as carriers of nucleic acids because of their tunable pore morphology, large surface area, biocompatibility and ease of

surface functionalization, porous silica nanoparticles.[157, 158] Surface modification is used to enhance the nucleic acid loading into the pSNPs, cell uptake, and targeting efficiency.[159] Nucleic acid loading is achieved by functionalizing the silica surface with positive charge using aminosilanes, metal ions, cationic polymers and peptides to adsorb the negatively charged nucleic acid through covalent or electrostatic interactions. [155, 160] To reduce pSNPs aggregation and toxicity to damage the cell membrane during the delivery, surface coating of polyethyleneimine polymers (PEIs)[161, 162] or supported lipid bilayers[163] on the siRNA encapsulated pSNPs to eliminate the electrostatic interactions. Meanwhile, targeted moieties such as ligands or peptides are incorporated to the surface coating to enhance the specific binding to the targeted cells.[157]

While pSNPs have been highly investigated for protein and gene delivery, only recently has reliable synthesis of larger pore pSNPs allowed for direct loading of RNAs into the pores, providing control of loading/release characteristics as well as protection to the RNA.[164, 165] As a nucleic acid delivery vehicle, the pores of pSNPs are envisioned to allow the loading of large amount of nucleic acids and provide protection during the delivery to the target cells. Initial studies of nucleic acid delivery with pSNPs used nonporous particles or particles with small (2-2.5 nm) pores relative to the dimensions of the nucleic acids (17-21 bp and dsRNA with diameter of 3 nm).[166-168] Recently, the loading of nucleic acids with different lengths (20 bp siRNA, 20 bp DNA, 60 pb DNA and 90 DNA) into silica particles with pore size of 8 nm was throughout studied.[169] Steinbacher et al.[170] also reported effect of pores size (4 nm, 8 nm, and 15 nm) and extent of amine functionalization on the releasing and loading of siRNA (20 bp, 6nm long\* 3 nm diameter). The benefits of pores for loading nucleic acids and protection from nucleases

during delivery to the cell is unclear. It is generally accepted that the interaction of dsRNA loaded on mesoporous silica particles can be illustrated as in **Figure 6.1** where the RNA appears as a string in the pores.[171]

Despite the rapid development of delivery strategy of nucleic acid by pSNPs, improving the loading capacity of pSNPs and controlling release of the siRNA are of particularly importance. In this context, fully understanding the siRNA loading behavior, interaction between siRNA and functionalized pSNPs, and diffusion dynamics of siRNA inside particles are essential for designing efficient siRNA carriers. Considering the relative dimension of siRNA to the pore of silica particles, the pore sizes and lengths siRNA are important factors affecting the RNA loading and mobility in pores. The goal of this work is to demonstrate the loading, protection and release of siRNA in porous silica nanoparticles. Also, dsRNA with distinct lengths difference (84 bp and 282 bp) from inhibitor of apoptosis (IAP) genes of *Spodoptera frugiperda* and silica with various pore sizes (3.6 nm, 7.4 nm, 11.8 nm) are used to cover most possible combination of RNA with RNA.



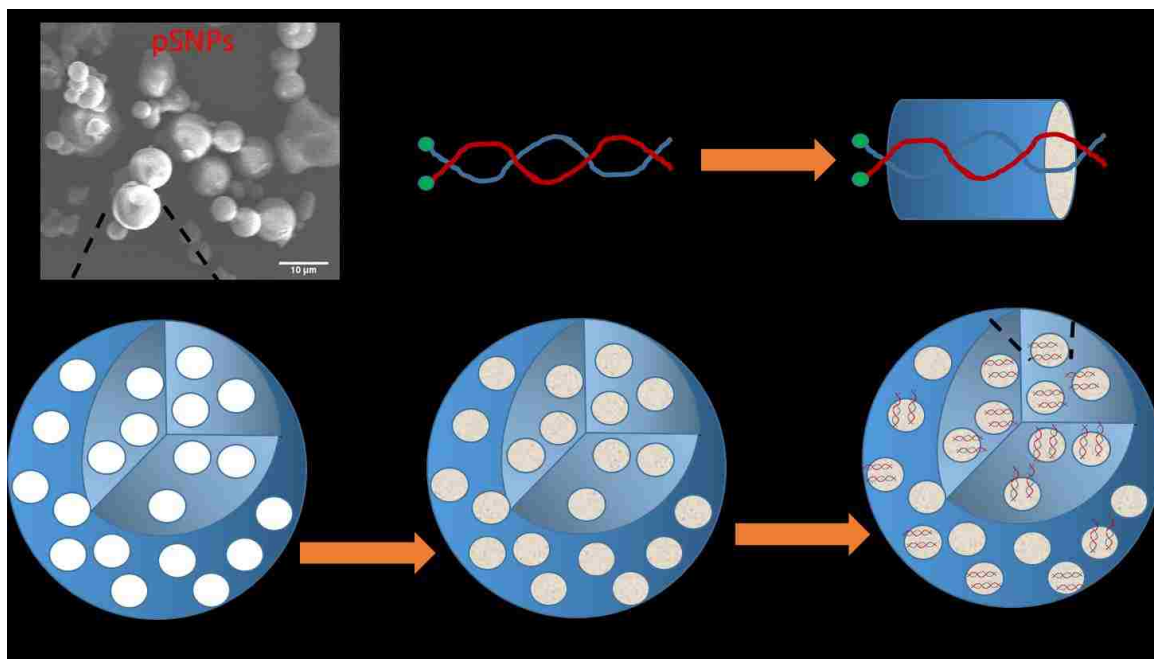


**Figure 6.1** Scheme of dsRNA loading into amine group functionalized micron-sized porous silica nanoparticles (pSNPs), modified from Na et al. [172]

Micron-sized pSNPs (SBA-15 type) with controllable pore size (2-12 nm) large enough ( $\sim 10 \mu\text{m}$ ) for confocal imaging were synthesized by hydrothermal aging with Pluronic surfactant P123 and cetyltrimethyl-ammonium bromide.[100] The SEM image (**Figure 6.1**) confirms their spherical shape and large diameters between  $5 \mu\text{m}$  and  $15 \mu\text{m}$ . Our previous study demonstrated that the particles has accessible ordered mesoporous structure and interconnected pores throughout the particles as characterized by XRD and FIB/SEM,[64] which allows the encapsulation of dsRNA. The template extracted silica particles were further functionalized with amines using (3-aminopropyl) triethoxy silane (APTES). Within our group, we found that the grafting location of amine group on the silica particles by APTES was controllable. 10 mins of reaction time was found to only graft the amine groups on the exterior surface of the particles, while 20 mins functionalized both the exterior particle surface and the surface of the pores. Previous studies[170]

indicate that low extents of amine functionalization (only the exterior particle surface or lightly functionalized pores) result in dsRNA adsorption only on the particle surface, which does not offer efficient protection of dsRNA during delivery RNases. Thus, amine functionalization procedure of Schlipf et al.[173] was used to achieve functionalization of 906.0 mg APTES/g particles to providing a network of amines corresponding to greater than monolayer coverage. For comparison, nonporous micron-sized silica particles that allow only for dsRNA on the surface were synthesized by a method adapted from Nakabayashi, Yamada [174] and also amine functionalized. The loading of dsRNA with various lengths into silica particles as a function of pore sizes was investigate by confocal laser scanning microscopy. Fluorescence Recovery after Photobleaching (FRAP), was used the diffusion dynamics of the dsRNA at the particle surface and the core of the particles as a function of the pore sizes (3.6 nm, 7.4 nm, 11.8 nm), which provides evidence for protection and release of functional dsRNA.

## **6.3 Experimental methods**

### **6.3.1 Materials**

Tetraethyl orthosilicate (TEOS, 98%), cetyltrimethylammonium bromide (CTAB, 99%), polyethylene oxide (PEO)-polypropylene oxide (PPO)-PEO triblock copolymer (P123, average Mn ~5,800), (3-Aminopropyl)triethoxysilane (APTES, 99%) potassium phosphate buffer tablets, fluorescamine (98%) were supplied by Sigma Aldrich. Ethanol (anhydrous) was purchased from DLI and hydrogen chloride (HCl, 6N), ammonium hydroxide (NH<sub>4</sub>OH 29% solution), sodium hydroxide (NaOH, 99%) were purchased from Fisher Scientific. The dsRNA used in this work is supplied by Dr. Bruce Webb's lab in department of Entomology.

### **6.3.2 Synthesis of micron-sized porous silica nanoparticle (pSNP)**

Spherical SBAS (Santa Barbara Amorphous Batch) materials were prepared using Schlipf's synthesis procedure.[63] Initially, 0.465 g of Cetyltrimethylammonium bromide (CTAB) dissolved in 20 mL of deionized water was added to 3.10 g poly (ethylene glycol)-block-poly (propylene glycol)-block-poly (ethylene glycol) (P123). This solution was placed in a water bath at 30 °C and stirred vigorously while 7.8 mL of 200 proof ethanol and 45.9 mL of 1.5 M HCl were added. After the P123 completely dissolved, 10 mL of tetraethoxysilane (TEOS) was slowly added drop wise. This solution was mixed for 2 h. At the end of 2 h, the solution was poured into a Parr 4748 Teflon lined bomb, which had been acclimated to the hydrothermal aging temperature, between 60°C and 120°C, prior to use. The sample was kept at the desired hydrothermal aging temperature in an oven for 3 days. At the end of the 3 day period, the sample was removed from the bomb and mixed in a high speed mixer to homogenize the solution. After homogenization, the sample was filtered and rinsed with deionized water. After filtration, the sample was placed into a single walled Whatman cellulose extraction thimble, and the surfactants were removed using Soxhlet extraction with 200 mL of 200 proof ethanol over 24 h. The pore dimension (5-12nm) increases as the hydrothermal aging (60-120°C) temperature increase.

### **6.3.3 Synthesis of micron-sized nonporous particles**

Spherical up to 6 micron sized nonporous particles were synthesized using electrolyte-added semi-batch synthesis procedure developed by Nakabayashi, Yamada [174] 150 mL of 0.5 M TEOS in ethanol solution (solution-I) was fed continuously using a Masterflex L/S PTFE-tubing pump (Barnant Co., Barrington, IL) for the semi-batch particles synthesis (4.7 mmol TEOS/h for 16 h) to 300 mL of ethanolic solution (solution-II) of 5 M water, 1

M NH<sub>3</sub> (20.2 mL of 29% NH<sub>4</sub>OH solution) and 3 mM KCl. Temperature of the solution-II was maintained at 35 °C throughout the addition of solution-I and feeding tube outlet was cleaned every 30 min to prevent clogging. Particles were separated by centrifugation (5000 rpm) and washed with ethanol and water. Smaller particles (<3 micron) were separated out by repeated gravitational setting (1h) and decantation followed by ultrasonication.

#### **6.3.4 Nitrogen adsorption**

Average pore diameter, pore size distribution and surface area were estimated from nitrogen sorption conducted at 77 K using Micromeritics TriStar 300. Samples were degassed at 120°C for a minimum of 4 h under flowing dry N<sub>2</sub> gas before the nitrogen sorption experiment. The specific surface area was estimated using the Brunauer, Emmett and Teller (BET) isotherm, and average pore diameter and pore size distribution were estimated by the method of Barrett, Joyner and Halenda (BJH) for adsorption branch.

#### **6.3.5 Amine functionalization for heavily functionalized particles**

Amine functionalized particles were obtained by condensing (3-Aminopropyl) triethoxysilane (APTES) on particle surface using a modified version of the methods reported in literature. [175, 176] 200 mg of the particles (nonporous or any of the porous) was sonicated in 25 mL of dry ethanol for 15 min and uniformly dispersed solution obtained. 0.5 mL of APTES was added drop wise under constant stirring and the solution kept stirring overnight in closed environment at room temperature. Particles were centrifuged at 17,000 rpm followed by repeated washing with dry ethanol and cured at 84 °C overnight. After curing, particles were stirred in excess ethanol for 24 hours to remove

any remaining loosely bound amine groups. The functionalized particles were again washed 3 times with dry ethanol and dried in oven at 84 °C.

### **6.3.6 Amine quantification**

The amount of amine group on particle surface was determined by a modified version of the previously reported method,[177] where primary amine group in aminosilanes, following dissolution in alkaline solution, reacts with fluorescamine to produce fluorescent pyrrolinone. [178] 30 mg of functionalized particles were dissolved over an 8 hour period in 30 mL of 0.02 M NaOH solution at room temperature under vigorous stirring. 100  $\mu$ L of this solution and 1.0 mL of 1.0 mM fluorescamine in acetone solution were mixed with 2.0 mL of PBS solution at pH 7.4. Maximum fluorescent intensity of this solution was measured at emission wavelength of 480 nm after excitation at 366 nm using Varian Cary Eclipse fluorescent spectrophotometer with both excitation and emission slits held at 5 nm. Calibration curve was prepared using same procedure by dissolving known amounts of APTES and 30 mg of non-functionalized pSNPs.

### **6.3.7 Reversibility of dsRNA loaded on the silica nanoparticles**

To visualize dsRNA saturated silica nanoparticles exchanging dsRNA with surrounding, firstly, 1  $\mu$ L of unlabeled dsRNA (13  $\mu$ g/ $\mu$ L, 84bp) was mixed with 5  $\mu$ L of 11.8 nm porous nanoparticles (10 mg/mL) and 44  $\mu$ L of RNase-free water. The mixture was incubated on shaker table at speed 5 for 1 hour at room temperature. After 1 hour, the dsRNA loaded-particles was washed with RNase-free H<sub>2</sub>O three times to remove excess RNA. After washing, same amount of labelled RNA was added to the particles, and incubated in the solution for 10 mins and 40 mins before confocal imaging.

### **6.3.8 Confocal imaging and Fluorescence Recovery after Photobleaching**

1  $\mu\text{L}$  of fluorescein labelled dsRNA (12.7  $\mu\text{g}/\mu\text{L}$ ) was mixed with 5  $\mu\text{L}$  of porous or nonporous silica nanoparticles (10  $\text{mg}/\text{mL}$ ), 44  $\mu\text{L}$  of RNase-free water and incubate on shaker table at speed 5 for 1 hour at room temperature. After 1 hour, the dsRNA loaded-particles was washed with RNase-free  $\text{H}_2\text{O}$  three times to remove excess RNA. For fluorescence imaging, the labelled RNA was excited at 488 nm with an argon laser at 8% laser power for imaging and emission was collected between 500 nm and 600 nm using confocal laser scanning microscopy (Leica TCS SP5). Experiments were performed at 20°C over a x63/1.3 oil immersion objective. For FRAP experiments, one image was captured prior to bleaching, a 500 nm diameter disk was bleached once at 75% laser power, 5 images were captured at the fastest capture rate (1.3 seconds), 5 images were captured at 3 second intervals and finally 20 images were captured at 10 second intervals.

## **6.4 Results and discussion**

### **6.4.1 Amine functionalization of silica particles for RNA loading**

The pore size and surface area of the particles before and after amine functionalization was characterized by nitrogen adsorption (**Table 6.1**). The particle pore size and surface area before and after amine functionalization characterized by nitrogen adsorption. The introduction of amine groups caused the reduction of mean pore diameter and BET surface area, consistent with the incorporation of the amine groups in the pores of particles. Micron-sized nonporous silica particles were also amine modified. Due the small surface area of nonporous silica particles comparing the mesoporous silica, the amine amount used to functionalizing the nonporous was carefully controlled to avoid overdose. The non-

functionalized silica particle is named as pSNP-pore size. And the amine functionalized silica particles is named as Amine-pSNP-pore size.

**Table 6.1** Brunauer–Emmett–Teller (BET) specific surface area, amount of amine grafted and % of monolayer silica surface coverage by amine group for amine functionalized micron-sized nonporous and porous particles.

Particle type	Average pore diameter (nm) <sup>a</sup>	BET surface area (m <sup>2</sup> /g)	mmol APTES/g particles	% of monolayer coverage
Nonporous	-	0.54 <sup>b</sup>	-	-
Amine-Nonporous	-	0.54	0.0065	364
pSNP-3.6	3.6 ± 1.4	551	-	-
Amine-pSNP-3.6	3.0 ± 0.9	191	2.19	233
pSNP -7.4	7.4 ± 1.1	668	-	-
Amine-pSNP -7.4	7.2 ± 1.2	400	1.93	170
pSNP -11.8	11.8 ± 2.6	367	-	-
Amine-pSNP -11.8	11.3 ± 3.0	319	1.64	212

<sup>a</sup>The average and range were determined from the peak and full width at half maximum (FWHM) of the BJH pore distribution, respectively; <sup>b</sup>Surface area determined by considering all particles as 5 μm diameter spheres;

The extent of amine modification was determined from dissolution of the particle, followed by reaction of fluorescein to produce fluorescent pyrrolinone. [173, 178] The extent of amine functionalization reported on a per gram particle basis decreases with increasing pore size (**Table 6.1**) Bauer et al. reported different types of aminosilane grafting on silica support based on trace amount of water presents during hydrolysis process, where linear cross-linked oligomeric structures or monolayer type coverage form on a hydrophilic surface (silica), whereas neutral or hydrophobic surface induces isolated

tridental aminosilane grafting (less than monolayer coverage).[179] Ritter et al. [180] measured the amine groups accessibility of SBA-15 silica particles with 7.6 nm pores directly by the post-synthesis reaction of amines with fluorescein isothiocyanate (FITC), and found the amine on the accessible mesoporous is about 0.33 mmol FITC/g particles for total amine group density of 1.02 and 1.41 mmol amine/g particles. This indicates the mesoporous is completely and uniformly covered by the amine and the rest of the amine groups were grafted in the intrawall micropores, which is inaccessible to the FITC. The lowest amount of amine incorporation (1.64 mmol amine/g particles for pSNP-11.8) in this work is higher than the total amine group density of 1.02 and 1.41 mmol amine/g particles, therefore the mesopores walls of silica is completely cover by amine groups and results in uniform functionalization on the pore surface for the particles present in the **Table 6.1**.

#### **6.4.2 Loading of dsRNA to silica particles and its mobility**

To investigate effect of dsRNA length on loading, protection and release on pSNPs of various pore size using confocal laser scanning microscopy, varying lengths of dsRNA were templated from inhibitor of apoptosis (IAP) genes of *Spodoptera frugiperda* fragments using T7 polymerase promoter regions. To visualize the dsRNA loading and uptake by cells, fluorescent nucleotides were labelled at the end of strands of the dsRNA. **Figure 6.2** shows the confocal images through the middle cross section of the silica particles as a function of fragment length (84 bp and 282 bp) and pore size (nonporous, 3.6nm, 7.4nm and 11.8nm) after incubating in the labelled dsRNA solution at a ratio of 0.25 mg dsRNA /mg particles for 1 hours. A halo of fluorescence at the surface of the spherical particle indicates that the dsRNA is adsorbed to the surface but excluded from the pores (and also observed in the case of nonporous particles for both lengths of dsRNA).



Continuous fluorescence throughout the particle indicates that the dsRNA is present at both the surface and also in the pores. The 84 bp dsRNA was present throughout 3.6, 7.4 and to 11.8 nm pores of the pSNPs. In contrast, the 3.6 nm pores are inaccessible to the 282 bp RNA, which can reside in the 7.4 and 11.8 nm pores.

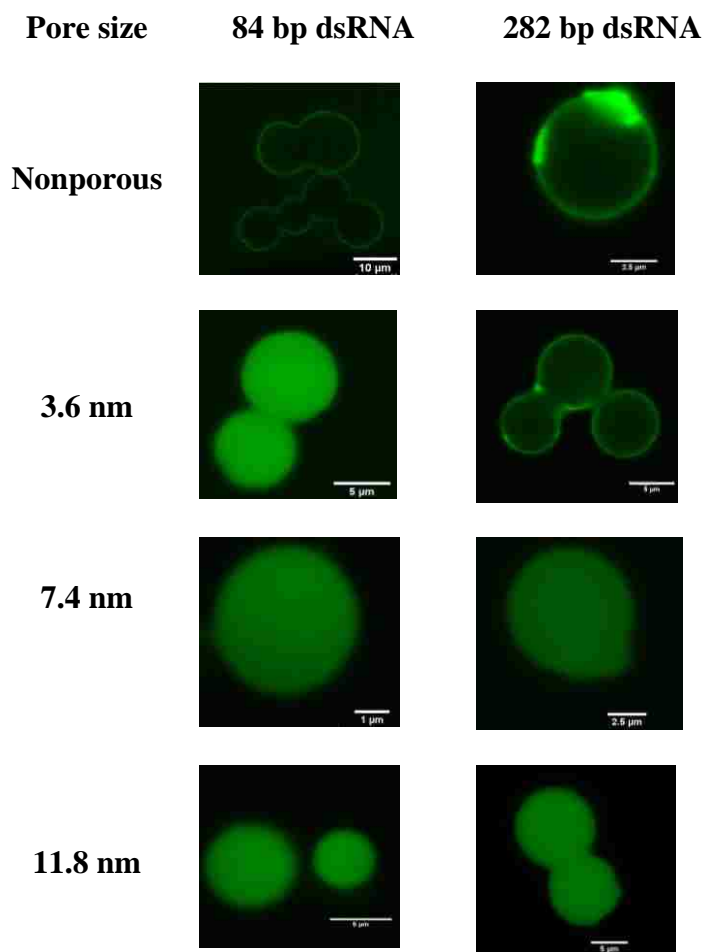


**Figure 6.2** Confocal images through the middle section of silica particles as a function of fragment length and pore size.

The 84 bp and 282 bp RNA are estimated to have a diameter of about 3 nm and lengths of 25 nm, 85 nm respectively.[181] The fact that dsRNA can fit into the pores far smaller than its lengths suggests the dsRNA inserted into the pores like a hard rod (**Figure 6.1**). Li

et al. [171] measured the hydrodynamic size change of silica particle with 20 -30 nm pore depth and diameter of 3 nm after the interaction with 50 nm long DNA and found that the hydrodynamic size of particles increased from 130 nm to 220 nm. This observation was consistent with the insertion of DNA into the length of these short pores, leaving the remaining DNA outside of the pore and contributing to the hydrodynamic size increase of the particle.[171] The depth of the pores and their tortuous pathway may explain why the 84 bp dsRNA fits into the 3.6 nm pores while the 282 bp dsRNA is excluded from the pores, although they have the same diameter. When the longer dsRNA fails to enter the pores, it can adsorb to the particle surface and blocks the pores. In the case of the 84 bp dsRNA in the 3.6 nm pores, one molecule layer can fit into pores. For larger pores, a geometric pore-filling model based on the dsRNA adsorption isotherms was developed to predict the maximum numbers of dsRNA can accommodate into the pores, [170, 182] which is useful for predicting particles capacities as functions of pore sizes.

The interaction of dsRNA with the pSNP and the accessibility of the pores of the pSNP can be described from the diffusivity (mobility) of the dsRNA in dsRNA-loaded pSNPs. Using FRAP, the effect of both pore size (nonporous, 3.6 nm, 7.4, and 11.8 nm diameter) and length of dsRNA (84 bp and 282 bp) on the diffusivity at the surface and in the core of dsRNA-loaded pSNPs has been examined. For FRAP experiments, a 500 nm diameter disk at the surface or the core of dsRNA-loaded pSNPs was bleached by high intensity laser beam vertically passing through the focal plane of interest. The fluorescence recovery of the bleached spot was collected as a function of time and fitted to a one dimensional radial diffusion model previously reported to extract oligonucleotides diffusivity inside the porous network of silica particles. [183]

**Figure 6.3** presents the dsRNA diffusivity as a function of fragment length (84 bp and 282 bp), pore size (nonporous, 3.6nm, 7.4nm and 11.8nm) and dsRNA location (external surface (cap) and the porous core of the particle) after incubating the pSPNs in the labelled dsRNA solution at a ratio of 0.25 mg dsRNA /mg particles (higher than saturation concentration) for one hour. As shown, regardless of dsRNA length, the dsRNA diffusivity increased as the pore size increased, as larger pore size allows to accommodate more dsRNA molecules in one single pore. Overall, the mobility of 282 bp dsRNA was smaller than that of 84 bp dsRNA, which is consistent with the assembly of dsRNA inside the pores and longer dsRNA need to diffuse through longer path. In addition, when the dsRNA was disturbed throughout the particles (corresponding to **Figure 6.2**), the diffusivity measured at the surface and core of the particle was similar. This is consistent with a mobile network of dsRNA throughout the particle, and was also observed in our previous study of lipid diffusivity in lipid-filled pSPNs.[64] However, when dsRNA only adsorbed to the particles surface (both lengths of dsRNA on nonporous particle and 282 bp dsRNA in 3.6 nm pores), the mobility is not measurable at the particle surface, as there is limited amount of dsRNA on the surface to diffuse to the photobleached spot without the dsRNA supply from the pores. Thus, loading sufficient dsRNA into porous particle is important for creating a mobile dsRNA network, which has important implications to design strategies for dsRNA protection and release from porous particles.

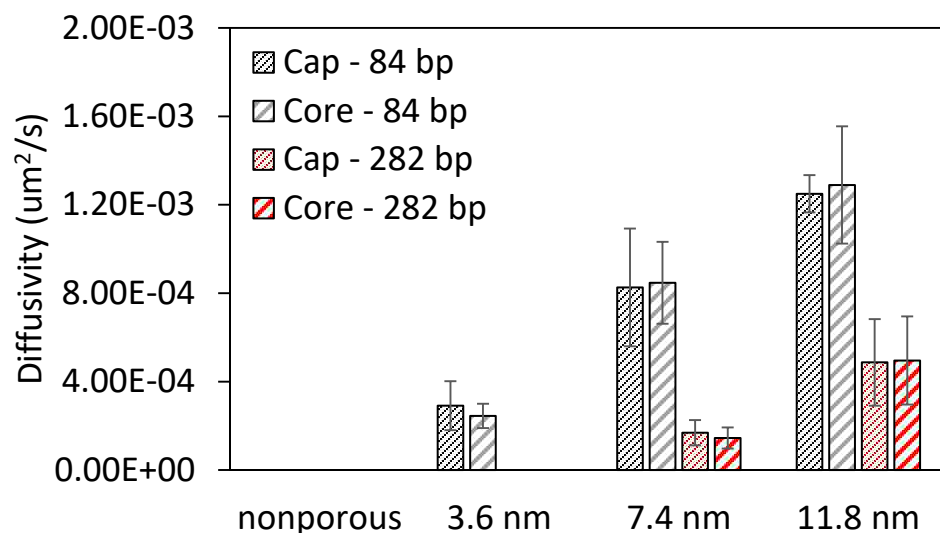


**Figure 6.3** 84 bp and 282 bp dsRNA diffusivity as a function of pore size and dsRNA location (cap and core) at a loading concentration of 0.25 mg dsRNA /mg particles. The role of RNA concentration on mobility is important designing dsRNA loading strategy.

For the most mobile system (the smallest dsRNA with the largest pores), the fluorescence halo formed at low concentration (0.07 mg dsRNA /mg particles) and the dsRNA penetrated into the pores when the concentration increased to 0.13 mg/mg and 0.25 mg/mg (**Figure 6.4**). Correspondingly, the mobility of dsRNA loaded in pores increased with dsRNA concentration while the mobility of surface adsorbed dsRNA was not detectable. Thus, a initial dsRNA concentration sufficient to achieve maximum loading of dsRNA into the porous network is required to achieve high mobility on amine functionalized silica with high (greater than monolayer) surface coverage.

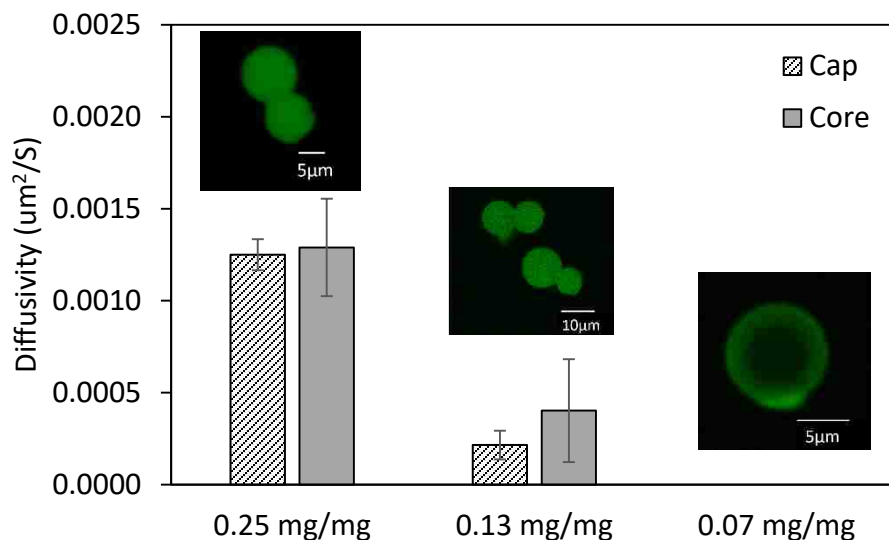


**Figure 6.4** Loading (confocal images) and corresponding diffusivity of 84 bp dsRNA in pSNPs of 11.8 nm pores with varying loading concentration.

The diffusivity of 21 bp DNA oligonucleotides when adsorbed on the APTES functionalized glass surface was reported to be around  $0.2 \mu\text{m}^2/\text{s}$ , [184] which is about two orders magnitude higher than the values reported here. However, it is well known that molecular in liquid-filled pores of molecular dimensions have reduced diffusivities due to the steric restrictions. [185] In fact, these measured diffusivities of dsRNA confined in pores and at porous surfaces are comparable to the diffusivity of large molecules such as lipid, dyes, protein inside mesoporous materials, which is on the scale of  $0.001 \mu\text{m}^2/\text{s}$ . [64, 186] In addition, Lu et al. [187] also reported pore-size dependent diffusivity of porcine pancreatic lipase (PPL) encapsulated in mesoporous silica particles, where diffusivity of PPL in 9.7 nm pores was 42 times higher than that of 5.6 nm pores. In contrast, the mobility of 84 bp dsRNA mobility in 11.8 nm pores is only 4 times higher than that of 3.6 nm pores. This may result from the differences in the relative dimensions of the PPL and dsRNA.

The dimensional sizes of PPL is  $2 \text{ nm} \times 4.5 \text{ nm}$ , which allows it pack closely in  $9.7 \text{ nm}$  pores comparing to  $5.6 \text{ nm}$  pores, meanwhile the assembly of 48 dsRNA ( $3 \text{ nm} \times 25 \text{ nm}$ ) is restricted by its length.

In order to understand if mobility contributes to a functional aspect of RNA delivery, such as RNA release from the particle, the reversibility of dsRNA loading on the mesoporous SNPs was examined. Reversibility of RNA loading was demonstrated on  $11.8 \text{ nm}$  pore diameter particles by first saturating the particles with unlabeled dsRNA (84 bp), washing the particles, and then exposing the particles to labeled dsRNA. The dynamic exchange of dsRNA on mesoporous nanoparticles is captured in confocal images (**Figure 6.5**) for particles incubated with labeled dsRNA for 10 and 40 minutes. The increase in fluorescence intensity represents the exchange of dsRNA in the mesoporous particles. Thus, the mobility of dsRNA in the nanopores of the pSNPs is expected to have a functional effect on delivery of dsRNA to insects.

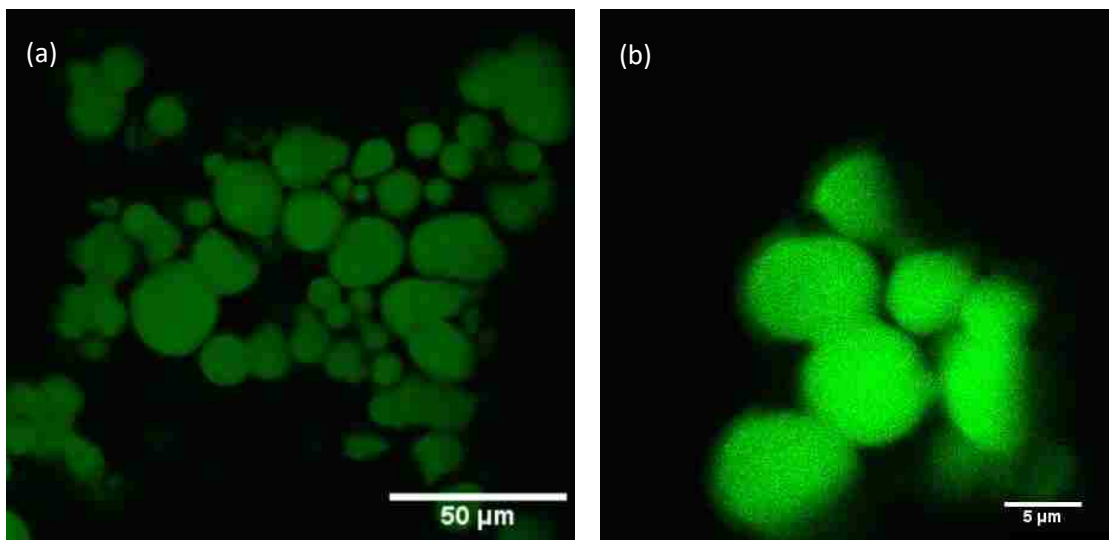


**Figure 6.5** Fluorescence recovery after incubating pSNPs (11.8 nm pore) saturated with unlabeled dsRNA (84 bp) in labelled dsRNA solution for (a) 10min; (b) 40mins.

### 6.5 Conclusion

The siRNA loading behavior, interaction of dsRNA - amine functionalized pSNPs, and diffusion dynamics of siRNA inside particles were successfully examined using confocal imaging and FRAP. 84 bp dsRNA was found to penetrate into the pores of 3.6 nm, 7.4 nm and 11.8 nm, while 282 bp dsRNA can't fit into 3.6 nm pores and is able to load into pores of 7.4 and 11.8 nm. This suggests that the relative dimension of dsRNA length to pore diameter is an important factor for designing carrier that can efficiently encapsulate dsRNA to provide protection from RNases during delivery. For the cases of dsRNA distribute throughout the particles, the mobility at the core of particle can be measured and was similar to that on the particle surface. However, for dsRNA only adsorbed to the particles surface (both lengths of dsRNA on nonporous particle and 282 bp dsRNA in 3.6 nm pores), dsRNA mobility at the surface was not detectable, suggesting the importance of loading sufficient dsRNA into pores to provide a mobile network of dsRNA. Furthermore, the mobility of pore confined dsRNA was dependent on the dsRNA lengths,

pores size and dsRNA concentration. The identification of these factors is of great importance, which will guide to the design of to the design of dsRNA-loaded pSNPs for effective delivery to insects.



## **Chapter 7: Conclusion and Future Directions**

### **7.1 Conclusion**

**Chapter 3** through **Chapter 5** examined the structure and separation efficiency of the biomimetic carrier-mediated separation membrane, which is supported by orthogonally oriented ordered mesoporous thin film membrane with 2-D hexagonal close packed (HCP) structure. In **Chapter 3**, the lipid pore-filled silica thin film membrane with a lipid-immobilized carrier is successfully demonstrated to facilitate the transport of hydrophilic molecules. Besides, the robust lipid-filled mesoporous membranes is proven to act as barriers to ions and small hydrophilic solutes that can be matched with biomimetic carriers to provide selective transport as a separation and sensing platform. The facilitated transport of glucose through the membrane with lipid-immobilized boronic acid carrier can also be improved by controlling environment factors like pH gradient (related to binding of glucose) and temperature (related to the lipid bilayer diffusivity). Opportunities to tune transport through the solute-carrier interactions can also be used to manipulate the flux and achieve selective separations. Thus, the biomimetic membrane which combines high surface area silica thin film membrane with selective permeable lipid bilayers has potential as an efficient aqueous-based separation technology through the selection of lipid-based carrier molecules

**In Chapter 4**, electrochemical impedance spectroscopy (EIS) is proved to be capable of quantifying the accessibility of the pore structure of the mesoporous silica thin films. The EIS then can be used to screen separation platforms for constructing biomimetic membrane for the incorporation of proteins and small hydrophilic carriers. The EIS is also demonstrated to be able to distinguish the configuration and ion transport through the

mesoporous silica thin film supported lipid membrane using lipid deposition method (in the form of lipid enveloping and lipid filling). The lipid filled system is demonstrated to be a superior barrier while providing effective mobility for functioning small lipophilic carriers. The application of EIS to mesoporous silica thin film supported lipid membrane enables the study of the fundamental properties of the biomimetic membrane, and provides insights for making better barriers on mesoporous support for carrier-mediated membrane separation process. This sets the ground work for exploring the application of lipid bilayers in biosensing, selective separations and drug delivery.

**Chapter 5** demonstrate the successful immobilization of biocatalyst on a carrier-mediated separation membrane, while maintaining significant enzyme activity. Thus it is promising to combine the reaction and selective separation in one single membrane process to achieve low cost, high product purity, high yield upgrading and recovery of dilute aqueous solute. A general mathematical model that describes the chemical reaction and selective mass transfer through composite is developed, and the Thiele modulus ( $\Phi^2 = k_1 d^2 / D$ ) which defined the diffusion rate and reaction rate in the enzyme layer appears to be a critical factors determining the membrane performance. Thus, factors that affects the diffusion rate coefficient ( $D$ ), enzyme layer thick ( $d$ ) and enzyme reaction rate ( $k_1$ ) need to be considered in the model. The mathematical model then can serve as a screening tool for optimizing operation conditions to achieve high selectivity and productivity of the desired product using biocatalyst and carrier-mediated separation integrated membrane.

In **Chapter 6**, the siRNA loading behavior, interaction of dsRNA - amine functionalized pSNPs, and diffusion dynamics of siRNA inside particles are successfully examined using confocal imaging and FRAP. Furthermore, the mobility of pore confined

dsRNA is dependent on the dsRNA lengths, pores size and dsRNA concentration. The identification of these factors is of great importance and guide the design of dsRNA-loaded pSNPs to efficiently encapsulate dsRNA in the pores and provide protection from RNases for effective delivery to insects.

## **7.2 Future directions**

In this work, the application of lipid pore-filled silica thin film membranes for biomimetic recovery of dilute carbohydrates is demonstrated. However, this novel biomimetic membrane is not limited to sugar separation. The biomimetic membrane design uses pore confined lipid for constructing defect-free bilayer on the high surface area silica thin film separation platform, while the boronic acid carrier is immobilized in the lipid to achieve selective separation. Thus, the boronic acid carrier can be further replaced by other specific carriers for separating molecules of interest. Meanwhile, the stability and solute rejection properties of phospholipid barrier can be further improved.

While the pore-confined DPPC lipid used in this work is proved to be an efficient barrier for investigating the function of boronic acid carrier, factors like types of lipid, lipid composition, surface chemistry and solution conditions (pH, presence of divalent cations), [96, 97] can be further examined to improve stability, solute rejection and selectivity of the biomimetic membrane. For example, lipid bilayers consisting of saturated phospholipids form more rigid and impermeable membranes than unsaturated phospholipids. [188] The addition of cholesterol, which is an important constituent in biological membrane, to the lipid can reduce the membrane permeability with increased stability. [111] The tethered lipid bilayer, with high electrical insulation, can also be confined into pores of mesoporous

silica.[64] The combination of tethering and pore confinement of lipid in mesoporous silica thin film could result better lipid membrane.

In addition to phospholipid, amphiphilic block copolymers, which can also assemble as vesicle and bilayer structures, have become attractive to mimic biological membranes, due to their high mechanical stability and resistance to severe surrounding environments, which may destroy traditional phospholipid membranes.[189, 190] Proteins have been successfully incorporated into planar triblock copolymer membranes and found to exhibit protein functionality in the membrane.[191] The electrochemical property of the biomimetic copolymer membrane can also examine by the EIS.

Inspired by the membranes proteins, some effort have been taken to synthesis artificial channel mimicking the function of proteins. These channels are also potential carriers that can be used in the biomimetic carrier mediated separation membrane. Wu et al. synthesized a peptide-appended pillar[n]arene (n = 5, 6) derivatives that selectively transported amino acids across liposomes.[192] Cho and Zhao [193] reported a synthetic macrocyclic oligocholate that can facilitate the transport of the molecules glucose, maltoriose and carboxyfluorescein.[194] Artificial water channels (hydrazide-appended pillar[5]arene derivatives) were also reported to mimic water-selective aquaporin proteins.[195] It is also promising to transfer the ligands used in the affinity chromatography, where the targeted analytes are attached to the immobilized ligands with specific affinity to achieve purification. In fact, the boronic acid carriers have been used as ligands in affinity chromatography for the separation of carbohydrates, nucleic acid components, glycoproteins, and other small biomolecules.[196] Nevertheless, the discovery of new carriers are based on molecules recognition. Quartz crystal microbalance (QCM), which

allows for in real-time measurements of surface interaction under controlled solution conditions (temperature, pH etc.), can be a powerful techniques to screen the carriers for targeted molecules and examine the solutions conditions that will affect the reversibly reaction.

It is also important to investigate the lipid bilayer structure deformation after the immobilization of carrier, which is often seen in membrane protein based biomimetic membranes due to the size mismatch between the transmembrane protein and hydrophobic region of the bilayer.[109] To extend this carrier-mediated biomimetic membrane to other carriers such as transmembrane proteins and ionophores, the incorporation in the lipid bilayer in an active configuration will be a concern. To analyze the lipophilicity of carrier, the interaction between the lipid molecules and carriers can be characterized using techniques such as DSC, Raman spectroscopy, Second-Harmonic spectroscopy and NMR spectroscopy.[108-110, 197, 198] As discussed in **Chapter 3**, DSC is a sensitive tool to identify the change in the thermodynamic lipid phase transition as a function of the concentration of components incorporated in the lipid bilayer. As a supplemental analysis to the DSC results, Raman spectroscopy can be applied to determine the location of the additive in the lipid bilayers, whether it resides near the polar headgroup or is dispersed among the alkyl chains.[110] The presence of the additives at different locations would cause intensity and frequencies change in the spectral regions that are related to the functional group (headgroup or alkyl chain of phospholipids). These techniques enable the screening and optimization of carriers to be incorporated in the model lipid bilayers, which is important to improve the membrane performance.

As discussed in **Chapter 5**, the enzyme can be immobilized on the surface of the biomimetic membrane to achieve one step upgrading and separation of solute. One of the advantages of the mesoporous thin film supported by the AAO support is that two identical silica thin film can be formed on the two side of the AAO support, which is promising for making composite membrane with multiple functional layer for continuous process. Again, using sugar separation as an example, fructose is the desired product in the model enzymatic membrane reactor after the upgrading and recovery of dilute aqueous glucose. Fructose can be converted into HMF (5-hydroxymethyl-furfural), a potential dehydration product of carbohydrates that can readily be converted into valued added chemicals, [199], using metal oxide catalysts.[199, 200] Furthermore, the catalyst systems, such as aluminum based catalyst, can potentially be immobilized on silica thin film, which then combines the glucose isomerization process, separation and fructose conversion in a single system (**Figure 7.1**). The double layered silica thin film membrane with easy surface functionalization can find numerous potential application in continuous processing.

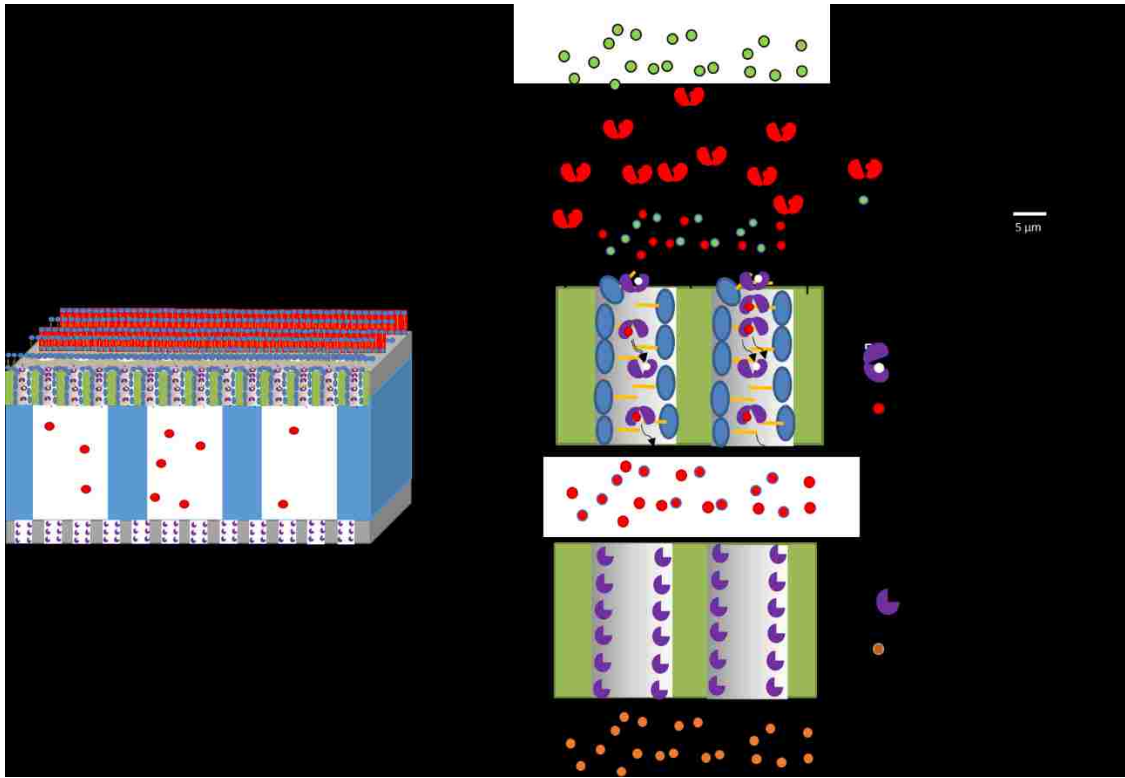


**Figure 7.1** Glucose upgrading process on composite silica thin film membranes

## Appendix A: Characterization of Orthogonally Oriented Silica Thin Film with 2-D HCP Structure Supported by AAO support

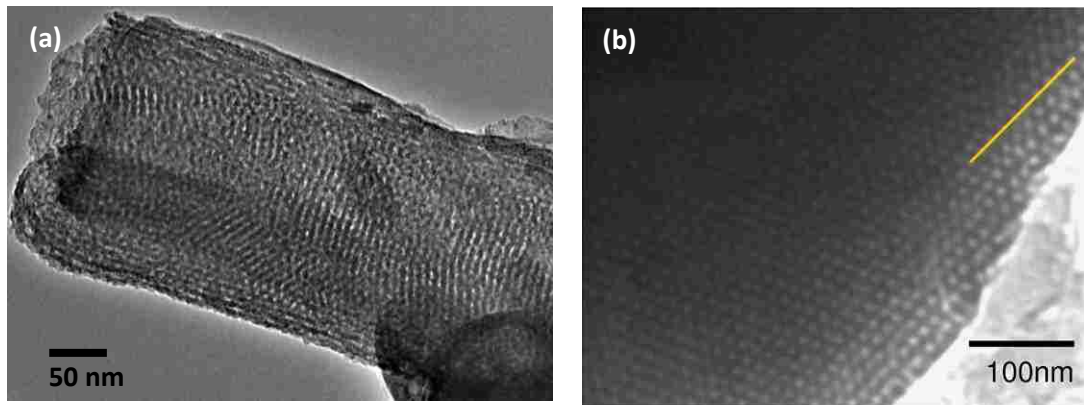


**Figure A.1** TEM image of oriented silica film after dissolving the AAO support in 5 M HCl.

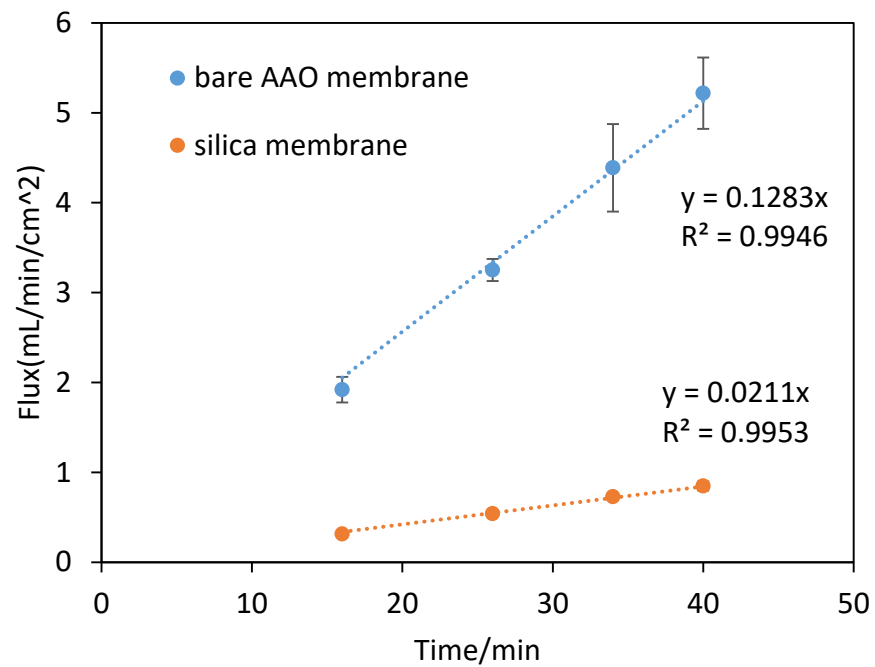


**Figure A.2** Ethanol flux as a function of pressure drop.



## Appendix B: MATLAB Code for the Model Describing the Transport Process in Biocatalysis and Selective Separation Integrated Membrane

```

function TransportModel
clear, clc, format long
warning off
global k1 k2 D Pa Pb CA0 A v1 v2

%-----
% Variables of interest

ratioP=1;           % relative permeability
ratioK=100000;     % relative reaction rate
ratioD=1;           % relative diffusion coefficient

%-----
%Initial values for the variables

Pb=0.206998596/10000*3600;           % permeability of substrate (A), unit
conversion: um/s --->cm/h
Pa=Pa/ratioP;                       % permeability of product (B), cm/h
k1=ratioK*0.015132952;              %forward reaction rate, h-1;
k2=0.015132952;                     %reverse reaction rate, h-1;
D=6.7/1000000*3600*ratioD;          % diffusion coefficient, unit
conversion: cm^2/s---->cm^2/h
CA0=1000;                             %initial substrate concentration, mg/L
A=2;                                  % area of the membrane exposed to the solution, cm^2
v1=0.01;                              % flow rate in donor phase, cm^3/h
v2=0.01;                              % flow rate in receptor phase,
cm^3/h

zspan=[0:1:200];                      %thickness of enzyme layer, nm
z=zspan/10000000;                     %thickness of enzyme layer, cm
d=z(size(z,2));

solinit =bvpinit (z,@guess);          % trial solution given by guess function
sol = bvp4c (@odes, @bcs, solinit);    % bvp solved,

y = deval(sol, z) ;                   %species profiles as a function of distance

CAd=(v1*CA0+D*y(2,1)*A)/v1;            % substrate conc. on the donor phase
CAi=y(1,size(z,2));                   % substrate conc. at the interface
between enzyme layer and membrane
CAR=Pa*A/(Pa*A+v2)*CAi;               % substrate conc. on the receptor phase

CBd=D*y(4,1)*A/v1;                    % product conc. on the donor phase
CBi=y(3,size(z,2));                   % product conc. at the interface
between enzyme layer and membrane
CBr=Pb*A/(Pb*A+v2)*CBi;               % product conc. on the receptor phase
S=CBr/CAR % selectivity of fructose over glucose on the receptor phase
Thiele=k1*d*d/D                       % Thiele modulus

```

```

Mass= (CAd+CBd)+(CAr+CBr)*v2/v1 % Total mass balance

%-----
% plot of species profiles as a function of distance
figure (1)
plot(zspan,y(1,:), 'b')
xlabel('d/nm');
ylabel('Concentration(mg/l) ');
title('Glucose')

figure (2)
plot(zspan,y(3,:), 'b')
xlabel('d/nm');
ylabel('Concentration(mg/l) ');
title('Fructose')

%-----
% provides a trial solution to start off
function yinit = guess (z)
global k1 k2 D Pa Pb CA0 A v1 v2
y1= exp(-sqrt(k1)*z);
y2= 0.*y1;
yinit = [y1 y2 y2 y2];

%-----
%ODEs
function dydz=odes(z,y)
global k1 k2 D Pa Pb CA0 A v1 v2

dy1dz=y(2); % y1: substrate concentration
dy2dz=k1*y(1)/D-k2*y(3)/D; % y2: derivative of y1
dy3dz=y(4); % y3: product concentration
dy4dz=-k1*y(1)/D+k2*y(3)/D; % y4: derivative of y3
dydz=[dy1dz;dy2dz;dy3dz;dy4dz];

%-----
% provides the boundary conditions at the end points a and b
function res = bcs ( ya,yb)

global k1 k2 D Pa Pb CA0 A v1 v2

res = [ ya(1)-(v1*CA0+D*ya(2)*A)/v1
ya(3)-D*ya(4)*A/v1
yb(2)+Pa/D*v2/(Pa*A+v2)*yb(1)
v1*(CA0-(v1*CA0+D*ya(2)*A)/v1-D*ya(4)*A/v1)-v2*Pa*A/(Pa*A+v2)*yb(1)-
v2*Pb*A/(Pb*A+v2)*yb(3) ];

```

## References

1. Kaghazchi, T., et al., *Emulsion liquid membrane pertraction of L-lysine from dilute aqueous solutions by D2EHPA mobile carrier*. Desalination, 2006. **190**(1-3): p. 161-171.
2. Zhang, H., et al., *Adsorptive Separation of Acetic Acid from Dilute Aqueous Solutions: Adsorption Kinetic, Isotherms, and Thermodynamic Studies*. Journal of Chemical & Engineering Data, 2016. **61**(1): p. 213-219.
3. Tian, M. and K.H. Row, *Separation of glucose and bioethanol in biomass with current methods and sorbents*. J Chromatogr Sci, 2013. **51**(8): p. 819-24.
4. Taherzadeh, M.J. and K. Karimi, *Enzyme-based hydrolysis process for ethanol from lignocellulosic materials: a review*. BioResources, 2007. **2**(4): p. 707-738.
5. Kurian, J.K., et al., *Bioconversion of hemicellulose hydrolysate of sweet sorghum bagasse to ethanol by using pichia stipitis NCIM 3497 and debaryomyces hansenii sp*. BioResources, 2010. **5**(4): p. 2404-2416.
6. Brooks, A.A., *Ethanol production potential of local yeast strains isolated from ripe banana peels*. Journal of Biotechnology, 2008. **7**(20): p. 3749-3752.
7. Abels, C., et al., *Membrane-based recovery of glucose from enzymatic hydrolysis of ionic liquid pretreated cellulose*. Bioresour Technol, 2013. **149**: p. 58-64.
8. Malmali, M., J.J. Stickel, and S.R. Wickramasinghe, *Sugar concentration and detoxification of clarified biomass hydrolysate by nanofiltration*. Separation and Purification Technology, 2014. **132**: p. 655-665.
9. Assary, R.S., et al., *Glucose and fructose to platform chemicals: understanding the thermodynamic landscapes of acid-catalysed reactions using high-level ab initio methods*. Phys Chem Chem Phys, 2012. **14**(48): p. 16603-11.
10. Luccioa, M.D., et al., *Separation of fructose from a mixture of sugars using supported liquid membranes*. Journal of Membrane Science, 2000. **174**: p. 217-224.
11. Goux, A., et al., *Oriented Mesoporous Silica Films Obtained by Electro-Assisted Self-Assembly (EASA)*. Chem. Mater, 2009. **21**: p. 731-741.

12. Trewyn, B.G., et al., *Synthesis and Functionalization of a Mesoporous Silica Nanoparticle Based on the Sol–Gel Process and Applications in Controlled Release*. *Acc. Chem. Res.*, 2007. **40**(9): p. 846-853.
13. Jin, Y., Y. Zhu, and W. Zhang, *Development of organic porous materials through Schiff-base chemistry*. *CrystEngComm*, 2013. **15**(8): p. 1484.
14. Argyo, C., et al., *Multifunctional Mesoporous Silica Nanoparticles as a Universal Platform for Drug Delivery*. *Chemistry of Materials*, 2014. **26**(1): p. 435-451.
15. Zhao, X.S., G.Q.M. Lu, and G.J. Millar, *Advances in Mesoporous Molecular Sieve MCM-41*. *Ind. Eng. Chem. Res.* , 1996. **35**: p. 2075-2090.
16. Koganti, V.R., *Controlled evaporation driven synthesis and applications of order nanoporous ceramic films*, in *Chemical and material engineering*. 2006, University of Kentucky: Lexington. KY.
17. Walcarius, A. and A. Kuhn, *Ordered porous thin films in electrochemical analysis*. *TrAC Trends in Analytical Chemistry*, 2008. **27**(7): p. 593-603.
18. WEST, L.L.H.a.J.K., *The Sol-Gel Process*. *Chem. Rev.* , 1990. **90**: p. 33-72.
19. Kresge, C.T., et al., *Ordered mesoporous molecular sieves synthesized by a liquid-crystal template mechanism*. *NATURE*, 1992. **359**: p. 710-712.
20. Beck, J.S., et al., *A New Family of Mesoporous Molecular Sieves Prepared with Liquid Crystal Templates*. *J. Am. chem. Soc.*, 1992. **114**: p. 10834-20843.
21. BERETTA, M., *NANOSTRUCTURED MESOPOROUS MATERIALS OBTAINED BY TEMPLATE SYNTHESIS AND CONTROLLED SHAPE REPLICA*, in *Department of Materials Science*. 2009, University of Milano - Bicocca: Italy.
22. Sanchez, C., et al., *Design, Synthesis, and Properties of Inorganic and Hybrid Thin Films Having Periodically Organized Nanoporosity*. *Chem. Mater.* , 2008. **20**: p. 682-737.
23. Nicole, L., et al., *Mesostructured hybrid organic–inorganic thin films*. *J. Mater. Chem.*, 2005. **15**: p. 3598-3627.
24. Guliyants, V.V., M.A. Carreon, and Y.S. Lin, *Ordered mesoporous and macroporous inorganic films and membranes*. *Journal of Membrane Science*, 2004. **235**(1-2): p. 53-72.

25. Alberius, P.C.A., et al., *General Predictive Syntheses of Cubic, Hexagonal, and Lamellar Silica and Titania Mesostructured Thin Films*. Chem. Mater., 2002. **14**(8): p. 3284-3294.
26. Lu, Y., et al., *Continuous formation of supported cubic and hexagonal mesoporous films by sol-gel dip-coating*. NATURE, 1997. **389**: p. 364-368.
27. Platschek, B., *Ordered Mesoporous Silica Control of Morphology and Exploration with Single Molecules*, in *Faculty of Chemistry and Pharmacy*. 2007, Ludwig Maximilian University of Munich: Germany.
28. Wooten, M.K., *NANOFILTRATION MEMBRANES FROM ORIENTED MESOPOROUS SILICA THIN FILMS*, in *Chemical and Materials Engineering*. 2014, University of Kentucky: Lexington, KY.
29. Zhao, D., et al., *Nonionic Triblock and Star Diblock Copolymer and Oligomeric Surfactant Syntheses of Highly Ordered, Hydrothermally Stable, Mesoporous Silica Structures*. J. Am. Chem. Soc., 1998. **120**(24): p. 6024-6036.
30. Zhao, D., et al., *Continuous Mesoporous Silica Films with Highly Ordered Large Pore Structures*. Adv. Mater., 1998. **16**: p. 1380-1385.
31. Walcarius, A., et al., *Electrochemically assisted self-assembly of mesoporous silica thin films*. Nature Materials, 2007. **6**: p. 602-608.
32. Koganti, V.R. and S.E. Rankin, *Synthesis of Surfactant-Templated Silica Films with Orthogonally Aligned Hexagonal Mesophase*. J. Phys. Chem. B 2005. **109**: p. 3279-3283.
33. Clark Wooten, M.K., et al., *Synthesis and Nanofiltration Membrane Performance of Oriented Mesoporous Silica Thin Films on Macroporous Supports*. ACS Appl Mater Interfaces, 2016. **8**(33): p. 21806-15.
34. Scott Freeman, M.H., Joan C. Sharp *Biological Science*. 2009, Toronto: Pearson Education Canada.
35. Eeman, M. and M. Deleu, *From biological membranes to biomimetic model membranes*. Biotechnol. Agron. Soc. Environ. , 2010. **14**(4): p. 719-736.
36. Smith, B.D., et al., *Facilitated Transport of Carbohydrates, Catecholamines, and Amino Acids Through Liquid and Plasticized Organic Membranes*. Journal of

- Inclusion Phenomena and Molecular Recognition in Chemistry, 1998. **32**: p. 121-131.
37. Li, Y., et al., *Facilitated transport of small molecules and ions for energy-efficient membranes*. Chem Soc Rev, 2015. **44**(1): p. 103-18.
  38. Tang, C.Y., et al., *Desalination by biomimetic aquaporin membranes: Review of status and prospects*. Desalination, 2013. **308**: p. 34-40.
  39. Pohlmeier, K., et al., *Isolation and characterization of an amino acid-selective channel protein present in the chloroplastic outer envelope membrane*. Proc Natl Acad Sci U S A. , 1997. **94**(17): p. 9504–9509.
  40. Kelkar, D.A. and A. Chattopadhyay, *The gramicidin ion channel: A model membrane protein*. Biochimica et Biophysica Acta (BBA) - Biomembrane, 2007. **1768**(9): p. 2011–2025.
  41. Naumann, R., et al., *Kinetics of valinomycin-mediated K<sup>+</sup> ion transport through tethered bilayer lipid membranes*. Journal of Electroanalytical Chemistry, 2003. **550-551**: p. 241-252.
  42. Zhao, Y.H. and D.F. Shantz, *Phenylboronic acid functionalized SBA-15 for sugar capture*. Langmuir, 2011. **27**(23): p. 14554-62.
  43. Mohapatra, S., N. Panda, and P. Pramanik, *Boronic acid functionalized superparamagnetic iron oxide nanoparticle as a novel tool for adsorption of sugar*. Materials Science and Engineering: C, 2009. **29**(7): p. 2254-2260.
  44. Striegler, S., *Selective Carbohydrate Recognition by Synthetic Receptors in Aqueous Solution*. Current Organic Chemistry, 2003. **7**: p. 81-102.
  45. Cheema, M.K., *Design and Synthesis of FRET-Based Boronic Acid Receptors to Detect Carbohydrate Clustering and Development of Diacylglycerol-Based Lipid Probesto Investigate Lipid-Protein Binding Interactions*. 2009, University of Tennessee.
  46. Tamm, L.K. and H.M. McConnell, *Supported phospholipid bilayers*. Biophys. J. , 1985. **47**(1): p. 105-113.
  47. Loose, M. and P. Schwille, *Biomimetic membrane systems to study cellular organization*. J Struct Biol, 2009. **168**(1): p. 143-51.

48. Mingeot-Leclercq, M.P., et al., *Atomic force microscopy of supported lipid bilayers*. Nat Protoc, 2008. **3**(10): p. 1654-9.
49. Sackmann, E., *Supported Membranes: Scientific and Practical Applications* Science, 1996. **271**(5245): p. 43-48.
50. Brian, A.A. and H.M. McConnell, *Allogeneic stimulation of cytotoxic T cells by supported planar membranes*. Proc. Natl. Acad. Sci., 1984. **81**: p. 6159-6153.
51. Reimhult, E., Fredrik Hook, and B. Kasemo, *Intact Vesicle Adsorption and Supported Biomembrane Formation from Vesicles in Solution: Influence of Surface Chemistry, Vesicle Size, Temperature, and Osmotic Pressure*. Langmuir, 2003. **19**: p. 1681-1691.
52. Brinker, C.J., et al., *Neutron Reflectivity Study of Lipid Membranes Assembled on Ordered Nanocomposite and Nanoporous Silica Thin Films*. Langmuir, 2005. **21**(2865-2870).
53. Jing, Y., et al., *Formation of supported lipid bilayers on silica: relation to lipid phase transition temperature and liposome size*. Soft Matter, 2014. **10**(1): p. 187-95.
54. Guidelli, R. and L. Becucci, *Model Lipid Bilayers at Electrode Surfaces*. 2012: p. 189-227.
55. Zhu, Z.W., et al., *Electrochemical impedance spectroscopy and atomic force microscopic studies of electrical and mechanical properties of nano-black lipid membranes and size dependence*. Langmuir, 2012. **28**(41): p. 14739-46.
56. Isaksson, S., et al., *Protein-Containing Lipid Bilayers Intercalated with Size-Matched Mesoporous Silica Thin Films*. Nano Lett, 2017. **17**(1): p. 476-485.
57. Lin, J., et al., *Effect of a polymer cushion on the electrical properties and stability of surface-supported lipid bilayers*. Langmuir, 2010. **26**(5): p. 3544-8.
58. Lehmann, T.R., J ; Knoll, W ; Frank, C ; Frank, C Frank, C, *The Polymer-Supported Phospholipid Bilayer: Tethering as a New Approach to Substrate-Membrane Stabilization*. Biomacromolecules, 2001. **3**(1): p. 27-35.
59. Vockenroth, I.K., et al., *Stable insulating tethered bilayer lipid membranes*. Biointerphases, 2008. **3**(2): p. FA68.

60. Rebaud, S., O. Maniti, and A.P. Girard-Egrot, *Tethered bilayer lipid membranes (tBLMs): interest and applications for biological membrane investigations*. Biochimie, 2014. **107 Pt A**: p. 135-42.
61. Andersson, J. and I. Koper, *Tethered and Polymer Supported Bilayer Lipid Membranes: Structure and Function*. Membranes (Basel), 2016. **6(2)**.
62. Koper, I., *Insulating tethered bilayer lipid membranes to study membrane proteins*. Mol Biosyst, 2007. **3(10)**: p. 651-7.
63. Schlipf, D.M., *Biomolecule localization and surface engineering within size tunable nanoporous silica particles*, in *Chemical and Materials Engineering*. 2015, University of Kentucky: Lexington, KY.
64. Schlipf, D.M., et al., *Effects of Pore Size and Tethering on the Diffusivity of Lipids Confined in Mesoporous Silica*. Adv. Mater. Interfaces, 2017: p. 1601103.
65. Park, J.Y. and S.M. Park, *DNA hybridization sensors based on electrochemical impedance spectroscopy as a detection tool*. Sensors (Basel), 2009. **9(12)**: p. 9513-32.
66. Cañas, A.A., M.J. ; Benavente, J., *Characterization of active and porous sublayers of a composite reverse osmosis membrane by impedance spectroscopy, streaming and membrane potentials, salt diffusion and X-ray photoelectron spectroscopy measurements*. Journal of Membrane Science, 2001. **183(1)**: p. 135-146.
67. Wei, T.-C. and H.W. Hillhouse, *Mass Transport and Electrode Accessibility Through Periodic Self-Assembled Nanoporous Silica Thin Films*. Langmuir, 2007. **23(10)**: p. 5689–5699.
68. Naumann, R., et al., *Tethered Lipid Bilayers on Ultraflat Gold Surfaces*. Langmuir, 2003. **19(13)**: p. 5435-5443.
69. Römer, W. and C. Steinem, *Impedance Analysis and Single-Channel Recordings on Nano-Black Lipid Membranes Based on Porous Alumina*. Biophysical Journal 2004. **86**: p. 955-965.
70. Venkatesan, B.M., et al., *Lipid bilayer coated Al(2)O(3) nanopore sensors: towards a hybrid biological solid-state nanopore*. Biomed Microdevices, 2011. **13(4)**: p. 671-82.



71. David Loveday, P.P., Bob Rodgers, *Evaluation of Organic Coatings with Electrochemical Impedance Spectroscopy Part 1: Fundamentals of Electrochemical Impedance Spectroscopy*. JCT CoatingsTech, 2004: p. 46-52.
72. Allen J. Bard, L.R.F., *Electrochemical Methods: Fundamentals and Applications*. 2nd ed. 2001: Wiley Interscience Publications.
73. Freger, V. and S. Bason, *Characterization of ion transport in thin films using electrochemical impedance spectroscopyI. Principles and theory*. Journal of Membrane Science, 2007. **302**(1-2): p. 1-9.
74. Chang, B.Y. and S.M. Park, *Electrochemical impedance spectroscopy*. Annu Rev Anal Chem (Palo Alto Calif), 2010. **3**: p. 207-29.
75. Dunphy, D.R., et al., *Characterization of lipid-templated silica and hybrid thin film mesophases by grazing incidence small-angle X-ray scattering*. Langmuir, 2009. **25**(16): p. 9500-9.
76. Lee, B., et al., *Structural Analysis of Block Copolymer Thin Films with Grazing Incidence Small-Angle X-ray Scattering*. Macromolecules 2005. **38**: p. 4311-4323.
77. Jiang, Z., et al., *The dedicated high-resolution grazing-incidence X-ray scattering beamline 8-ID-E at the Advanced Photon Source*. J Synchrotron Radiat, 2012. **19**(Pt 4): p. 627-36.
78. Smarsly, B.G., Alain ; Ruland, Wilhelm ; Sturmayer, Dietmar ; Brinker, C Jeffrey, *Quantitative SAXS analysis of oriented 2D hexagonal cylindrical silica mesostructures in thin films obtained from nonionic surfactants*. Langmuir 2005. **21**(9): p. 3858-66.
79. Das, S., et al., *Pore orientation effects on the kinetics of mesostructure loss in surfactant templated titania thin films*. Phys Chem Chem Phys, 2016. **18**(4): p. 2896-905.
80. Nagpure, S., et al., *In SituGISAXS Investigation of Low-Temperature Aging in Oriented Surfactant-Mesostructured Titania Thin Films*. The Journal of Physical Chemistry C, 2015. **119**(40): p. 22970-22984.
81. *Handbook of Biological Confocal Microscopy*. 3rd ed. 2006: Springer US.
82. Prasad, V., D. Semwogerere, and E.R. Weeks, *Confocal microscopy of colloids*. J. Phys.: Condens. Matter 2007. **19**: p. 113102.

83. Axelrod, D., et al., *Mobility measurement by analysis of fluorescence photobleaching recovery kinetics*. Biophys J. , 1976. **16**(9): p. 1055-1069.
84. Song, L., et al., *Photobleaching kinetics of fluorescein in quantitative fluorescence microscopy*. Biophys J. , 1995. **68**(6): p. 2588-2600.
85. Kang, M. and A. Kenworthy, *Complex Applications of Simple FRAP on Membranes*, in *Biomembrane Frontiers*, R. Faller, et al., Editors. 2009, Humana Press: New York,USA. p. 187-221.
86. Cussler, E.L., *Diffusion: Mass transfer in fluid systems*. 3rd ed. 2009: Cambridge University Press.
87. Ferraz, H.C., et al., *Recent achievements in facilitated transport membranes for separation processes*. Brazilian Journal of Chemical Engineering, 2007. **24**(1): p. 101-118.
88. Yan, J., et al., *The relationship among pKa, pH, and binding constants in the interactions between boronic acids and diols—it is not as simple as it appears*. Tetrahedron, 2004. **60**(49): p. 11205-11209.
89. Tsukagoshi, K. and S.J. Shinkai, *Specific Complexation with Mono- and Disaccharides That Can Be Detected by Circular Dichroism*. J. Org. Chem., 1991. **56**: p. 4089-4091.
90. Igawa, M., T. Sekimoto, and H. Okochi, *Facilitated transport of carbohydrates via complexation with borate ion fixed on an anion-exchange membrane*. Journal of Membrane Science, 1995. **98**: p. 177-180.
91. Duggan, P.J., et al., *Enhanced fructose, glucose and lactose transport promoted by a lipophilic 2-(aminomethyl)-phenylboronic acid*. Tetrahedron, 2008. **64**(30-31): p. 7122-7126.
92. Westmark, P.R., S.J. Gardiner, and B.D. Smith, *Selective Monosaccharide Transport through Lipid Bilayers Using Boronic Acid Carriers*. J. Am. Chem. Soc. , 1996. **118**: p. 11093-11100.
93. Weirich, K.L., J.N. Israelachvili, and D.K. Fygenson, *Bilayer edges catalyze supported lipid bilayer formation*. Biophys J, 2010. **98**(1): p. 85-92.
94. Worsfold, O., N.H. Voelcker, and T. Nishiya, *Biosensing Using Lipid Bilayers Suspended on Porous Silicon*. Langmuir 2006. **22**: p. 7078-7083.

95. Claesson, M., et al., *Pore spanning lipid bilayers on mesoporous silica having varying pore size*. Langmuir, 2011. **27**(14): p. 8974-82.
96. Richter, R.P., R. Bérat, and A.R. Brisson, *Formation of Solid-Supported Lipid Bilayers: An Integrated View*. Langmuir, 2006. **22**(8): p. 3497-3505.
97. El Kirat, K., S. Morandat, and Y.F. Dufrene, *Nanoscale analysis of supported lipid bilayers using atomic force microscopy*. Biochim Biophys Acta, 2010. **1798**(4): p. 750-65.
98. Koganti, V.R., et al., *Generalized coating route to silica and titania films with orthogonally tilted cylindrical nanopore arrays*. Nano Letters, 2006. **6**(11): p. 2567-2570.
99. Brinker, C.J., et al., *Evaporation-induced self-assembly: Nanostructures made easy*. Advanced Materials, 1999. **11**(7): p. 579-585.
100. Schlipf, D.M., S.E. Rankin, and B.L. Knutson, *Pore-size dependent protein adsorption and protection from proteolytic hydrolysis in tailored mesoporous silica particles*. ACS Appl Mater Interfaces, 2013. **5**(20): p. 10111-7.
101. Lundbaek, J.A., et al., *Lipid bilayer regulation of membrane protein function: gramicidin channels as molecular force probes*. J R Soc Interface, 2010. **7**(44): p. 373-95.
102. Kaufman, Y., A. Berman, and V. Freger, *Supported lipid bilayer membranes for water purification by reverse osmosis*. Langmuir, 2010. **26**(10): p. 7388-95.
103. Arai, N., K. Yasuoka, and X. Zeng, *Phase diagrams of confined solutions of dimyristoylphosphatidylcholine (DMPC) lipid and cholesterol in nanotubes*. Microfluidics and Nanofluidics, 2013. **14**(6): p. 995-1010.
104. Mütter, D., et al., *Surfactant Self-Assembly in Cylindrical Silica Nanopores*. J. Phys. Chem. Lett., 2010. **1**(9): p. 1442–1446.
105. Karp, E.S., et al., *Characterization of lipid bilayer formation in aligned nanoporous aluminum oxide nanotube arrays*. J Magn Reson, 2007. **187**(1): p. 112-9.
106. Wattraint, O. and C. Sarazin, *Diffusion measurements of water, ubiquinone and lipid bilayer inside a cylindrical nanoporous support: a stimulated echo pulsed-*

- field gradient MAS-NMR investigation*. Biochim Biophys Acta, 2005. **1713**(1): p. 65-72.
107. Kucerka, N., M.P. Nieh, and J. Katsaras, *Fluid phase lipid areas and bilayer thicknesses of commonly used phosphatidylcholines as a function of temperature*. Biochim Biophys Acta, 2011. **1808**(11): p. 2761-71.
  108. Gardikis, K., et al., *A DSC and Raman spectroscopy study on the effect of PAMAM dendrimer on DPPC model lipid membranes*. Int J Pharm, 2006. **318**(1-2): p. 118-23.
  109. Barry, J., et al., *Determining the Effects of Lipophilic Drugs on Membrane Structure by Solid-State NMR Spectroscopy: The Case of the Antioxidant Curcumin*. J. Am. Chem. Soc., 2009. **131**(12): p. 4490–4498.
  110. Gardikis, K., et al., *Effect of a bioactive curcumin derivative on DPPC membrane: A DSC and Raman spectroscopy study*. Thermochemica Acta, 2006. **447**(1): p. 1-4.
  111. Fritzsche, K.J., J. Kim, and G.P. Holland, *Probing lipid-cholesterol interactions in DOPC/eSM/Chol and DOPC/DPPC/Chol model lipid rafts with DSC and <sup>13</sup>C solid-state NMR*. Biochim Biophys Acta, 2013. **1828**(8): p. 1889-98.
  112. McMullen, T.P.W., R.N.A.H. Lewis, and R.N. McElhaney, *Differential scanning calorimetric study of the effect of cholesterol on the thermotropic phase behavior of a homologous series of linear saturated phosphatidylcholines*. Biochemistry, 2002. **32**(2): p. 516-522.
  113. Voskuhl, J. and B.J. Ravoo, *Molecular recognition of bilayer vesicles*. Chem Soc Rev, 2009. **38**(2): p. 495-505.
  114. R, L., K. M., and C. SI, *The formation and annealing of structural defects in lipid bilayer vesicles*. Biochim Biophys Acta. , 1976. **443**(3): p. 313-330.
  115. Pande, A.H., S. Qin, and S.A. Tatulian, *Membrane fluidity is a key modulator of membrane binding, insertion, and activity of 5-lipoxygenase*. Biophys J, 2005. **88**(6): p. 4084-94.
  116. Lande, M., J. Donovan, and M. Zeidel, *The relationship between membrane fluidity and permeabilities to water, solutes, ammonia, and protons*. J Gen Physiol., 1995. **106**(1): p. 67-84.

117. Springsteen, G. and B. Wang, *A detailed examination of boronic acid–diol complexation*. Tetrahedron, 2002. **58**(26): p. 5291-5300.
118. Paugam, M.-F., J.A. Riggs, and B.D. Smith, *High fructose syrup production using fructose-selective liquid membranes*. Chem. Commun., 1996. **1**(22): p. 2539-2540.
119. Korman, C.E., et al., *Nanopore-spanning lipid bilayers on silicon nitride membranes that seal and selectively transport ions*. Langmuir, 2013. **29**(14): p. 4421-5.
120. Verma, P., *Engineering the interface between lipid bilayers and inorganic materials*, in *Department of materials science and engineering*. 2011, Stanford university: Stanford, CA.
121. Tantawi, K.H., et al., *Porous silicon membrane for investigation of transmembrane proteins*. Superlattices and Microstructures, 2013. **58**: p. 72-80.
122. Drexler, J. and C. Steinem, *Pore-Suspending Lipid Bilayers on Porous Alumina Investigated by Electrical Impedance Spectroscopy*. J. Phys. Chem. B 2003. **107**: p. 11245-11254.
123. Phung, T., et al., *Bilayer lipid membranes supported on Teflon filters: a functional environment for ion channels*. Biosens Bioelectron, 2011. **26**(7): p. 3127-35.
124. Khan, M.S., N.S. Dosoky, and J.D. Williams, *Engineering lipid bilayer membranes for protein studies*. Int J Mol Sci, 2013. **14**(11): p. 21561-97.
125. Purruicker, O.H., Heiko ; Adlkofer, Klaus ; Tanaka, Motomu, *Deposition of highly resistive lipid bilayer on silicon–silicon dioxide electrode and incorporation of gramicidin studied by ac impedance spectroscopy*. Electrochimica Acta, 2001. **47**(5): p. 791-798.
126. Chen, V., *Non-invasive observation of synthetic membrane processes ? a review of methods*. Journal of Membrane Science, 2004. **241**(1): p. 23-44.
127. Koganti, V.R.D., Darren ; Gowrishankar, Vignesh ; Mcgehee, Michael D ; Li, Xuefa ; Wang, Jin ; Rankin, Stephen E, *Generalized coating route to silica and titania films with orthogonally tilted cylindrical nanopore arrays*. Nano letters, 2006. **6**(11): p. 2567-70.

128. Nagpure, S.R., *Synthesis of titania thin films with controlled mesopore orientation: nanostructure for energy conversion and storage*, in *Chemical and Materials Engineering*. 2016, University of Kentucky: Lexington, KY.
129. Karman, C., N. Vilà, and A. Walcarius, *Amplified Charge Transfer for Anionic Redox Probes through Oriented Mesoporous Silica Thin Films*. *ChemElectroChem*, 2016. **3**(12): p. 2130-2137.
130. Tanaka, S., et al., *Mass transport and electrolyte accessibility through hexagonally ordered channels of self-assembled mesoporous carbons*. *Journal of Power Sources*, 2013. **228**: p. 24-31.
131. Wiegand, G., et al., *Electrical Properties of Supported Lipid Bilayer Membranes*. *J. Phys. Chem. B*, 2002. **106**: p. 4245–4254.
132. Heimburg, T., *The capacitance and electromechanical coupling of lipid membranes close to transitions: the effect of electrostriction*. *Biophys J*, 2012. **103**(5): p. 918-29.
133. Yarrow, F. and B.W. Kuipers, *AFM study of the thermotropic behaviour of supported DPPC bilayers with and without the model peptide WALP23*. *Chem Phys Lipids*, 2011. **164**(1): p. 9-15.
134. Pantoja, R., et al., *Bilayer Reconstitution of Voltage-Dependent Ion Channels using a Microfabricated Silicon Chip*. *Biophysical Journal* 2001. **81**: p. 2389-2394.
135. Giess, F., et al., *The protein-tethered lipid bilayer: a novel mimic of the biological membrane*. *Biophys J*, 2004. **87**(5): p. 3213-20.
136. Tantawi, K.H.C., R.; Berdiev, B.; Williams, J., *Investigations on Transmembrane Ion Channels Suspended over Porous Silicon Membranes*. *Nanotechnology* 2013. **3**: p. 198–201.
137. Atanasov, V., et al., *Membrane on a chip: a functional tethered lipid bilayer membrane on silicon oxide surfaces*. *Biophys J*, 2005. **89**(3): p. 1780-8.
138. Garcia, O.J., P.A. Quintela, and A.E. Kaifer, *Electrodes modified with a film of phosphatidylcholine: electrochemistry inside a lipid layer*. *Anal. Chem.*, 1989. **61**(9): p. 979–981.

139. Trusek-Holownia, A. and A. Noworyta, *A catalytic membrane for hydrolysis reaction carried out in the two-liquid phase system—Process modelling*. Journal of Membrane Science, 2005. **259**(1-2): p. 85-90.
140. Agustian, J., A.H. Kamaruddin, and S. Bhatia, *Enzymatic membrane reactors: the determining factors in two separate phase operations*. Journal of Chemical Technology & Biotechnology, 2011. **86**(8): p. 1032-1048.
141. du Preez, R., et al., *Modelling of immobilised enzyme biocatalytic membrane reactor performance*. Journal of Molecular Catalysis B: Enzymatic, 2015. **119**: p. 48-53.
142. Giorno, L., et al., *Hydrolysis and regioselective transesterification catalyzed by immobilized lipases in membrane bioreactors*. Journal of Membrane Science, 1997. **125**(1): p. 177-187.
143. Giorno, L., J. Zhang, and E. Drioli, *Study of mass transfer performance of naproxen acid and ester through a multiphase enzyme-loaded membrane system*. Journal of Membrane Science, 2006. **276**(1-2): p. 59-67.
144. Leitgeb, M., Ž. Knez, and K. Vasić, *Micro- and Nanocarriers for Immobilization of Enzymes*. 2016.
145. Liu, D. and E.Y.X. Chen, *Ubiquitous aluminum alkyls and alkoxides as effective catalysts for glucose to HMF conversion in ionic liquids*. Applied Catalysis A: General, 2012. **435-436**: p. 78-85.
146. Gaily, M.H., A.K. Sulieman, and A.E. Abasaeed, *Kinetics of a Three-Step Isomerization of Glucose to Fructose Using Immobilized Enzyme*. International Journal of Chemical Engineering and Applications, 2013: p. 31-34.
147. Gaily, M.H., et al., *Isomerization and Kinetics of Glucose into Fructose*. International Journal of Engineering & Technology 2010. **10**(3): p. 1-6.
148. Xu, J., et al., *Immobilization of lipase by filtration into a specially designed microstructure in the CA/PTFE composite membrane*. Journal of Molecular Catalysis B: Enzymatic, 2006. **42**(1-2): p. 55-63.
149. Jung, D., C. Streb, and M. Hartmann, *Covalent anchoring of chloroperoxidase and glucose oxidase on the mesoporous molecular sieve SBA-15*. Int J Mol Sci, 2010. **11**(2): p. 762-78.

150. Zhang, D., et al., *Immobilization of cellulase on a silica gel substrate modified using a 3-APTES self-assembled monolayer*. Springerplus, 2016. **5**: p. 48.
151. Pugazhenthii, G. and A. Kumar, *Enzyme membrane reactor for hydrolysis of olive oil using lipase immobilized on modified PMMA composite membrane*. Journal of Membrane Science, 2004. **228**(2): p. 187-197.
152. Suekane, M., M. Tamura, and C. Tomimura, *Physico-chemical and Enzymatic Properties of Purified Glucose Isomerases from Streptomyces olivochromogenes and Bacillus stearothermophilus*. Agricultural and Biological Chemistry, 2014. **42**(5): p. 909-917.
153. Hu, Y., et al., *Modeling of a biphasic membrane reactor catalyzed by lipase immobilized in a hydrophilic/hydrophobic composite membrane*. Journal of Membrane Science, 2008. **308**(1-2): p. 242-249.
154. Trusek-Holownia, A., *A catalytic membrane for hydrolysis reaction carried out in the two-liquid phase system—Membrane preparation and characterisation, mathematical model of the process*. Journal of Membrane Science, 2005. **259**(1-2): p. 74-84.
155. Xiong, L. and S.Z. Qiao, *A mesoporous organosilica nano-bowl with high DNA loading capacity - a potential gene delivery carrier*. Nanoscale, 2016. **8**(40): p. 17446-17450.
156. Yu, N., et al., *Delivery of dsRNA for RNAi in insects: an overview and future directions*. Insect Sci, 2013. **20**(1): p. 4-14.
157. Tarn, D., et al., *Mesoporous Silica Nanoparticle Nanocarriers: Biofunctionality and Biocompatibility*. Acc. Chem. Res., 2013. **46**(3): p. 792–801.
158. Tao, Z., *Mesoporous silica-based nanodevices for biological applications*. RSC Advances, 2014. **4**(36): p. 18961.
159. Rosenholm, J.M., et al., *Nanoparticles in targeted cancer therapy: mesoporous silica nanoparticles entering preclinical development stage*. Nanomedicine, 2012. **7**(1): p. 111-120.
160. Lin, D., et al., *Intracellular cleavable poly(2-dimethylaminoethyl methacrylate) functionalized mesoporous silica nanoparticles for efficient siRNA delivery in vitro and in vivo*. Nanoscale, 2013. **5**: p. 4291-4301.



161. Buchman, Y.K., et al., *Silica nanoparticles and polyethyleneimine (PEI)-mediated functionalization: a new method of PEI covalent attachment for siRNA delivery applications*. *Bioconjug Chem*, 2013. **24**(12): p. 2076-87.
162. Xia, T., et al., *Polyethyleneimine Coating Enhances the Cellular Uptake of Mesoporous Silica Nanoparticles and Allows Safe Delivery of siRNA and DNA Constructs*. *ACS Nano*, 2009. **3**(10): p. 3273-86.
163. Ashley, C.E., et al., *Delivery of Small Interfering RNA by Peptide-Targeted Mesoporous Silica Nanoparticle-Supported Lipid Bilayers*. *ACS Nano*, 2012. **6**(3): p. 2174-2188.
164. Zhu, R., et al., *Optical brightener M2R destroys the peritrophic membrane of *Spodoptera exigua* (Lepidoptera: Noctuidae) larvae*. *Pest Manag Sci*, 2007. **63**(3): p. 296-300.
165. Wang, P. and R.R. Granados, *Calcofluor disrupts the midgut defense system in insects*. *Insect Biochemistry and Molecular Biology* 2000. **30**: p. 135–143.
166. Beh, C.W., et al., *Efficient Delivery of Bcl-2-Targeted siRNA Using Cationic Polymer Nanoparticles: Downregulating mRNA Expression Level and Sensitizing Cancer Cells to Anticancer Drug*. *Biomacromolecules* 2009. **10**: p. 41–48.
167. Huan Meng, et al., *Engineered Design of Mesoporous Silica Nanoparticles to Deliver Doxorubicin and P-Glycoprotein siRNA to Overcome Drug Resistance in a Cancer Cell Line*. *ACS nano*, 2010. **4**(8): p. 4539–4550.
168. Chen, A.M., et al., *Co-delivery of doxorubicin and Bcl-2 siRNA by mesoporous silica nanoparticles enhances the efficacy of chemotherapy in multidrug-resistant cancer cells*. *Small*, 2009. **5**(23): p. 2673-7.
169. Lebold, T., et al., *Controlling The Mobility Of Oligonucleotides In The Nanochannels Of Mesoporous Silica*. *Adv. Funct. Mater.* , 2012. **22**: p. 106-112.
170. Steinbacher, J.L. and C.C. Landry, *Adsorption and Release of siRNA from Porous Silica*. *Langmuir*, 2014. **30**: p. 4396-4405.
171. Li, X., J. Zhang, and H. Gu, *Adsorption and desorption behaviors of DNA with magnetic mesoporous silica nanoparticles*. *Langmuir*, 2011. **27**(10): p. 6099-106.
172. Na, H.K., et al., *Efficient functional delivery of siRNA using mesoporous silica nanoparticles with ultralarge pores*. *Small*, 2012. **8**(11): p. 1752-61.

173. Schlipf, D.M., S.E. Rankin, and B.L. Knutson, *Selective external surface functionalization of large-pore silica materials capable of protein loading*. Microporous and Mesoporous Materials, 2017. **244**: p. 199-207.
174. Nakabayashi, H., et al., *Electrolyte-Added One-Pot Synthesis for Producing Monodisperse, Micrometer-Sized Silica Particles up to 7  $\mu\text{m}$* . Langmuir, 2010. **26**(10): p. 7512-7515.
175. Ezzeddine, Z., et al., *Divalent heavy metals adsorption onto different types of EDTA-modified mesoporous materials: Effectiveness and complexation rate*. Microporous and Mesoporous Materials, 2015. **212**: p. 125-136.
176. Na, H.-K., et al., *Efficient Functional Delivery of siRNA using Mesoporous Silica Nanoparticles with Ultralarge Pores*. Small, 2012. **8**(11): p. 1752-1761.
177. Schlipf, D.M., S.E. Rankin, and B.L. Knutson, *Selective external surface functionalization of large-pore silica materials capable of protein loading*. Microporous and Mesoporous Materials, 2016.
178. Ritter, H., et al., *A comparative study of the functionalization of mesoporous silica MCM-41 by deposition of 3-aminopropyltrimethoxysilane from toluene and from the vapor phase*. Microporous and Mesoporous Materials, 2009. **121**(1-3): p. 79-83.
179. Bauer, F., et al., *Water-based functionalization of mesoporous siliceous materials, Part I: Morphology and stability of grafted 3-aminopropyltriethoxysilane*. Microporous and Mesoporous Materials, 2017. **250**: p. 221-231.
180. Ritter, H. and D. Bruhwiler, *Accessibility of Amino Groups in Postsynthetically Modified Mesoporous Silica*. J. Phys. Chem. C 2009. **113**: p. 10667-10674.
181. Bloomfield, V.A., D.M. Crothers, and I. Tinoco, *Nucleic Acids: Structures, Properties, and Functions*. 2000, Sausalito, CA: University Science Books
182. Sang, L.C., A. Vinu, and M.O. Coppens, *General description of the adsorption of proteins at their iso-electric point in nanoporous materials*. Langmuir, 2011. **27**(22): p. 13828-37.
183. Lebold, T., et al., *Controlling The Mobility Of Oligonucleotides In The Nanochannels Of Mesoporous Silica*. Advanced Functional Materials, 2012. **22**(1): p. 106-112.

184. Chan, V., et al., *Adsorption and Surface Diffusion of DNA Oligonucleotides at Liquid/Solid Interfaces*. Langmuir 1997. **13**: p. 320-329.
185. Dechadilok, P. and W.M. Deen, *Hindrance Factors for Diffusion and Convection in Pores*. Ind. Eng. Chem. Res. , 2006. **45**: p. 6953-6959.
186. Lebold, T., et al., *Tuning single-molecule dynamics in functionalized mesoporous silica*. Chemistry, 2009. **15**(7): p. 1661-72.
187. Lu, S., Z. Song, and J. He, *Diffusion-controlled protein adsorption in mesoporous silica*. J Phys Chem B, 2011. **115**(24): p. 7744-50.
188. Akbarzadeh, A., et al., *Liposome: classification, preparation, and applications*. Nanoscale Res Lett, 2013. **8**(1): p. 102.
189. Kita-Tokarczyk, K., et al., *Block copolymer vesicles—using concepts from polymer chemistry to mimic biomembranes*. Polymer, 2005. **46**(11): p. 3540-3563.
190. Kowal, J., et al., *Planar Biomimetic Membranes Based on Amphiphilic Block Copolymers*. ACS Macro Letters, 2014. **3**(1): p. 59-63.
191. Mecke, A., C. Dittrich, and W. Meier, *Biomimetic membranes designed from amphiphilic block copolymers*. Soft Matter, 2006. **2**: p. 751-759.
192. Chen, L., et al., *Chiral selective transmembrane transport of amino acids through artificial channels*. J Am Chem Soc, 2013. **135**(6): p. 2152-5.
193. Cho, H. and Y. Zhao, *Translocation of hydrophilic molecules across lipid bilayers by salt-bridged oligocholates*. Langmuir, 2011. **27**(8): p. 4936-44.
194. Zhang, S. and Y. Zhao, *Oligocholate foldamers as carriers for hydrophilic molecules across lipid bilayers*. Chemistry, 2011. **17**(44): p. 12444-51.
195. Hu, X.B., et al., *Single-molecular artificial transmembrane water channels*. J Am Chem Soc, 2012. **134**(20): p. 8384-7.
196. Liu, X.-C., *Boronic Acids as Ligands for Affinity Chromatography*. Chinese Journal of Chromatography, 2006. **24**(1): p. 73-80.
197. Varshney, G.K., et al., *Effect of Bilayer Partitioning of Curcumin on the Adsorption and Transport of a Cationic Dye Across POPG Liposomes Probed by Second-Harmonic Spectroscopy*. Langmuir, 2016. **32**(40): p. 10415-10421.
198. Ikeda, A., et al., *Location of [60]fullerene incorporation in lipid membranes*. Chem Commun (Camb), 2011. **47**(44): p. 12095-7.

199. Saha, B. and M.M. Abu-Omar, *Advances in 5-hydroxymethylfurfural production from biomass in biphasic solvents*. Green Chemistry, 2014. **16**(1): p. 24.
200. van Putten, R.J., et al., *Hydroxymethylfurfural, a versatile platform chemical made from renewable resources*. Chem Rev, 2013. **113**(3): p. 1499-597.

## VITA

### Shanshan Zhou

**Place of Birth:** Fujiang, China

**Educational institutions attended and degrees already awarded:**

Master in Chemical Engineering, University of Kentucky, Kentucky, USA (2014)

Bachelor of Science in Chemical Engineering, East China University of Science and Technology, Shanghai, China (2012)

**Professional Positions:**

Graduate Research Assistant, Chemical and Material Engineering Department, University of Kentucky (December, 2012-Present).

Teaching Assistant, Chemical and Material Engineering Department, University of Kentucky (August, 2012-May, 2013).

Undergraduate Research Assistant, Chemical Engineering Department, East China University of Science and Technology (December, 2011-June, 2012).

**Scholastic and Professional Honors:**

Center of Membrane Sciences Student Fellow Award, University of Kentucky (2016)

First-class Scholarship, East China University of Science and Technology (2008-2012).

Outstanding Student Award in Science and Engineering of ECUST (2012)

**Professional Publications:**

Zhou, S., Li, H., Garlapalli, R., Nokes, S. E., Flythe, M., Rankin, S. E., Knutson, B. L., Hydrolysis of Model Cellulose Films by *Clostridium thermocellum*: Extension of Quartz Crystal Microbalance Techniques to Cellulosomes, *Journal of Biotechnology*, 2016, 241, 42-49.

Wooten, K., Koganti, V. R., Zhou, S., Rankin, S. E., Knutson, B. L., Nanofiltration Membranes Synthesized from Oriented Mesoporous Silica Thin Films on Macroporous Supports, *Applied Material and Interface*, 2016, 8 (33), 21806–2181.

Schlipf, D. M., Zhou, S., Khan, A., Rankin, S. E., Knutson, B. L., Effects of Pore Size and Tethering on the Diffusivity of Lipids Confined in Mesoporous Silica, *Advanced Materials Interfaces*, In press.

Shanshan Zhou

August 14<sup>th</sup>, 2017